Supplementary Information

Ethylene-bridged Bis(borylamidinates) as Near-UV Fluorescent Emitters with Narrow Emission Bands

Alvaro Calderón-Díaz,[†[a]] Sanjay Dutta,[†[a]] Tomasz Kruczyński,[a] Colin D. McMillen,[b] Ajith Ashokan,[c] Seyhan Salman,[c] and Michael Stollenz*[a]

[a] Department of Chemistry and Biochemistry, Kennesaw State University, 370 Paulding Avenue NW, MD # 1203, Kennesaw, Georgia 30144. [b] Department of Chemistry, Clemson University, 379 Hunter Laboratories, Clemson, SC 29634-0973. [c] Chemistry Department, Clark Atlanta University, 223 James P. Brawley Dr. SW Atlanta, Georgia 30314.

[†]These authors contributed equally to this work.

*E-mail: Michael.Stollenz@kennesaw.edu

Table of Contents

Experimental and Computational Section

General Procedures. All synthetic procedures involving air- and moisture-sensitive compounds were carried out by using Schlenk or glovebox techniques under an atmosphere of dry argon. Glassware and NMR tubes were heat-sealed with a heat gun under vacuum. ***Caution!*** *Extreme care should be taken both in the handling of the cryogen liquid nitrogen and its use in the Schlenk line trap to avoid the condensation of oxygen from air.*

Solvents: Prior to use, tetrahydrofuran (THF, Thermo Fisher, ≥ 99.0%) and toluene (Thermo Fisher, 99.9%) were purified using a PPT Solvent Purification System. For non-inert manipulations, dichloromethane (CH_2Cl_2, Thermo Fisher, 99.9%), toluene (Thermo Fisher, 99.9%), ethyl acetate (Thermo Fisher, 99.9%), and hexanes (mixture of isomers, BDH, 99.9%) were used without further purification. *Deuterated solvents*: Chloroform-*d* (Cambridge Isotope Laboratories, Inc., D, 99.8% + 0.03% v/v tetramethylsilane, TMS) was dried over molecular sieves (4A beads).

Reactants: Triethylamine (Alfa Aesar, 99%) was distilled from sodium. $BF_3{\cdot}OEt_2$ (Acros) was distilled from CaH_2. Bis(amidine) ligands $\mathbf{L^{1-4}}H_2$[S2] were prepared according to the literature procedure.

Melting points were determined with an SRS (Stanford Research Systems) Digi Melt instrument using open capillaries. The heating rate was 2 K/min. The values are uncorrected.

NMR measurements were recorded on a Bruker Avance III 400 and a Bruker Avance III 600 spectrometers, equipped with a PRODIGY cryoprobe, at ambient probe temperatures regulated by a BCU unit unless noted at 400.1 MHz or 600.2 MHz (^{1}H) and 100.6 MHz or 150.9 MHz (^{13}C), respectively. ^{13}C NMR resonances were obtained with proton broadband decoupling and referenced to the solvent signals of $CDCl_3$ at 77.16 ppm (^{1}H NMR: 7.26 ppm ($CDCl_3$)).[S3] ^{13}C NMR assignments are based on COSY, NOESY, HSQC, and HMBC 2D experiments. ^{19}F NMR measurements were recorded on a Bruker Avance III 400 spectrometer at ambient probe temperatures unless otherwise noted. ^{19}F NMR resonances were indirectly referenced using the method described by *Harris et al*.[S4]

Mass spectrometric analyses were performed on a Waters Q-Tof API US quadrupole time-of-flight MS system (low resolution ESI) as well as on a Thermo Orbitrap Velos Pro MS system.

IR spectra were measured on a PerkinElmer Spectrum 100 FT-IR Spectrometer equipped with a Universal ATR Sampling Accessory.

Photoluminescence (PL) measurements were performed on a Horiba Scientific Fluorolog-QM (model: FL-QM-75-11C) spectrofluorometer equipped with variable-temperature setup using a Janis VPF-100 liquid nitrogen cryostat system with a sample holder window. Variable Temperature emission spectra were recorded in crystalline solid samples in flame-sealed quartz capillaries (diameter of 2 mm) under vacuum (0.2 mbar) in the temperature range of 77–300 K. Fluorescence lifetimes were measured using fluorescence intensity decay of a time-correlated single photon counting (TCSPC) setup coupled with

pulsed delta diode-LED (model: DD-340; peak wavelength: 339 nm). Fluorescence decay curves were obtained using a picosecond photon detection module (model PPD 900; Horiba scientific.) coupled with the TCSPC setup (Delta hub). The decay kinetics were fitted with powerFit-10 module incorporated in FelixFL 1.0.43.0 software from HORIBA. Photostability measurements were performed at room temperature (~293 K) using time-based scans at the respective maximum emission wavelengths. The samples were continuously irradiated at their corresponding maximum emission wavelengths (pulse rate was 1 pulse/second), and the emission intensity profiles were monitored for 30 minutes.

Absorbance spectra for all samples were recorded on a Cary 5000 UV-Vis-NIR spectrophotometer, in THF as solvent with a concentration of 10 μM.

Synthesis of 1–4. A solution of $BF_3{\cdot}OEt_2$ ($\mathbf{L^{1–4}}H_2$: 0.60 mL, 4.9 mmol) in toluene (10 mL) was added dropwise into a solution of $\mathbf{L^{1–4}}H_2$ (1.00 mmol) in toluene (30 mL) at 0 °C with stirring. After 15 min, triethylamine (0.60 mL, 4.3 mmol) was added dropwise. The reaction mixture was allowed to warm to room temperature after 30 min and stirred for additional 20 h. The mixture was treated with deionized water (10 mL) and stirred for 15 min. The organic phase was separated, washed with water (4 × 10 mL), and dried over Na_2SO_4. Subsequent filtration and removal of all volatiles from the filtrate by rotary evaporation resulted in a white solid ($\mathbf{L^{1–4}}H_2$) that was purified by automated flash column chromatography on silica gel using a linear gradient of hexanes and ethyl acetate mixtures starting from 100:0 to 20:80 v/v ratios of hexanes to ethyl acetate over a period of 25 minutes. After removal of all volatiles, subsequent drying in oil pump vacuum for 18 h, **1–4** were obtained as colorless microcrystalline powders.

1. Yield: 0.133 g, (0.28 mmol, 28%). Mp (decomposition): ≈ 188–194 °C (solid becomes brown within 188−194 °C, then gradual decomposition into a brown oil > 194 °C). ^{1}H NMR (600.2 MHz, $CDCl_3$): δ 1.52 (s, 18 H, CH_3, ^{t}Bu), 4.23 (s, 4 H, CH_2), 7.00 (t, $^3J_{H,H}$ = 6.5 Hz, 2 H, Py H^5), 7.19 (d, $^3J_{H,H}$ = 8.5 Hz, 2 H, Py H^3), 7.76 (t, $^3J_{H,H}$ = 7.6 Hz, 2 H, Py H^4), 8.10 ppm (d, $^3J_{H,H}$ = 5.9 Hz, 2 H, Py H^6). ^{13}C{^{1}H} NMR (150.9 MHz, $CDCl_3$): 29.9 (CH_3, ^{t}Bu), 39.7 (C, ^{t}Bu), 45.8 (CH_2), 116.5 (CH, Py C^5), 123.5 (CH, Py C^3) 136.2 (CH, Py C^6), 140.7 (CH, Py C^4), 153.9 (CH, Py C^2), 174.0 ppm (C, CN_2). ^{19}F NMR (376.5 MHz, $CDCl_3$): −134.3 ppm (q, $^1J_{B\text{-}F}$ = 32.2 Hz; B***F***$_2$). IR (neat, cm^{-1}): $\tilde{\nu}$ = 3131, 3077, 3048, 2991 (m, ν(CH)), 2979 (m, ν(CH)), 2948, 2921 (m, ν(CH)), 2855, 2584, 1987, 1927, 1918, 1871, 1842, 1740, 1631 (m), 1561 (m), 1506 (m), 1484 (w), 1466 (sh), 1435 (sh), 1417 (w), 1367 (m), 1338, 1312 (m), 1291 (m), 1263, 1245 (m), 1200 (sh), 1189 (m), 1160, 1144, 1106 (m), 1089 (sh), 1061 (w), 1027 (m), 1000 (w), 971 (sh), 960 (br sh), 938 (br), 926 (sh), 910 (m), 878 (m), 860 (m), 817 (m), 805 (m), 780 (s), 758 (s), 740 (sh). UV−Vis (THF), λ [nm] (ε [L·mol^{-1}·cm^{-1}]): 282 (2.56 × 10^4), 337 (2.90 × 10^4, broad shoulder), 350 (2.80 × 10^4). PL excitation and emission (powder, [nm]): λ_{ex} = 372, λ_{em} = 398. Absolute quantum yield: Φ_F = 15.9%. MS (ESI(+)): *m/z* (relative intensity): 477 (73) [M + H]$^+$, 239 (100) [M + 2 H]$^{2+}$. HRMS (ESI(+)): *m*/*z* calcd for $C_{22}H_{31}N_6B_2F_4$ [M + H]$^+$ 477.2732, found 477.2730.

2. Yield: 0.162 g (0.32 mmol, 32%). Mp (decomposition): ≈ 198–242 °C (solid becomes brown within 198−242 °C, then gradual decomposition into a brown oil > 242 °C). ^{1}H NMR (600.2 MHz, $CDCl_3$): δ 1.51 (s, 18 H, CH_3, ^{t}Bu), 2.71 (s, 6 H, CH_3, 6-Py), 4.25 (s, 4 H, CH_2), 6.77 (d, $^{3}J_{H,H}$ = 7.1 Hz 2 H, Py H^5), 7.05 (d, $^{3}J_{H,H}$ = 8.5 Hz 2 H, Py H^3), 7.60 ppm (t, $^{3}J_{H,H}$ = 7.8 Hz, 2 H, Py H^4). ^{13}C{^{1}H} NMR (150.9 MHz, $CDCl_3$): 21.3 (CH_3, Py C^6), 29.9 (CH_3, ^{t}Bu), 39.4 (C, ^{t}Bu), 45.7 (CH_2), 118.6 (CH, Py C^5), 121.6 (CH, Py C^3) 140.3 (CH, Py C^4), 149.9 (CH, Py C^6), 155.0 (C, Py C^2), 172.3 ppm (C, CN_2). ^{19}F NMR (376.5 MHz, $CDCl_3$): −124.3 ppm (q, $^{1}J_{B\text{-}F}$ = 35.1 Hz; B***F***$_2$). IR (neat, cm^{-1}): $\tilde{\nu}$ = 3252, 3106, 3075, 3010, 2991, 2965 (m, ν(CH)), 2917 (m, ν(CH)), 2878, 2850, 2280, 1997, 1981, 1888, 1824, 1778, 1733, 1706, 1625 (s), 1574 (s), 1503 (w), 1489 (w), 1466 (w), 1456, 1432 (m), 1392 (m), 1372 (sh), 1367 (m), 1337 (m), 1312 (m), 1259 (m), 1239 (m), 1207 (sh), 1191 (m), 1164, 1138, 1116 (m), 1094 (sh), 1076 (w), 1057 (sh), 1045 (w), 1021, 1004 (w), 964 (m), 944 (m), 916 (sh), 905 (m), 890 (m), 853, 817 (m), 803 (s), 773, 762 (m), 735 (m), 720 (sh). UV−Vis (THF), λ [nm] (ε [L·mol^{-1}·cm^{-1}]): 283 (2.45 × 10^4), 345 (2.55 × 10^4, br shoulder), 358 (2.79 × 10^4). PL excitation and emission (powder, [nm]): λ_{ex} = 383, λ_{em} = 403. Absolute quantum yield: Φ_F = 12.5%. MS (ESI(+)): *m/z* (relative intensity): 505 (39) [M + H]$^+$, 253 (100) [M + 2 H]$^{2+}$. HRMS (ESI(+)): *m/z* calcd for $C_{24}H_{35}N_6B_2F_4$ [M + H]$^+$ 505.3045, found 505.3041.

3. Yield: 0.167 g (0.33 mmol, 33%). Mp (decomposition): ≈ 205–217 °C (solid becomes brown within 205−217 °C, then gradual decomposition into a brown oil > 217 °C). ^{1}H NMR (600.2 MHz, $CDCl_3$): δ 1.50 (s, 18 H, CH_3, ^{t}Bu), 2.38 (s, 6 H, CH_3, 4-Py), 4.20 (s, 4 H, CH_2), 6.83 (d, $^{3}J_{H,H}$ = 7.8 Hz, 2 H, Py H^5), 7.00 (s, 2 H, Py H^3), 7.97 ppm (d, $^{3}J_{H,H}$ = 7.8 Hz, 2 H, Py H^6). ^{13}C{^{1}H} NMR 150.9 MHz, $CDCl_3$): 21.6 (CH_3, Py C^4), 29.9 (CH_3, ^{t}Bu), 39.6 (C, ^{t}Bu), 45.8 (CH_2), 118.5 (CH, Py C^5), 122.5 (CH, Py C^3) 135.6 (CH, Py C^6), 153.0 (CH, Py C^4), 153.6 (C, Py C^2), 173.9 ppm (C, CN_2). ^{19}F NMR (376.5 MHz, $CDCl_3$): −134.8 ppm (q, $^{1}J_{B\text{-}F}$ = 32.7 Hz; B***F***$_2$). IR (neat, cm^{-1}): $\tilde{\nu}$ = 3339, 3100, 3055, 3000 (m, ν(CH)), 2969 (m, ν(CH)), 2922 (m, ν(CH)), 2876, 2853, 2651, 2451, 2411, 1920, 1772, 1733, 1641 (s), 1557 (m), 1518 (sh), 1512 (sh), 1490 (w), 1472 (sh), 1444 (sh), 1421 (sh), 1411 (w), 1392 (sh), 1372, 1365 (m), 1340, 1313 (s), 1282 (m), 1269 (m), 1245 (m), 1215, 1193 (m), 1169, 1145 (m), 1136 (sh), 1104 (m), 1088, 1059 (m), 1029 (m), 1003 (s), 963 (m), 953 (m), 936 (m), 911 (m), 890 (m), 862 (m), 810 (s), 772, 758 (m), 736, 704 (m). UV−Vis (THF), λ [nm] (ε [L·mol^{-1}·cm^{-1}]): 282 (1.46 × 10^4), 332 (2.51 × 10^4, br shoulder), 345 (2.55 × 10^4). PL excitation and emission (powder, [nm]): λ_{ex} = 363, λ_{em} = 388. Absolute quantum yield: Φ_F = 7.8%. MS (ESI(+)): *m/z* (relative intensity): 505 (24) [M + H]$^+$, 253 (100) [M + 2 H]$^{2+}$. HRMS (ESI(+)): *m/z* calcd for $C_{24}H_{35}N_6B_2F_4$ [M + H]$^+$ 505.3045, found 505.3046.

4. Yield: 0.1.450 g (0.27 mmol, 27%). Mp (decomposition): ≈ 210–249 °C (solid becomes brown within 210−249 °C, then gradual decomposition into a brown oil > 249 °C). ^{1}H NMR (600.2 MHz, $CDCl_3$): δ 1.50 (s, 18 H, CH_3, ^{t}Bu), 2.30 (s, 6 H, CH_3, 4-Py), 2.66 (s, 6 H, CH_3, 6-Py), 4.22 (s, 4 H, CH_2), 6.61 (s, 2 H, Py H^5), 6.87 ppm (s, 2 H, Py H^3). ^{13}C{^{1}H} NMR (150.9 MHz, $CDCl_3$): 21.1 (CH_3, Py C^4), 21.1 (CH_3,

Py C^6), 30.0 (CH_3, ^{t}Bu), 39.3 (C, ^{t}Bu), 45.7 (CH_2), 120.5 (CH, Py C^5), 120.9 (CH, Py C^3) 149.1 (C, Py C^4), 152.3 (CH, Py C^6), 154.7 (C, Py C^2), 172.3 ppm (C, CN_2). ^{19}F NMR (376.5 MHz, $CDCl_3$): −125.2 ppm (q, $^1J_{B\text{-}F}$ = 34.4 Hz; B***F***$_2$). IR (neat, cm^{-1}): $\tilde{\nu}$ = 3283, 3098, 3060, 3000 (m, ν(CH)), 2971, (m, ν(CH)), 2927, (m, ν(CH)), 2877, 2850, 2529, 2412, 1981, 1894, 1784, 1769, 1727, 1640 (m), 1570 (m), 1508 (w), 1492 (w), 1477 (sh), 1467, 1453 (w), 1427 (w), 1406 (sh), 1380 (m), 1373 (sh), 1364, 1348, 1312 (m), 1264 (sh), 1248 (m), 1213, 1196 (m), 1158 (m), 1122 (m), 1095 (m), 1086 (sh), 1063 (sh), 1052 (m), 1031 (sh), 1025 (m), 1004 (m), 976 (m), 958 (sh), 937, 910, 898 (m), 885 (m), 842 (s), 804 (m), 773, 767, 733 (m). UV−Vis (THF), λ [nm] (ε [L·mol^{-1}·cm^{-1}]): 282 (2.11 × 10^4), 338 (2.98 × 10^4, br shoulder); 352 (3.41 × 10^4). PL excitation and emission (powder, [nm]): λ_{ex} = 371, λ_{em} = 399. Absolute quantum yield: Φ_F = 11.7%. MS (ESI(+)): *m/z* (relative intensity): 533 (16) [M + H]$^+$, 267 (100) [M + 2 H]$^{2+}$. HRMS (ESI(+)): *m/z* calcd for $C_{26}H_{39}N_6B_2F_4$ [M + H]$^+$ 533.3358, found 533.3361.

X-ray Crystallography. Colorless, rhomb-shaped single crystals of **1** and **3** were obtained by slow evaporation from solutions of DMSO-d_6 (**1**) and $CDCl_3$ (**3**) at room temperature over the course of two weeks. Colorless, rhomb-shaped single crystals of **2** and **4** were obtained by the slow evaporation of a mixture of ethyl acetate and hexanes at room temperature over the course of one week. All X-ray data were collected on a Bruker Venture X-ray diffractometer (MoKα radiation, λ = 0.71073 Å, Photon II detector) by using ω and φ scans at 100 K (Table S1). The integrated intensities for each reflection were obtained by reduction of the data frames with the program APEX3.[S5] Cell parameters were obtained and refined with 17856 (2241 unique, **1**), 16610 (2574 unique, **2**), 14845 (2441 unique, **3**), and 15035 (2787 unique, **4**) reflections, respectively. The integrated data were scaled and corrected for absorption by using a multi-scan approach in SADABS.[S6] The structures were solved by intrinsic phasing and refined (weighted least squares refinement on F^2) by using SHELXT and SHELXL.[S7] Reflections blocked by the beamstop were omitted from the refinements. The hydrogen atoms were placed in idealized positions, and refined by using a riding model. Non-hydrogen atoms were refined with anisotropic thermal parameters. For all structures, absence of additional symmetry and void space was confirmed using PLATON (ADDSYM).[S8] CCDC 2521021-2521024 contain the supplementary crystallographic data (CIF) for this paper. These data can be obtained free of charge from The Cambridge Crystallographic Data Centre *via* www.ccdc.cam.ac.uk/data_request/cif.

Computational details. All complexes were optimized using B3LYP,[S9] a hybrid density functional that uses 20% exact Hartree-Fock exchange and 80% DFT exchange energy. The 6-311+G** basis set was employed for all atoms. All ground state structures were validated to be at energy minima with vibrational frequency calculations, without any negative frequencies confirming the energy minima. Time dependent density functional (TD-DFT) calculations were performed on the ground optimized geometries for excited state calculations. The functional used for TD-DFT calculation is cam-B3LY[S10] to estimate excited state

properties and to take long-range electron–electron coulomb interaction correlations into account. The calculations were performed using Gaussian 16.[S11]

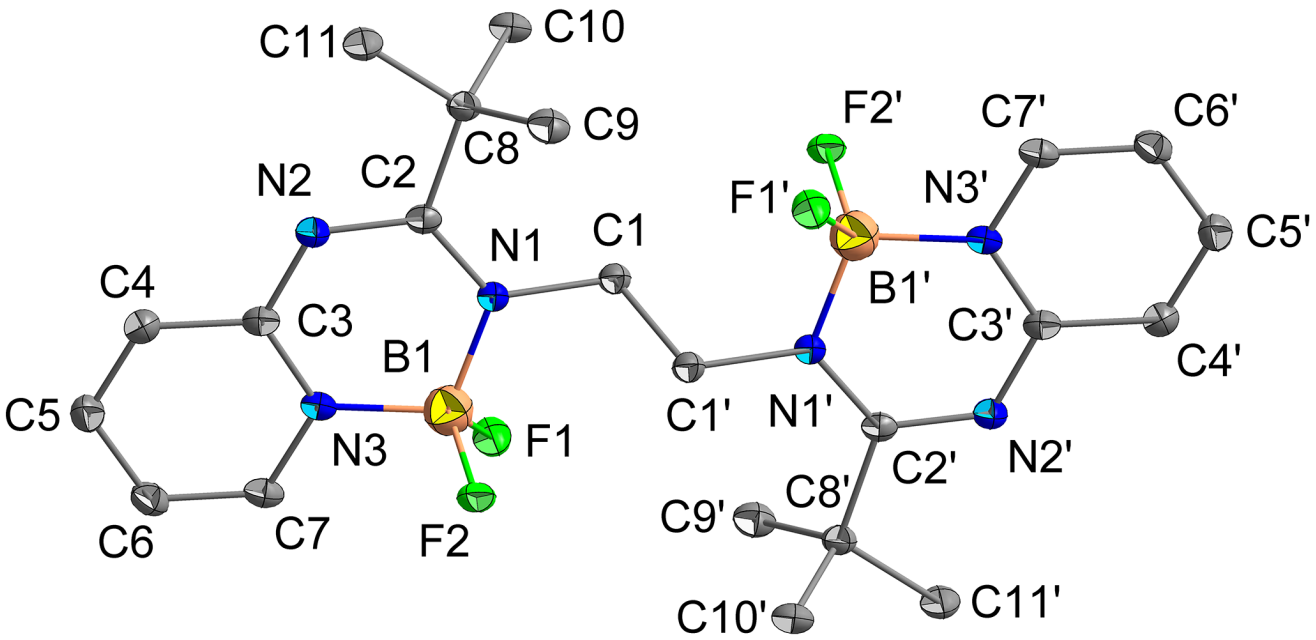

Figure S1. Molecular structure of **1** showing ellipsoids with anisotropic displacement factors of 50% probability. Selected interatomic distances (Å), bond angles (deg), and torsion angles (deg): C1–C1 1.538(3), F1–B1 1.3911(19), F2–B1 1.4040(19), N1–C1 1.4834(19), N1–C2 1.3455(19), N3–C3 1.3587(19), N1–B1 1.533(2), N3–B1 1.546(2), N2–C2 1.329(2), N2–C3 1.352(2), N1–B1–N3 109.56(12), F1–B1–F2 108.50(13), N2–C2–N1 123.16(13), C2–N1–C1 124.77(12), N2–C3–N3 122.52(14), C1–N1–B1 113.88(12), C2–N1–B1 121.16(13), C3–N3–B1 120.25(13), C2–N2–C3 121.55(13), N1–C1–C1' 112.13(15), N1–C1–C1'–N1' –180.0(1),[S12] C1–C1'–N1'–C2' –124.2(2),[S12] N3–B1–N1–C1 –162.1(1),[S12] F1–B1–N1–C1 –41.6(2),[S12] N2–C2–N1–B1 –4.0(2),[S12] F2–B1–N1–C1 79.4(2),[S12] F2–B1–N3–C3 106.9(2)[S12]. Symmetry operation used to generate equivalent atoms (') $-x + ½, -y + ½, -z + ½$.

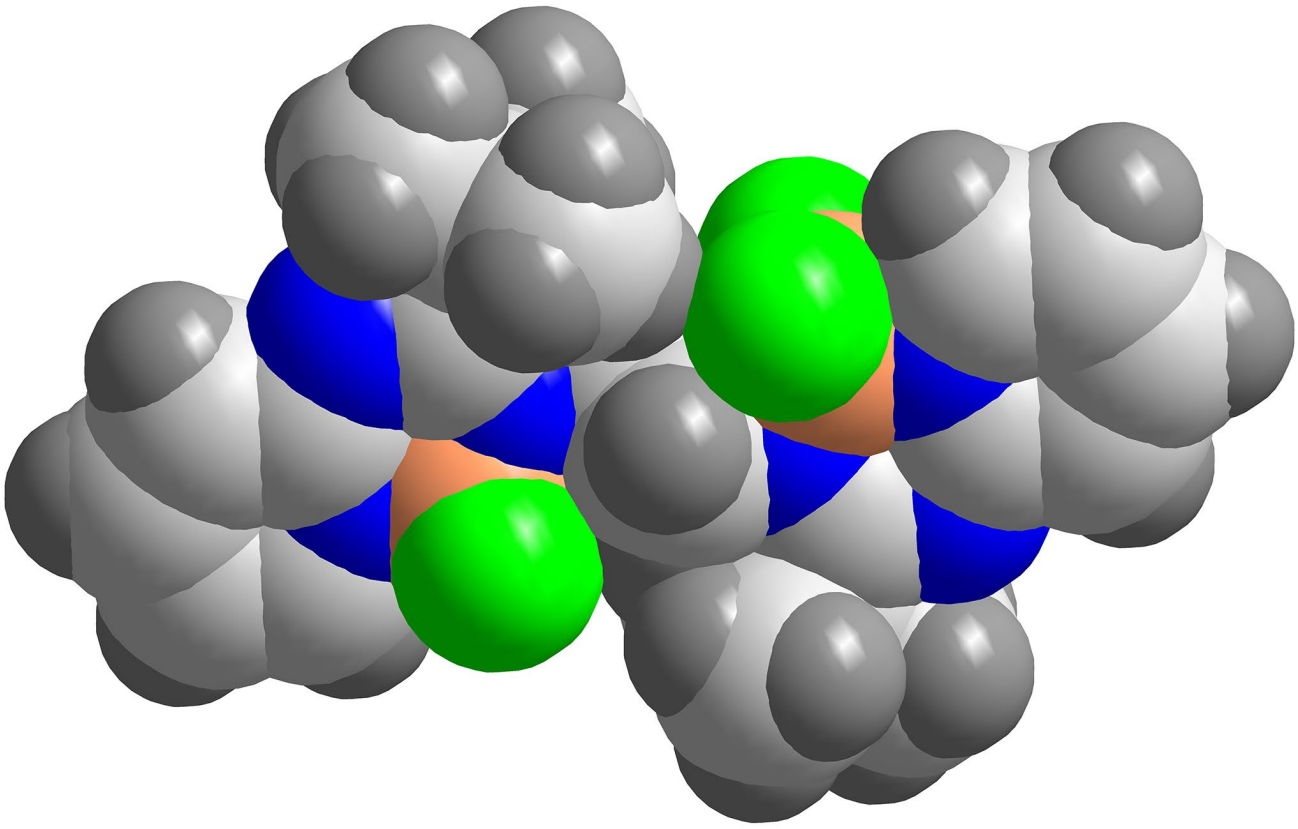

Figure S2. Space filling representation of the molecular structure of **1**.

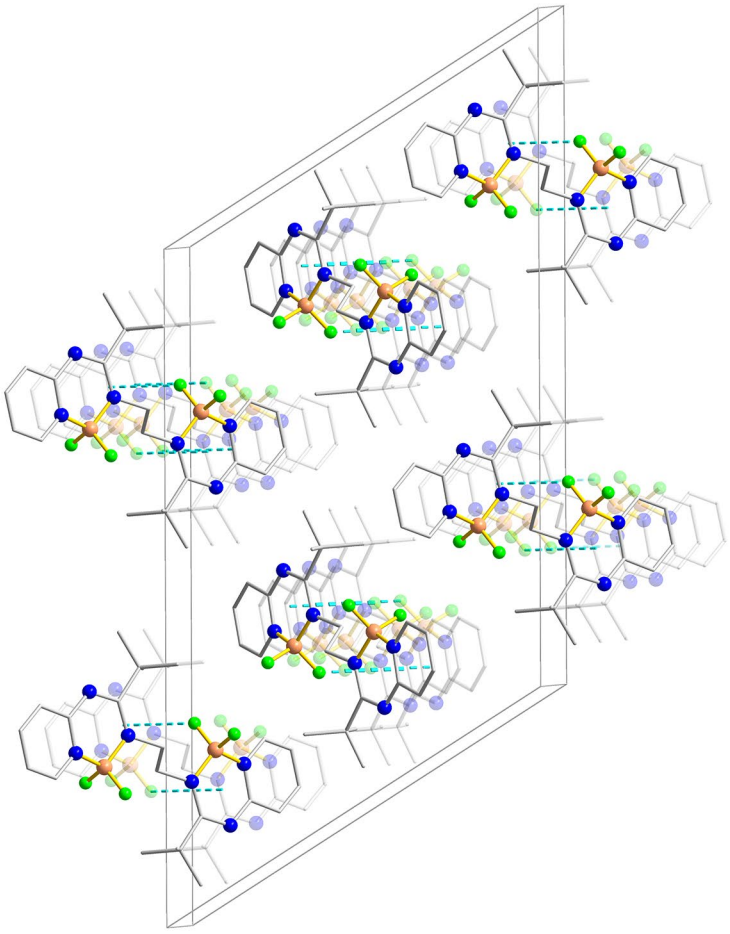

Figure S3. Crystal packing diagram and unit cell of **1**. Hydrogen atoms have been omitted for clarity. Dashed lines indicate the distances between F atoms and centroids of the difluoroboryl-heteroaromatic rings.

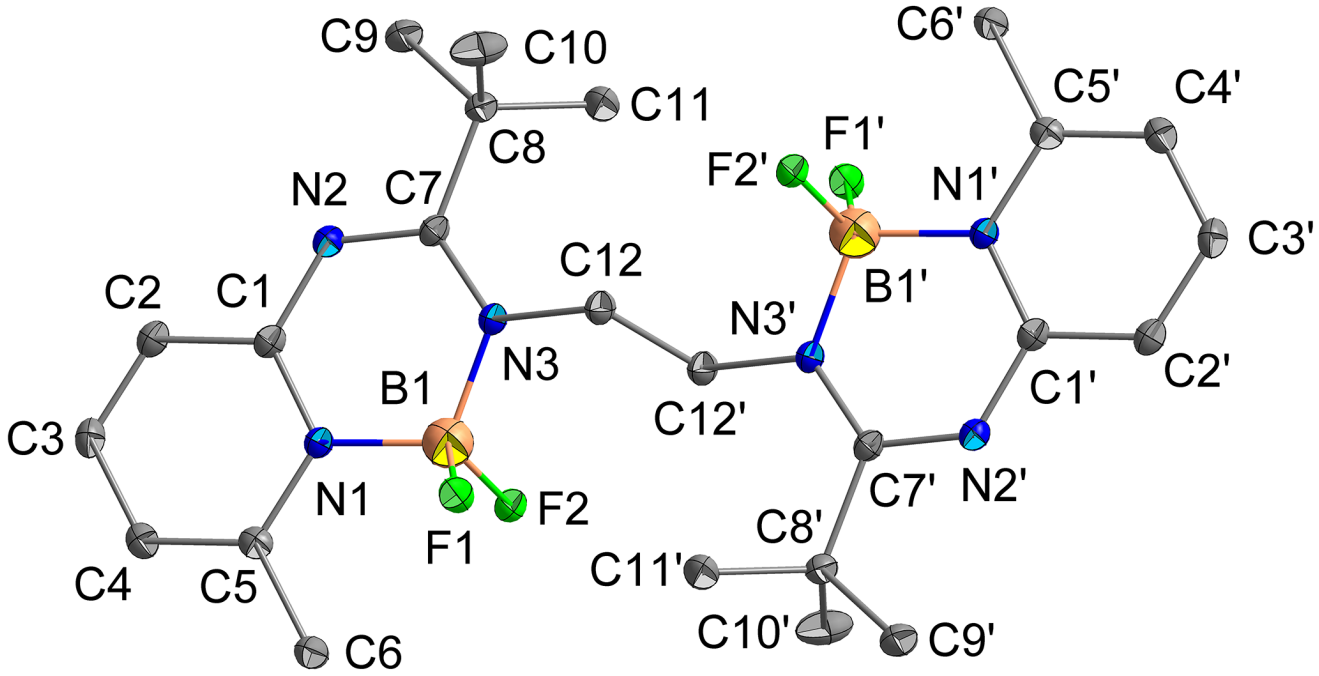

Figure S4. Molecular structure of **2** showing ellipsoids with anisotropic displacement factors of 50% probability. Selected interatomic distances (Å), bond angles (deg), and torsion angles (deg): C12–C12′ 1.542(2), F1–B1 1.3876(15), F2–B1 1.4013(16), N3–C12 1.4867(15), N3–C12 1.3545(16), N3–C7 1.3451(15), N1–C1 1.3671(15), N3–B1 1.5378(16), N1–B1 1.5713(16), N2–C7 1.3246(16), N2–C1 1.3545(16), N1–B1–N3 110.02(10), F1–B1–F2 110.04(10), N2–C1–N1 123.17(11), C12–N3–C7 124.41(10), N3–C7–N2 122.35(11), C12–N3–B1 113.69(9), C7–N3–B1 121.74(10), C1–N1–B1 118.78(10), C1–N2–C7 122.48(10), N3–C12–C12' 112.43(12), N3–C12–C12'–N3' –180.00(9),[S12] C12–C12'–N3'–C7' –118.5(1),[S12] N1–B1–N3–C12 162.48(9),[S12] F2–B1–N3–C12 –78.4 (1),[S12] N2–C7–N3–B1 9.0(2),[S12] F1–B1–N3–C12 42.9(1),[S12] F1–B1–N1–C1 127.3(1)[S12]. Symmetry operation used to generate equivalent atoms (') $-x + 1, -y + 1, -z + 1$.

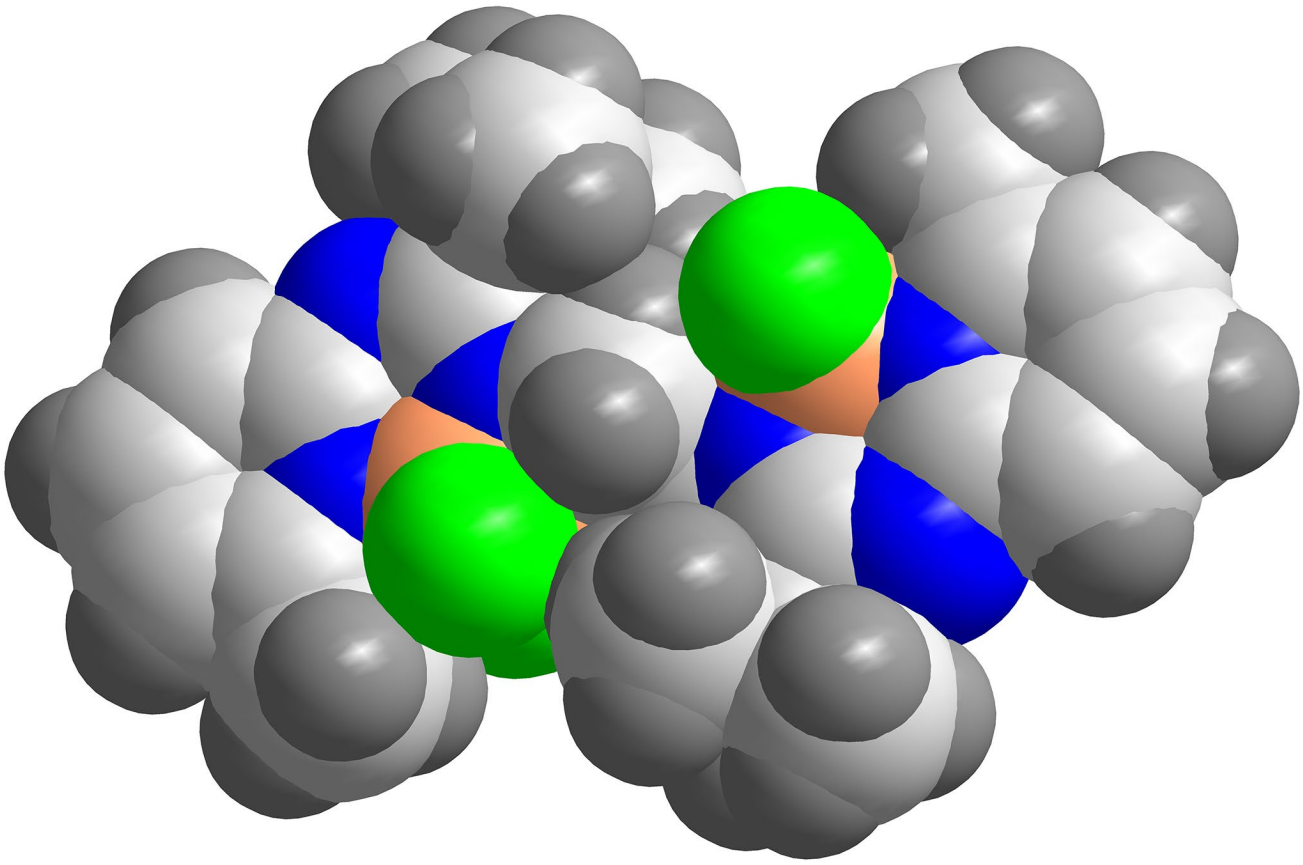

Figure S5. Space filling representation of the molecular structure of **2**.

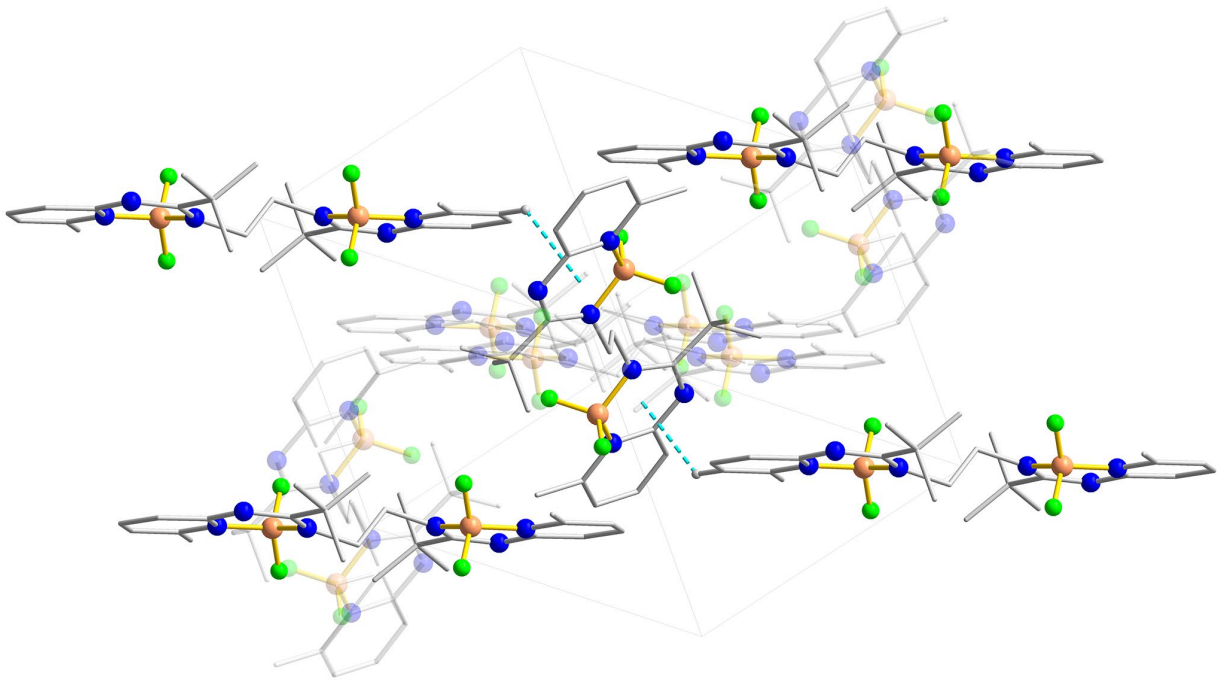

Figure S6. Crystal packing diagram and unit cell of **2**. Dashed lines indicate the distances between Py^5 H atoms and centroids of the difluoroboryl-heteroaromatic rings.

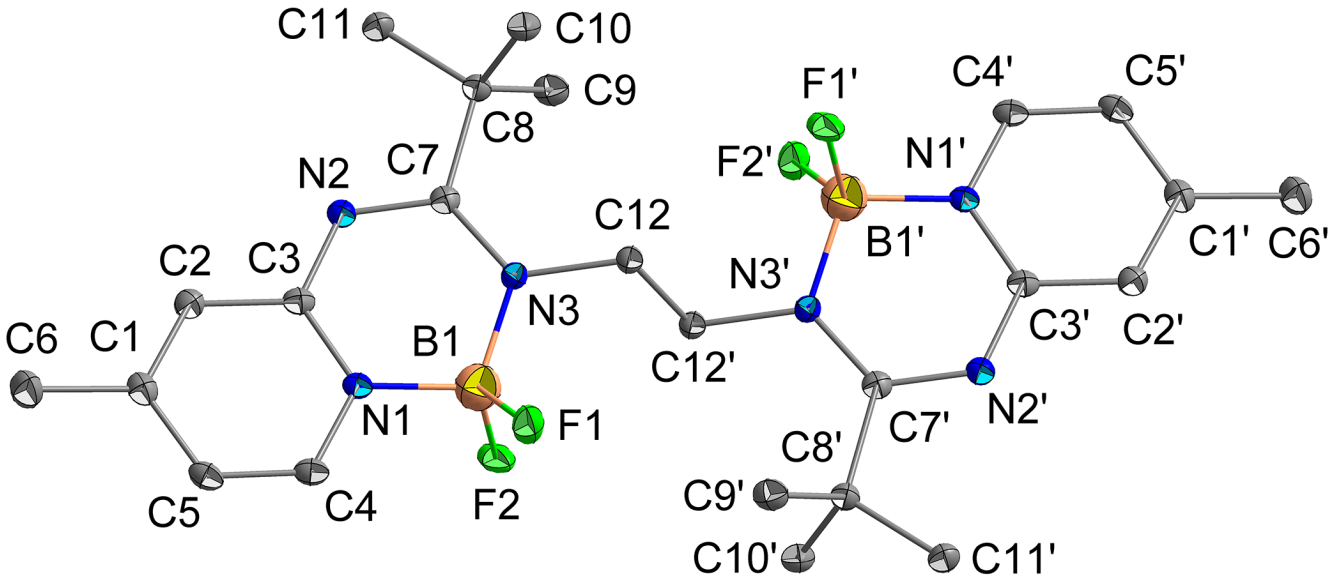

Figure S7. Molecular structure of **3** showing ellipsoids with anisotropic displacement factors of 50% probability. Hydrogen atoms have been omitted for clarity. Selected interatomic distances (Å), bond angles (deg), and torsion angles (deg): C12–C12' 1.541(18), F1–B1 1.388(2), F2–B1 1.404(2), N3–C12 1.4855(18), N3–C7 1.3494(18), N1–C3 1.3567(19), N3–B1 1.535(2), N1–B1 1.552(2), N2–C7 1.3263(19), N2–C3 1.3560(19), N1–B1–N3 109.07(12), F1–B1–F2 108.73(13), N1–C3–N2 122.47(13), C12–N3–C7 124.61(12), N3–C7–N2 122.69(14), C12–N3–B1 113.81(11), C7–N3–B1 121.49(12), C3–N1–B1 120.34(12), C7–N2–C3 121.62(13), N3–C12–C12' 111.99(15), N3–C12–C12'–N3' –180.0(1),[S12] C12'–C12–N3–C7 –117.1(1),[S12] N1–B1–N3–C12 161.5(1),[S12] F1–B1–N3–C12 42.2(2),[S12] N2–C7–N3–B1 5.5(2),[S12] F2–B1–N3–C12 –79.5(2),[S12] F2–B1–N1–C3 –107.5(1)[S12]. Symmetry operation used to generate equivalent atoms (') $-x, -y + 1, -z + 1$.

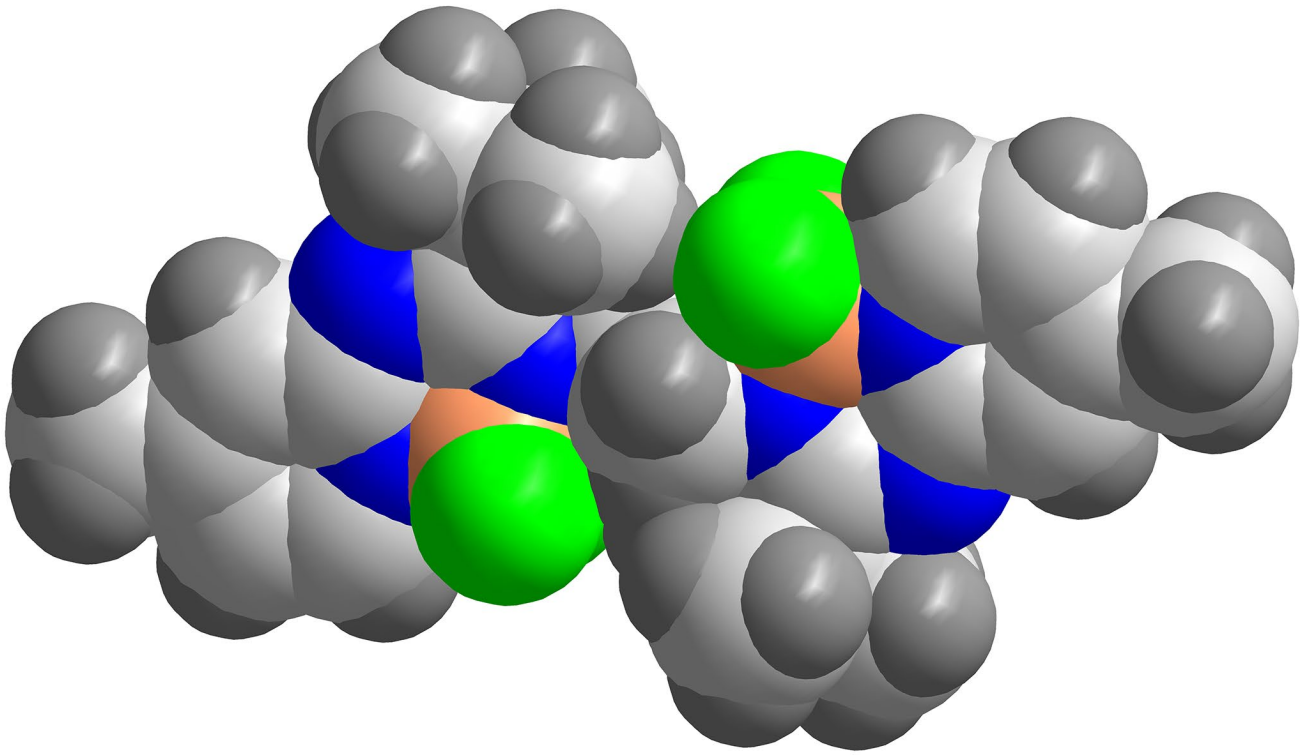

Figure S8. Space filling representation of the molecular structure of **3**.

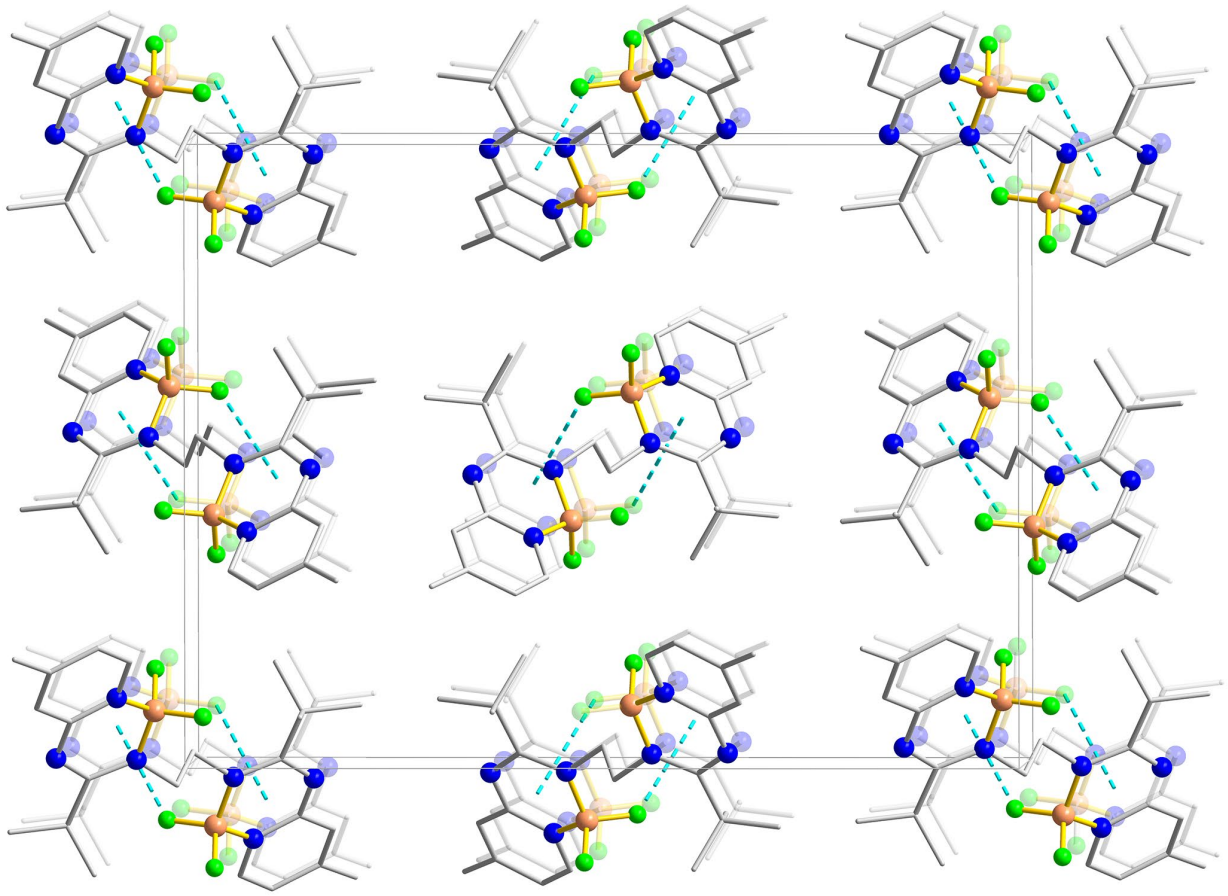

Figure S9. Crystal packing diagram and unit cell of **3**. Hydrogen atoms have been omitted for clarity. Dashed lines indicate the distances between F atoms and centroids of the difluoroboryl-heteroaromatic rings.

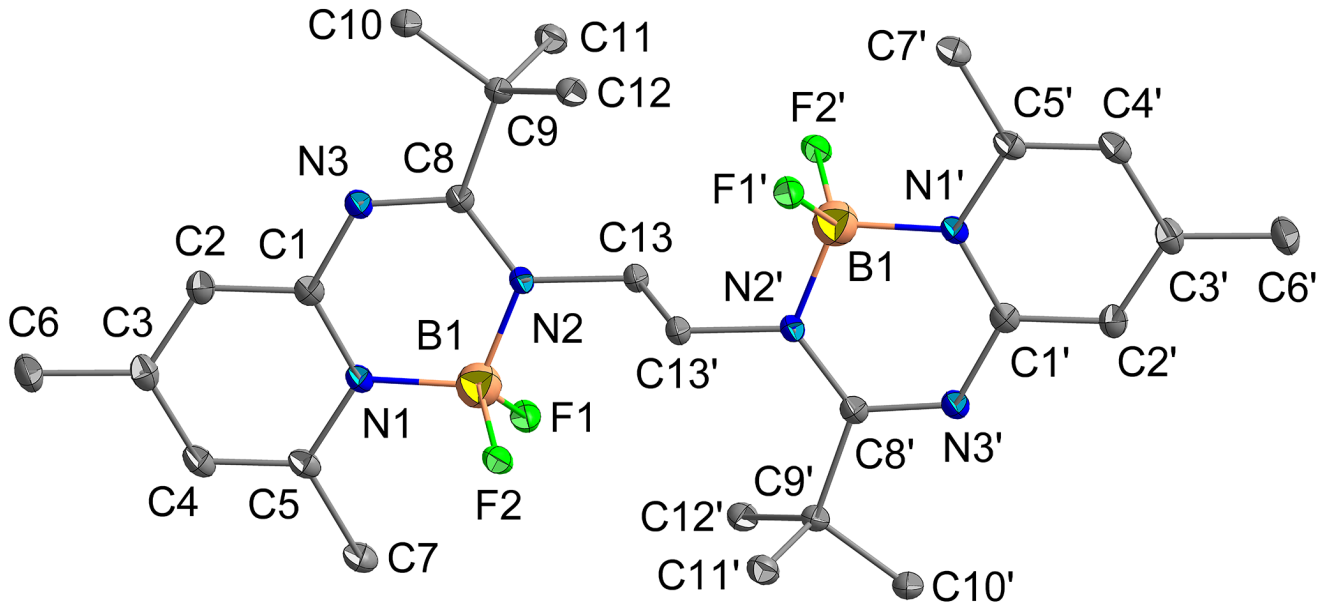

Figure S10. Molecular structure of **4** showing ellipsoids with anisotropic displacement factors of 50% probability. Hydrogen atoms have been omitted for clarity. Selected interatomic distances (Å), bond angles (deg), and torsion angles (deg): C13–C13' 1.546(2), F1–B1 1.3926(15), F2–B1 1.4060(15), N2–C13 1.4864(14), N2–C8 1.3482(15), N1–C1 1.3613(16), N2–B1 1.5382(16), N1–B1 1.5653(16), N3–C8 1.3222(15), N3–C1 1.3582(15), N2–B1–N1 110.28(10), F1–B1–F2 109.12(10), N1–C1–N3 123.00(11), C13–N2–C8 124.93(10), N2–C8–N3 122.40(11), C13–N2–B1 113.01(9), C8–N2–B1 121.99(10), C1–N1–B1 119.24(10), C8–N3–C1 122.74(10), N2–C13–C13' 112.13(12), N2–C13–C13'–N2' 180.0(1),[S12] C13'–C13–N2–C8 104.9(1),[S12] N1–B1–N2–C13 –173.6(1),[S12] F2–B1–N2–C13 67.9(1),[S12] N3–C8–N2–B1 0.8(2),[S12] F1–B1–N2–C13 –52.4(1),[S12] F1–B1–N1–C1 –128.0(1)[S12]. Symmetry operation used to generate equivalent atoms (') $-x + 1, -y, -z + 1$.

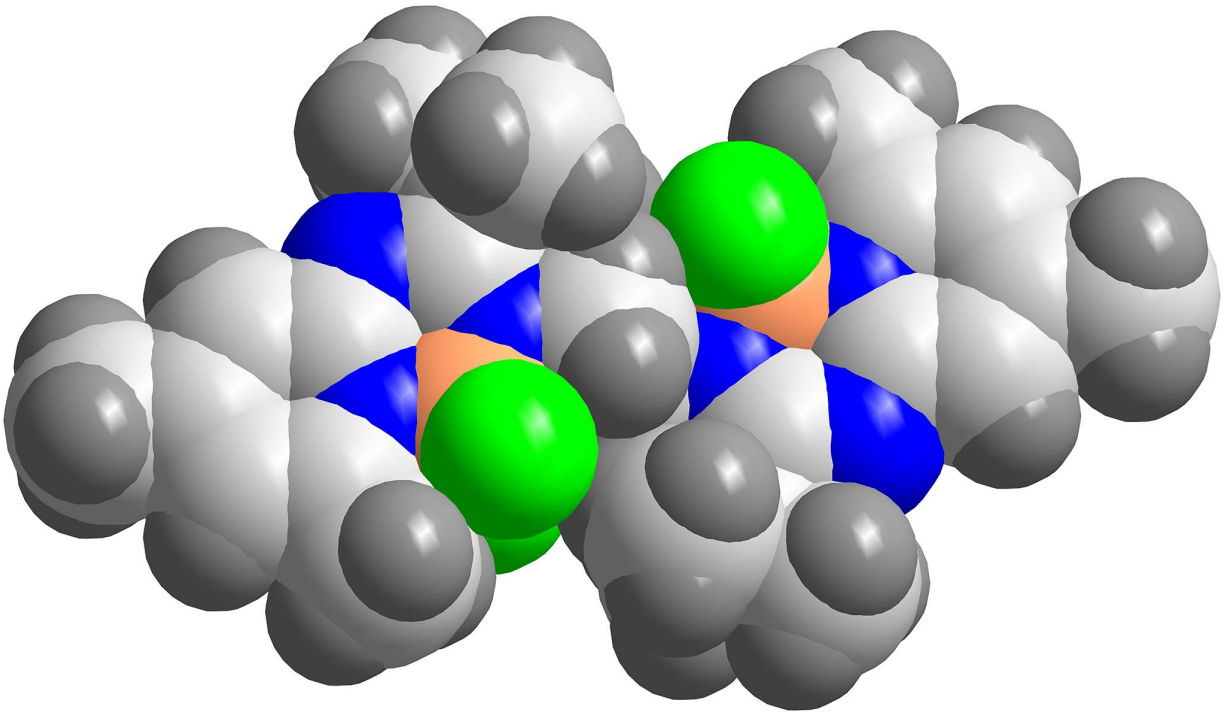

Figure S11. Space filling representation of the molecular structure of **4**.

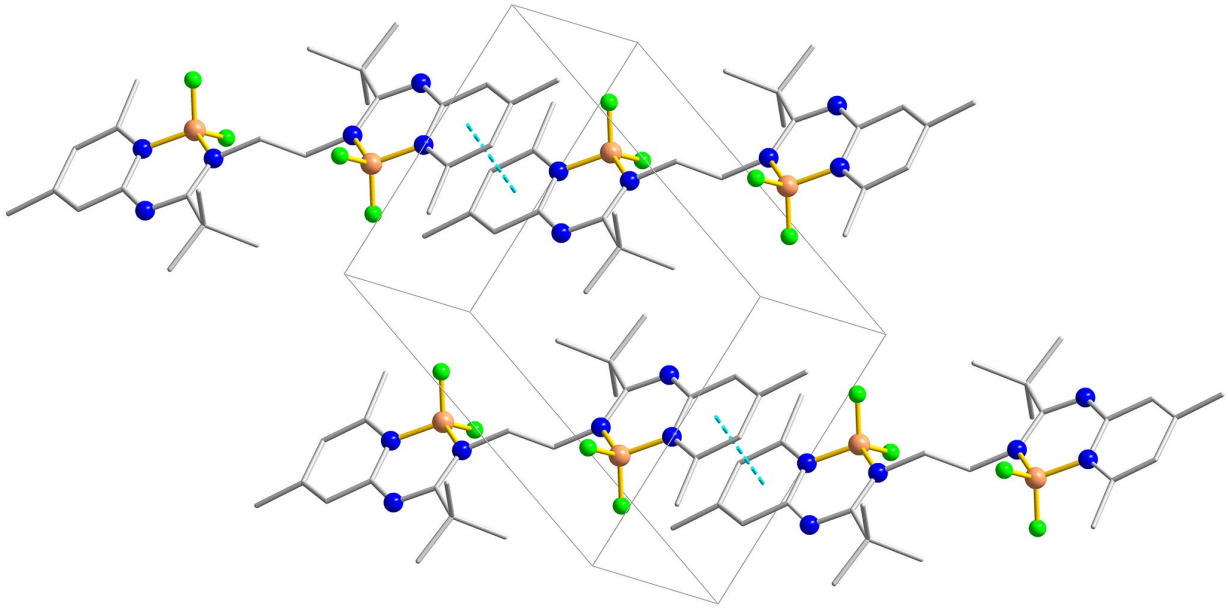

Figure S12. Crystal packing diagram and unit cell of **4**. Hydrogen atoms have been omitted for clarity. Dashed lines indicate the distances between the centroids of the 4,6-dimethylpyridyl-heteroaromatic rings.

Table S1. Crystal data and refinement details for **1**·and **2**.

	1	**2**
Empirical formula	$C_{22}H_{30}B_2F_4N_6$	$C_{24}H_{34}B_2F_4N_6$
M_r	476.14	504.19
Crystal size [mm]	0.051 × 0.122 × 0.237	0.087 × 0.162 × 0.171
Crystal system	monoclinic	monoclinic
Space group	*C*2/*c*	$P2_1/n$
a [Å], *α* [°]	24.988(3), 90	9.5180(7), 90
b [Å], *β* [°]	6.5629(7), 122.402(3)	9.9642(7), 99.837(3)
c [Å], *γ* [°]	16.5307(17), 90	13.3563(10), 90
V [Å^3]	2288.9(4)	1248.08(16)
Z	4	2
$\rho_{calcd.}$ [g cm^{-3}]	1.382	1.342
F(000)	1000	532
μ [mm^{-1}]	0.106	0.102
T_{max}/T_{min}	1.000 / 0.945	1.0000 / 0.9312
hkl range	±30, ±8, ±20	±11, ±12, ±16
θ range [°]	2.92 – 26.00	2.44 – 26.49
Measured refl.	17856	16610
Unique refl. [R_{int}]	2241 [0.0357]	2574 [0.0.283]
Data / restr. / param.	2241 / 0 / 157	2574 / 0 / 167
Goodness-of-fit	1.158	1.123
*R*1 (*I*>2σ(*I*))	0.0386	0.0347
*wR*2 (all data)	0.0955	0.1022
Largest diff. peak/hole [e Å^{-3}]	0.337 / −0.241	0.303 / −0.253

Table S2. Crystal data and refinement details for **3**·and **4**.

	3	**4**
Empirical formula	$C_{24}H_{34}B_2F_4N_6$	$C_{26}H_{38}B_2F_4N_6$
M_r	504.19	532.24
Crystal size [mm]	0.088 × 0.094 × 0.312	0.101 × 0.116 × 0.231
Crystal system	orthorhombic	triclinic
Space group	*Pbca*	$P\,\overline{1}$
a [Å], *α* [°]	6.9879(4), 90	8.2300(7), 107.216(3)
b [Å], *β* [°]	16.3090(12), 90	8.6335(7), 105.836(3)
c [Å], *γ* [°]	21.8166(14), 90	10.4627(8), 93.887(3)
V [Å^3]	2486.3(3)	674.17(10)
Z	4	1
$\rho_{calcd.}$ [g cm^{-3}]	1.347	1.311
F(000)	1064	282
μ [mm^{-1}]	0.102	0.098
T_{max}/T_{min}	1.000 / 0.9097	1.0000 / 0.9612
hkl range	±8, −20 +18, ±26	±10, ±10, ±13
θ range [°]	2.67 – 26.00	2.14 – 26.5
Measured refl.	14845	15035
Unique refl. [R_{int}]	2441 [0.0387]	2787 [0.0396]
Data / restr. / param.	2441 / 0 / 167	2787 / 0 / 177
Goodness-of-fit	1.076	1.086
*R*1 (*I*>2σ(*I*))	0.0392	0.0359
*wR*2 (all data)	0.0883	0.0975
Largest diff. peak/hole [e Å^{-3}]	0.245 / −0.203	0.311 / −0.203

Table S3: Key crystallographic interatomic distances and angles of **1**–**4**.

	1	**2**	**3**	**4**
	bond/angle [Å] / [°]			
B–F	1.3911(19) 1.4040(19)	1.3876(15) 1.4013(16)	1.388(2) 1.404(2)	1.3926(15) 1.4060(15)
B–N(CH_2)	1.533(2)	1.5378(16)	1.535(2)	1.5382(16)
B–N_{Py}	1.546(2)	1.5713(16)	1.552(2)	1.5653(16)
CH_2–CH_2	1.538(3)	1.542(2)	1.541(18)	1.546(2)
CH_2–N	1.4834(19)	1.4867(15)	1.4855(18)	1.4864(14)
(^{t}Bu)C–N(CH_2)	1.3455(19)	1.3451(15)	1.3494(18)	1.3482(15)
(^{t}Bu)C=N(C_{Py})	1.329(2)	1.3246(16)	1.3263(19)	1.3222(15)
(^{t}Bu)CN–C_{Py}	1.352(2)	1.3545(16)	1.3560(19)	1.3582(15)
C_{Py}–N_{Ar}	1.3587(19)	1.3671(15)	1.3567(19)	1.3613(16)
F–B–F	108.50(13)	110.04(10)	108.73(13)	109.12(10)
N–B–N	109.56(12)	110.02(10)	109.07(12)	110.28(10)
CH_2–N–C(^{t}Bu)	124.77(12)	124.41(10)	124.61(12)	124.93(10)
N–C(^{t}Bu)=N	123.16(13)	122.35(11)	122.69(14)	122.40(11)
(^{t}Bu)C=N–C_{Py}	121.55(13)	122.48(10)	121.62(13)	122.74(10)
N–C_{Py}–N_{Ar}	122.52(14)	123.17(11)	122.47(13)	123.00(11)
B–F···π_{NCNCN}[S12]	3.235(1)[S13] 3.374(1)[S14]	-	3.309(1)[S13] 3.367(1)[S14]	-
C–H···π_{NCNCN}[S12]	-	2.722[S15] 2.7456(2)[S16]	-	-
π_{Ar}···π_{Ar}[S12]	-	-	-	3.6630(3)[S17]

Table S4. Δ_{CN} parameter[S18] of **1**–**4**.

1	**2**	**3**	**4**
d(C–N) – d(C=N) [Å]			
0.017	0.021	0.023	0.026

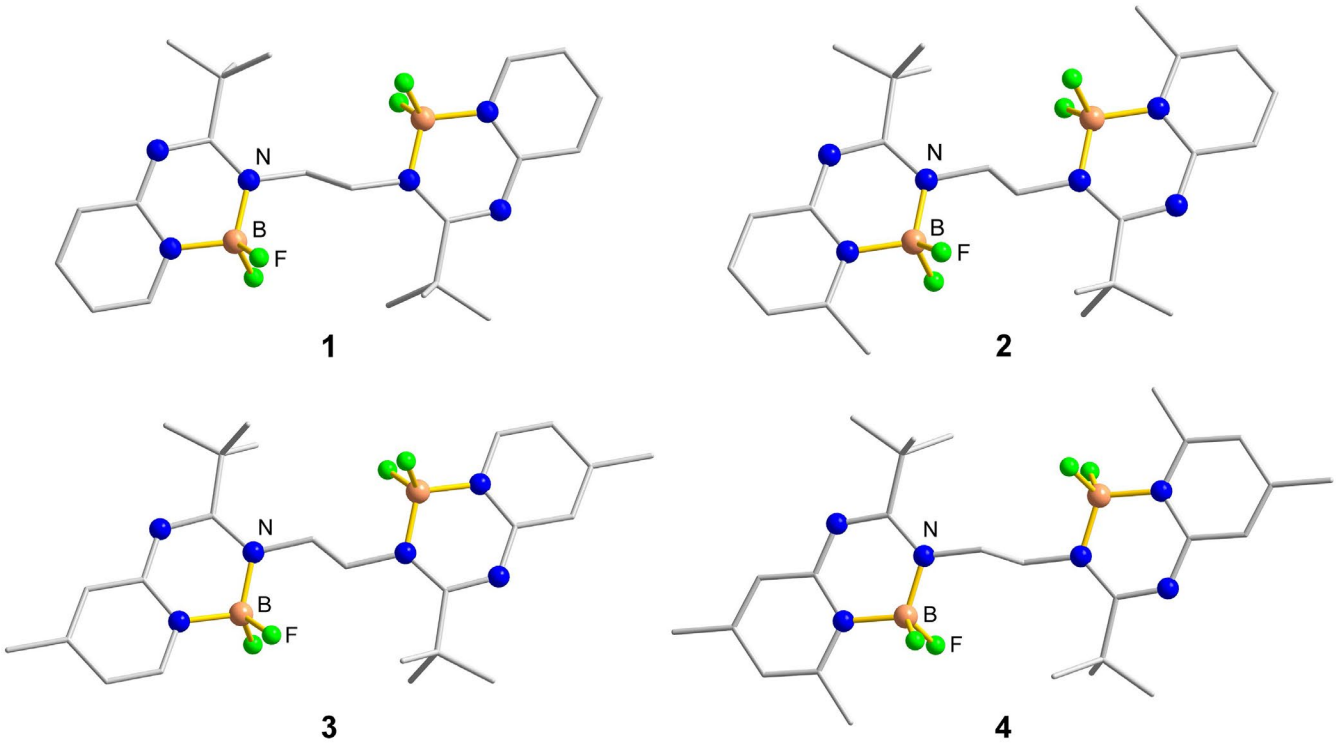

Figure S13. Computational geometry-optimized structures of **1**–**4**.

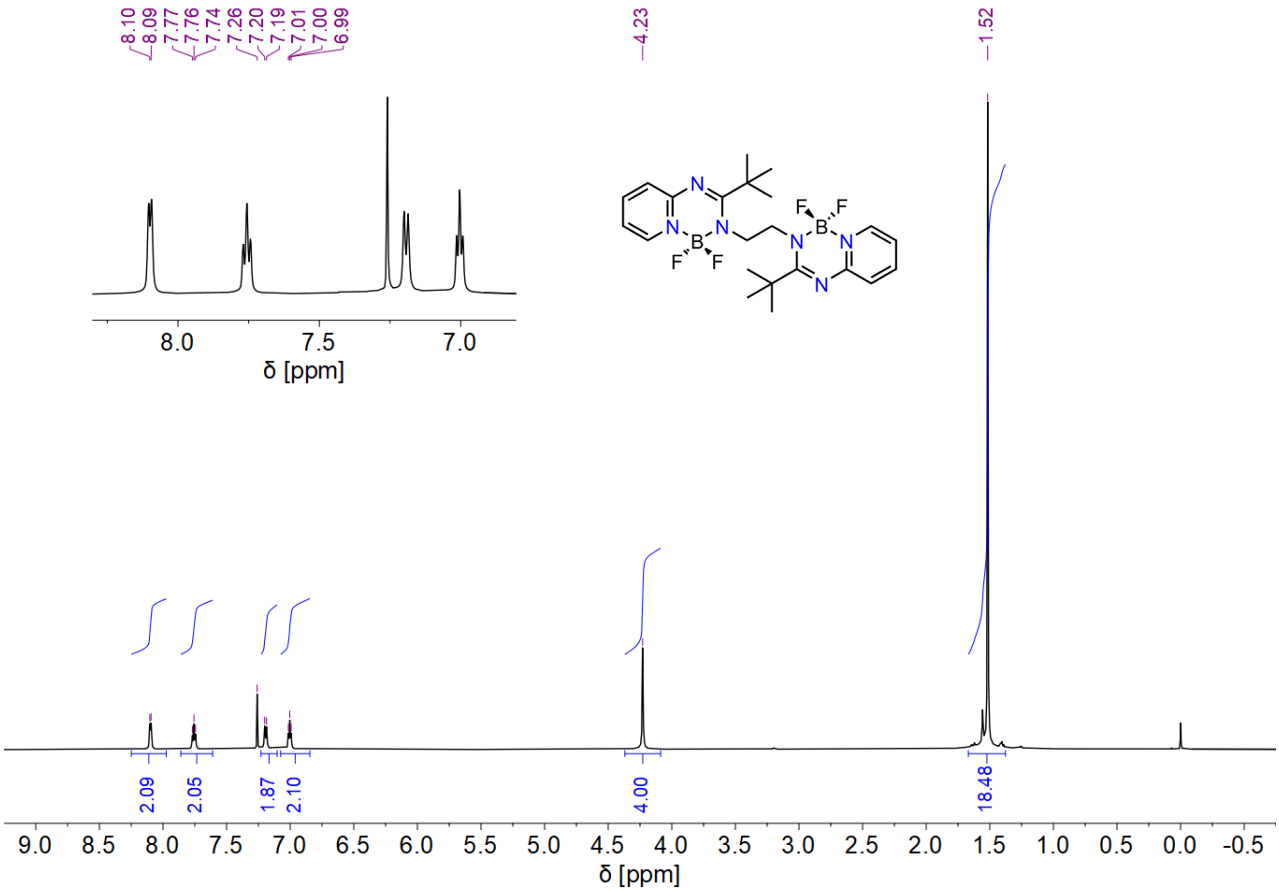

Figure S14. ^{1}H NMR spectrum of **1** ($CDCl_3$, 600.2 MHz).

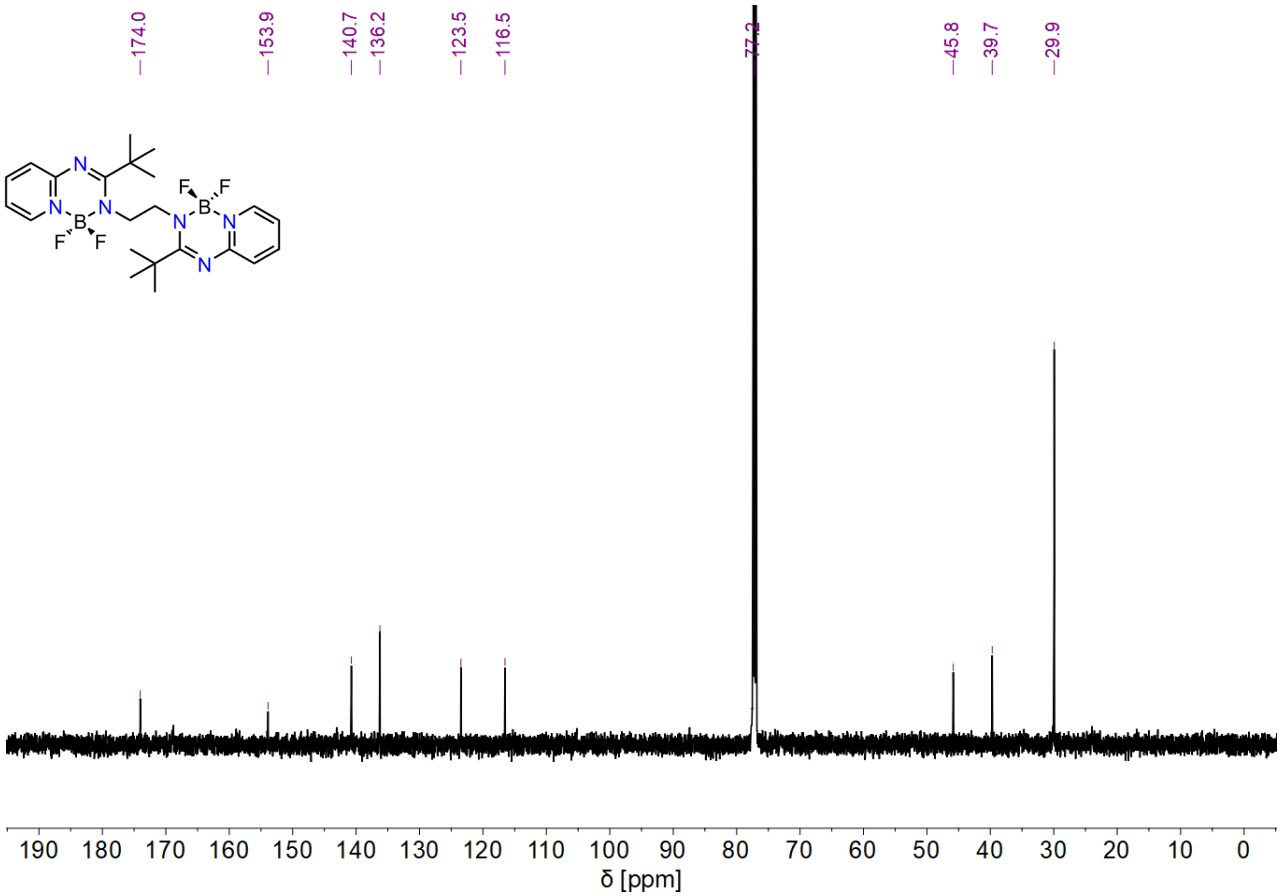

Figure S15. $^{13}C\{^{1}H\}$ NMR spectrum of **1** ($CDCl_3$, 150.9 MHz).

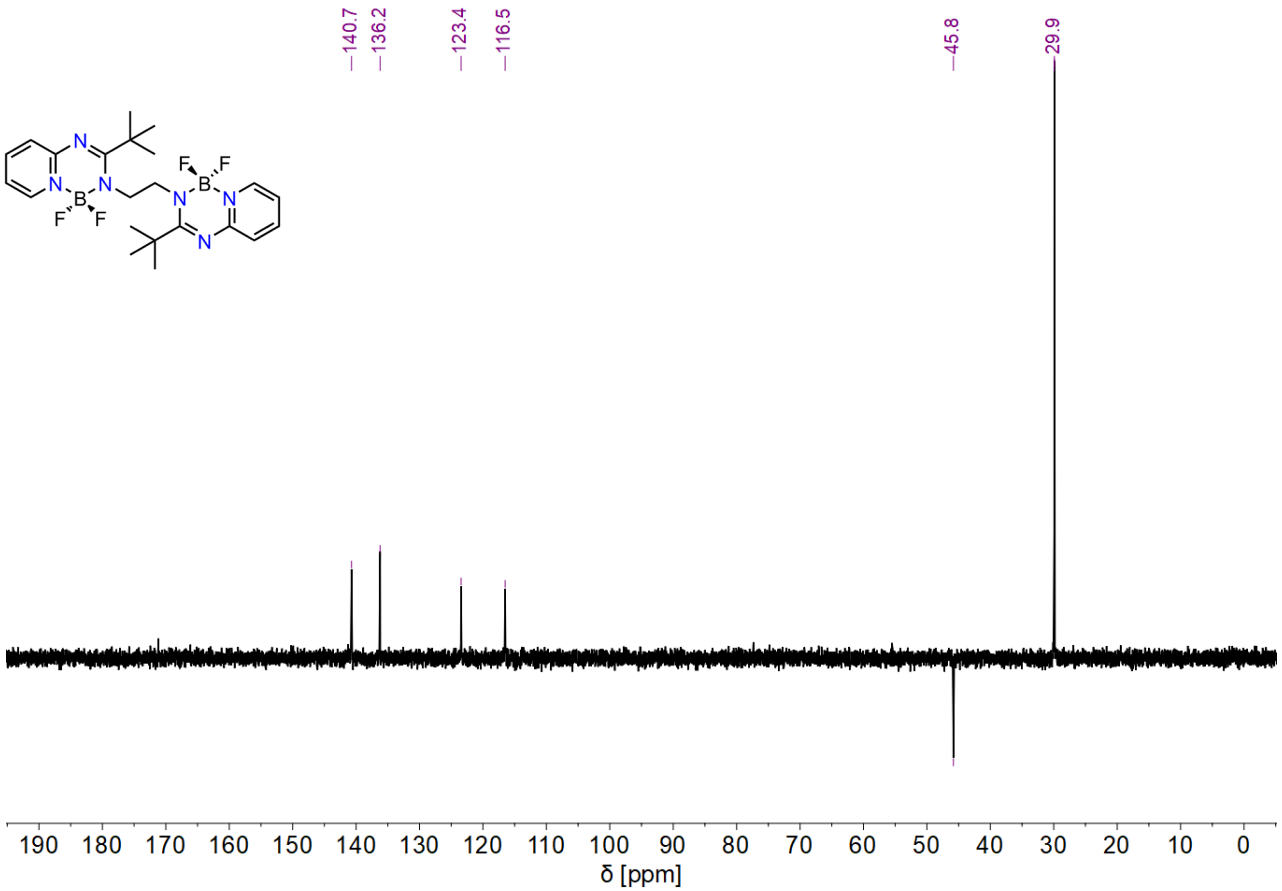

Figure S16. DEPT 135 NMR spectrum of **1** ($CDCl_3$, 150.9 MHz).

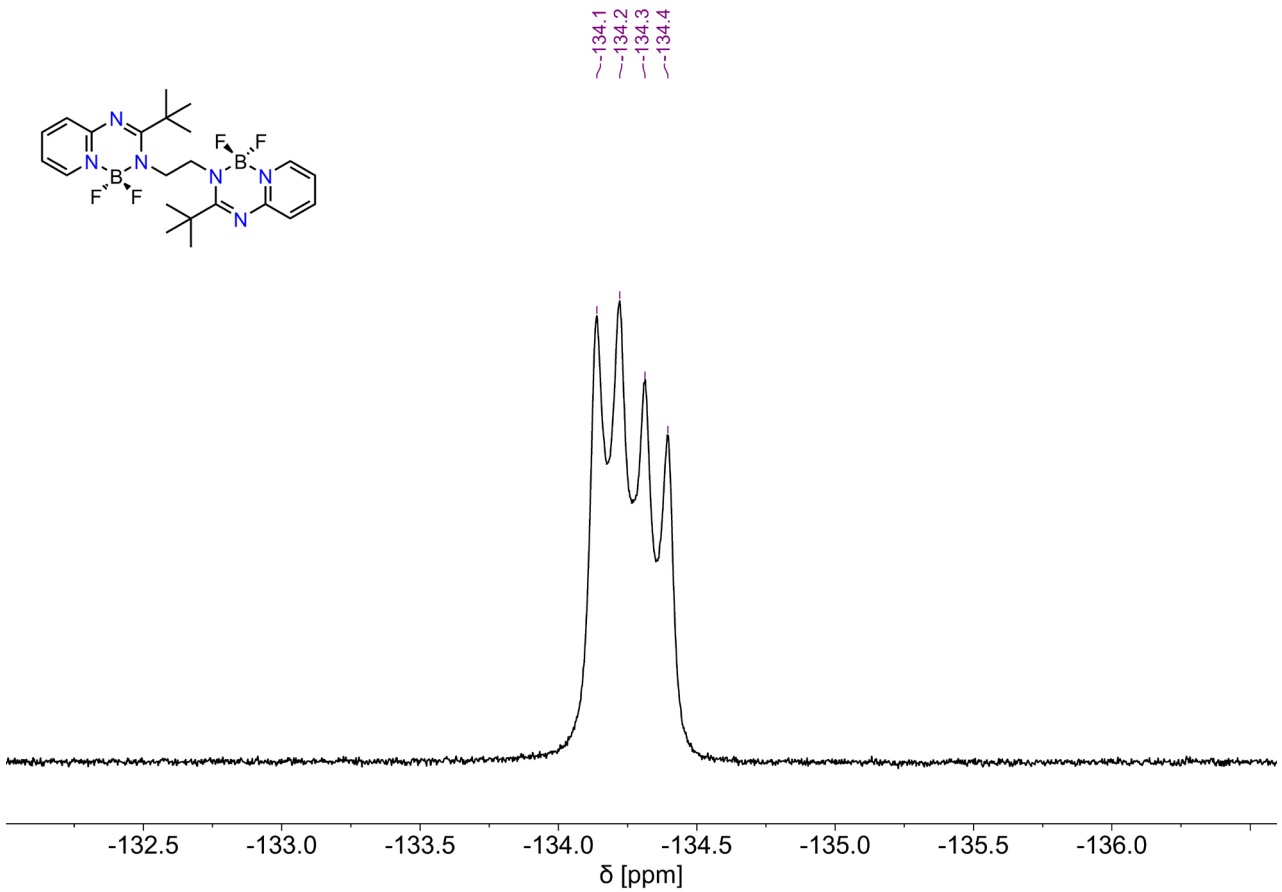

Figure S17. ^{19}F NMR spectrum of **1** ($CDCl_3$, 376.5 MHz).

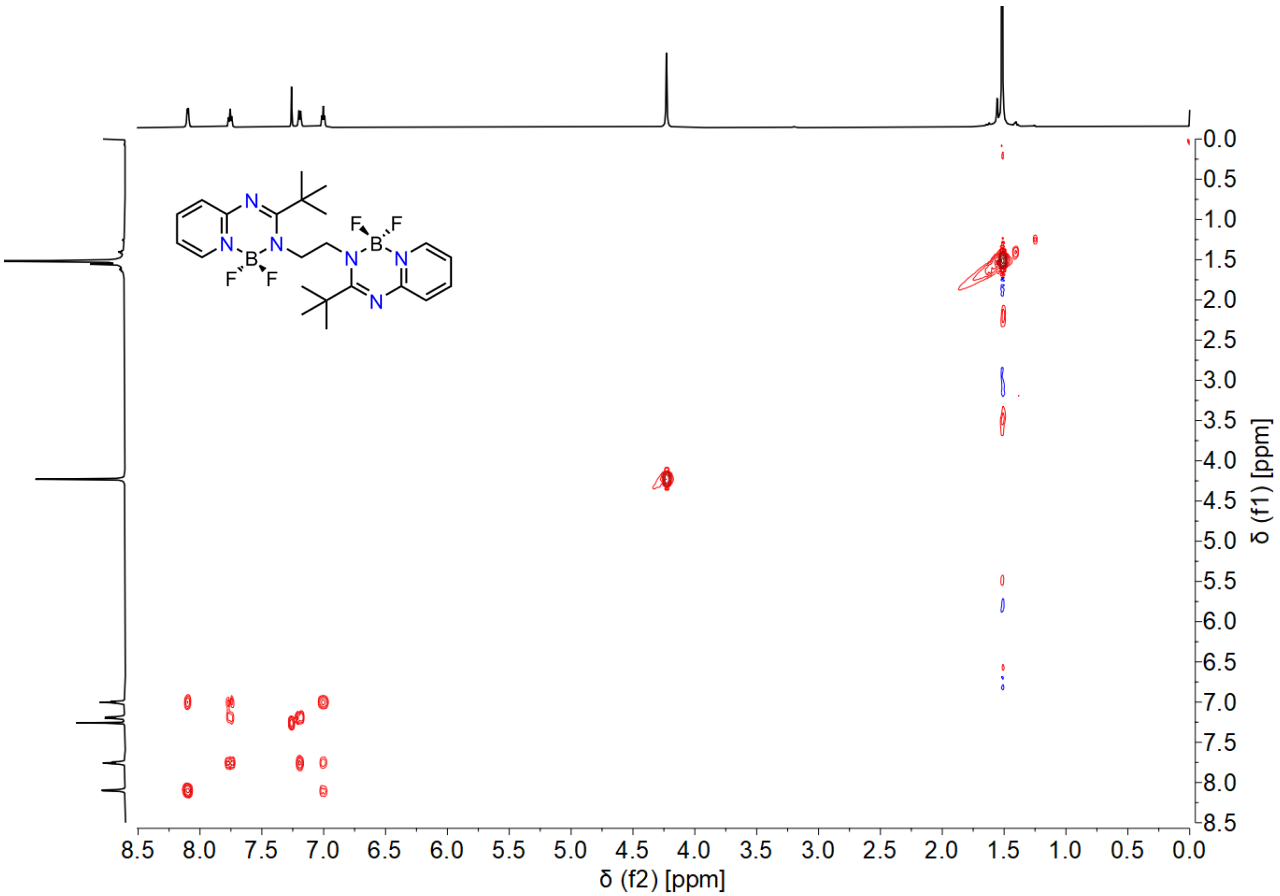

Figure S18. (^{1}H, ^{1}H)-COSY NMR spectrum of **1** ($CDCl_3$, 600.2 MHz).

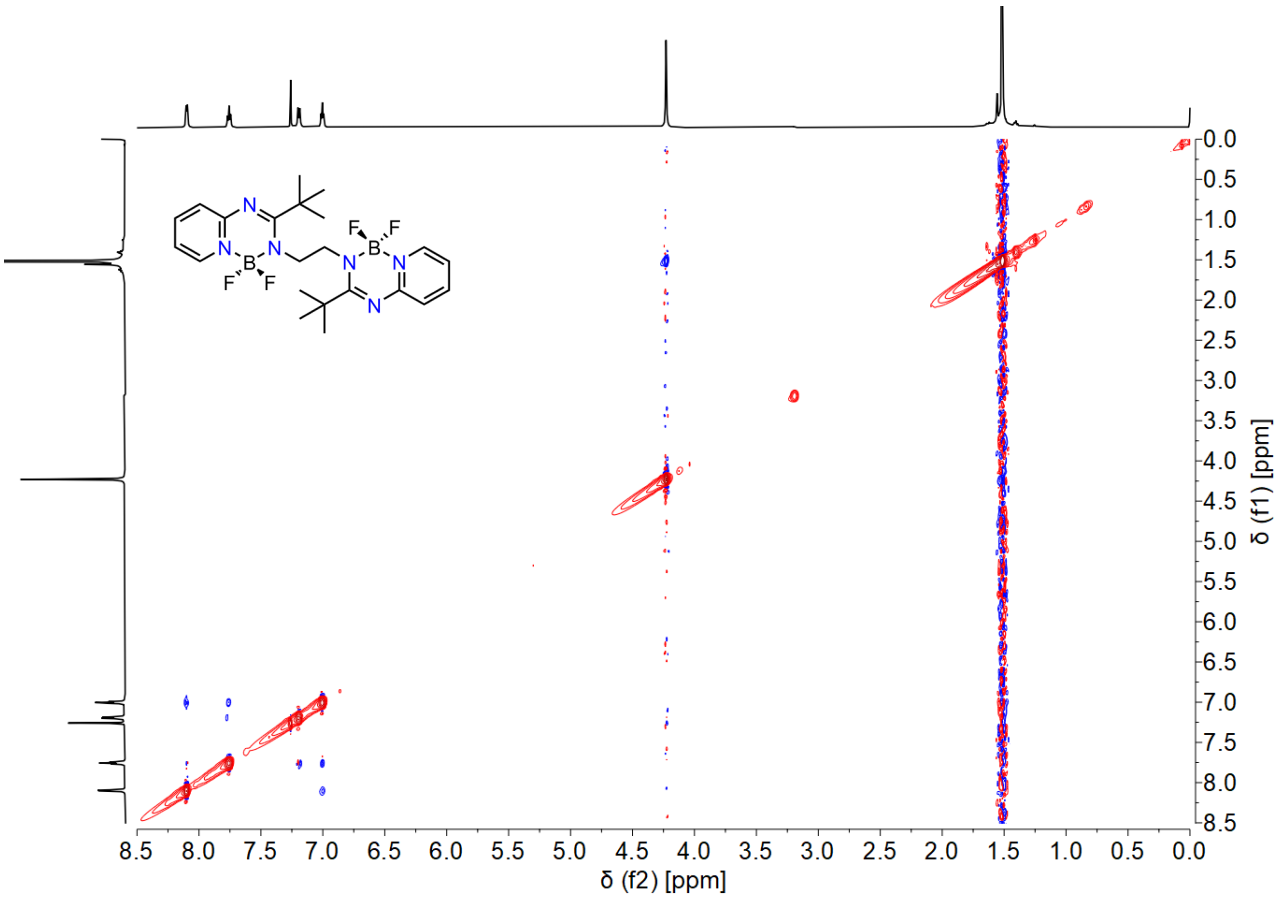

Figure S19. (^{1}H, ^{1}H)-NOESY NMR spectrum of **1** ($CDCl_3$, 600.2 MHz).

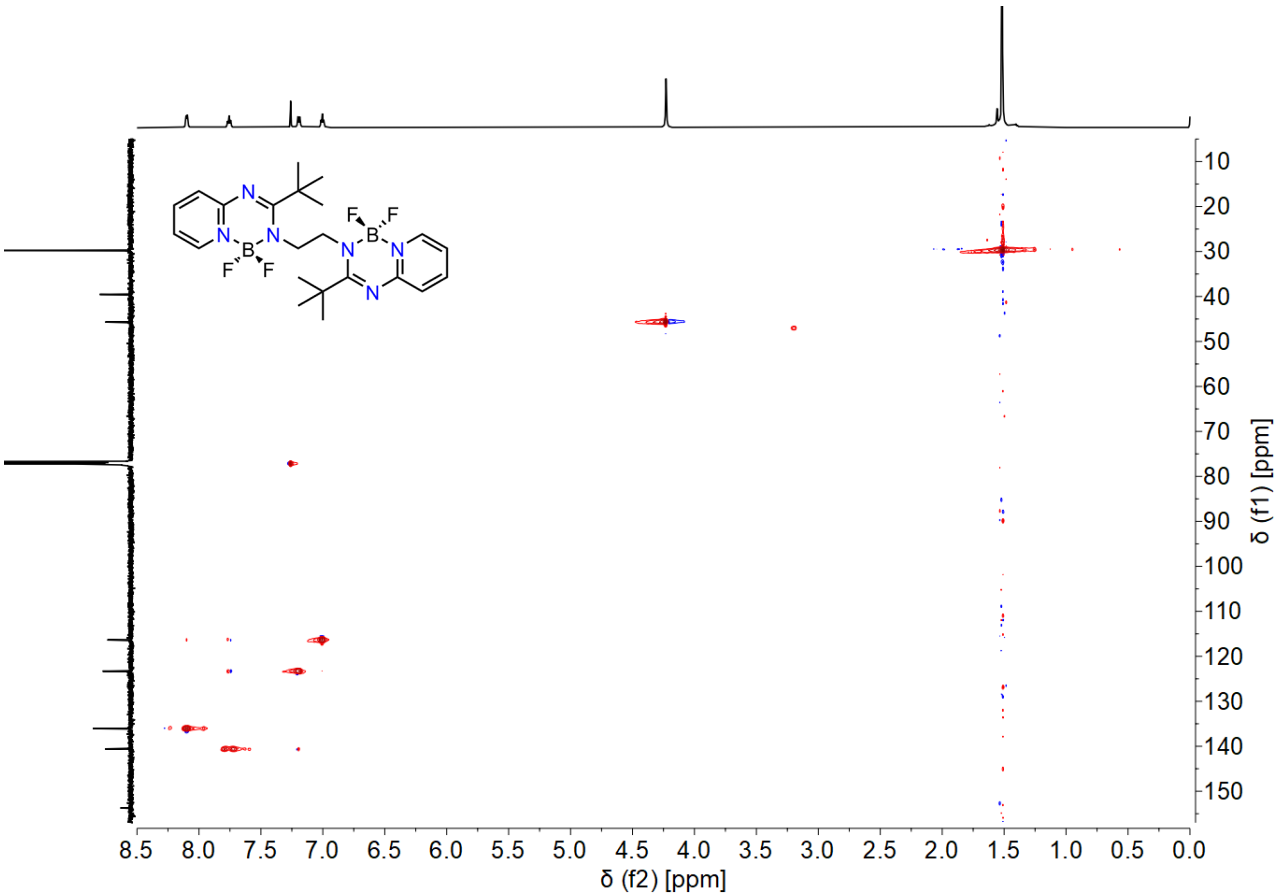

Figure S20. (^{1}H, ^{13}C)-HSQC NMR spectrum of **1** ($CDCl_3$, 600.2, 150.9 MHz).

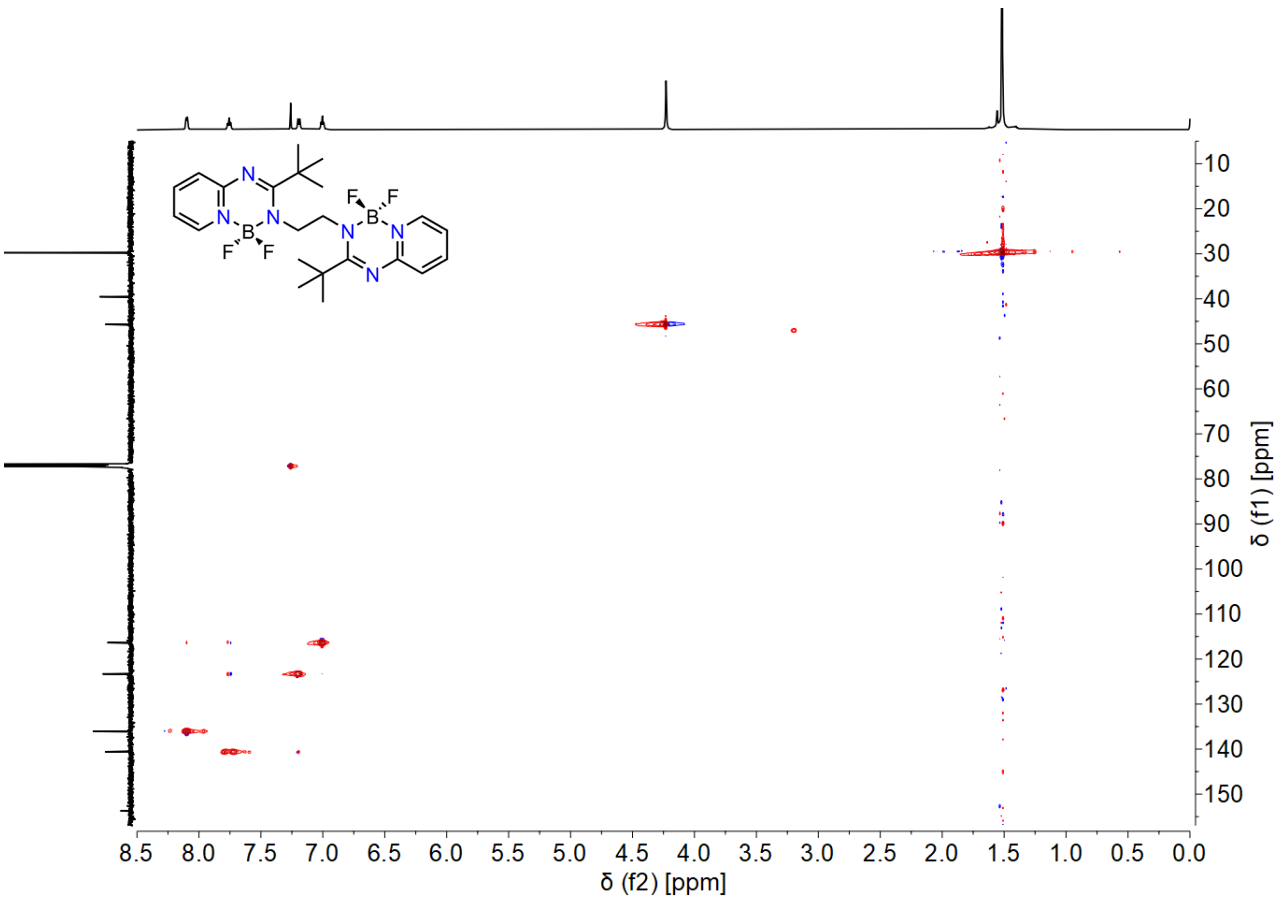

Figure S21. (^{1}H, ^{13}C)-HMBC NMR spectrum of **1** ($CDCl_3$, 600.2, 150.9 MHz).

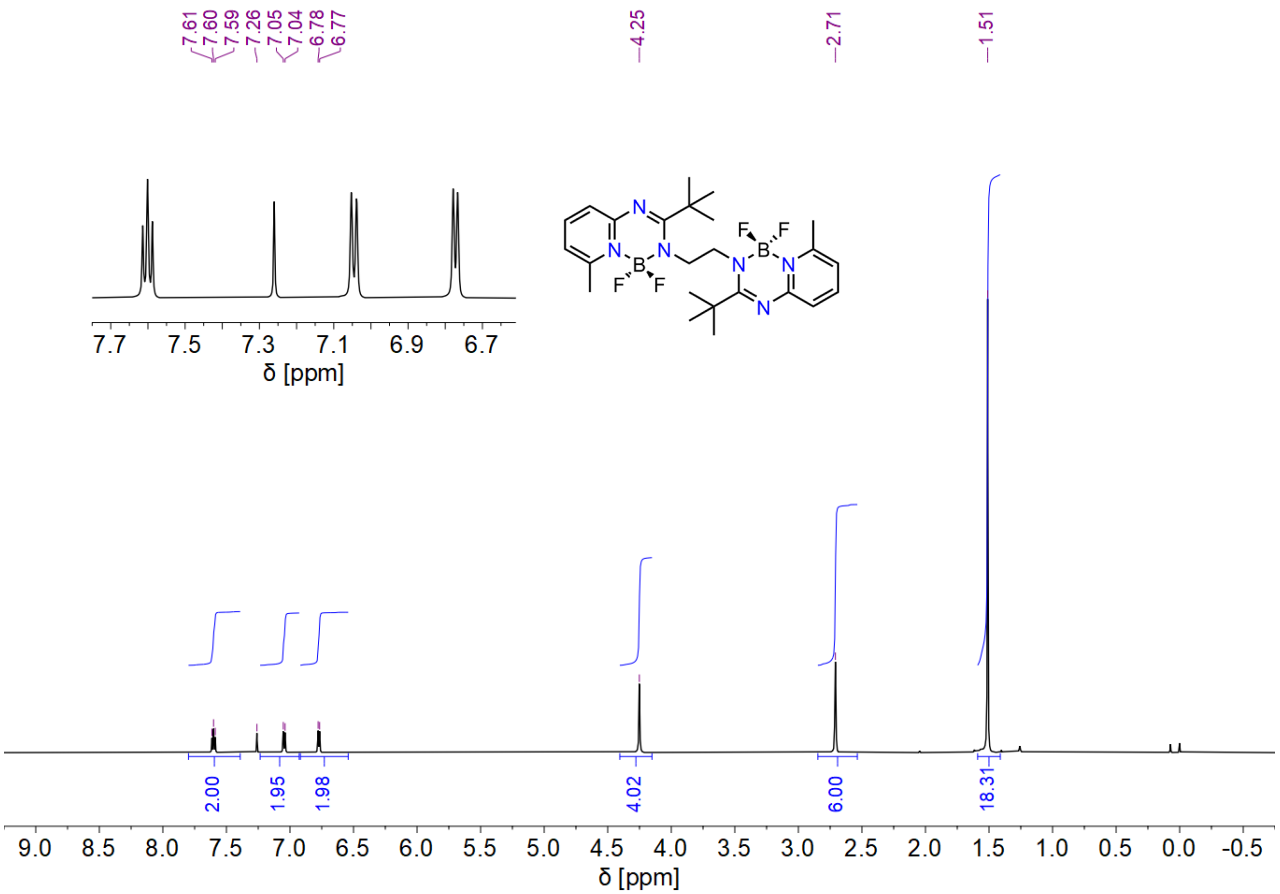

Figure S22. ^{1}H NMR spectrum of **2** ($CDCl_3$, 600.2 MHz).

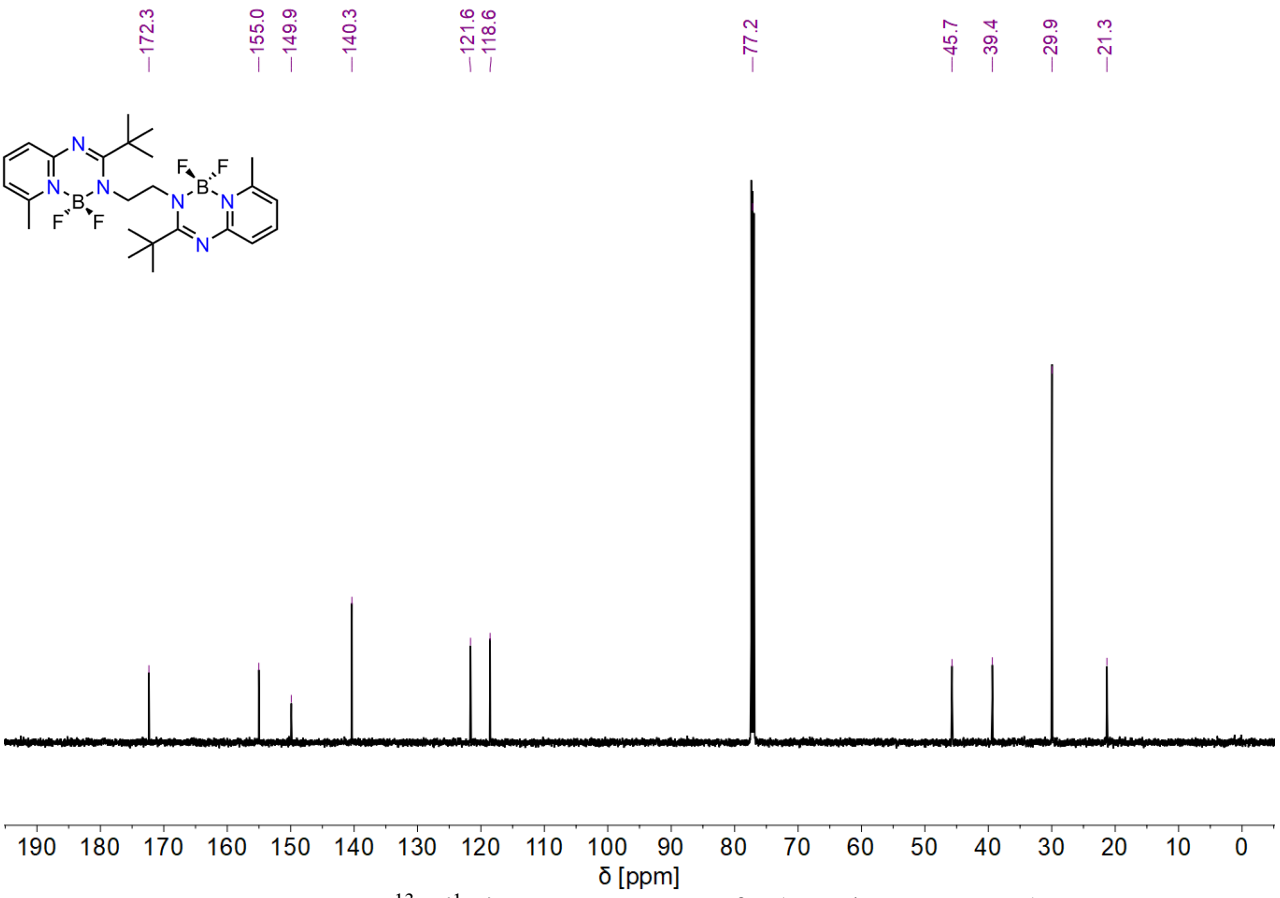

Figure S23. $^{13}C\{^{1}H\}$ NMR spectrum of **2** ($CDCl_3$, 150.9 MHz).

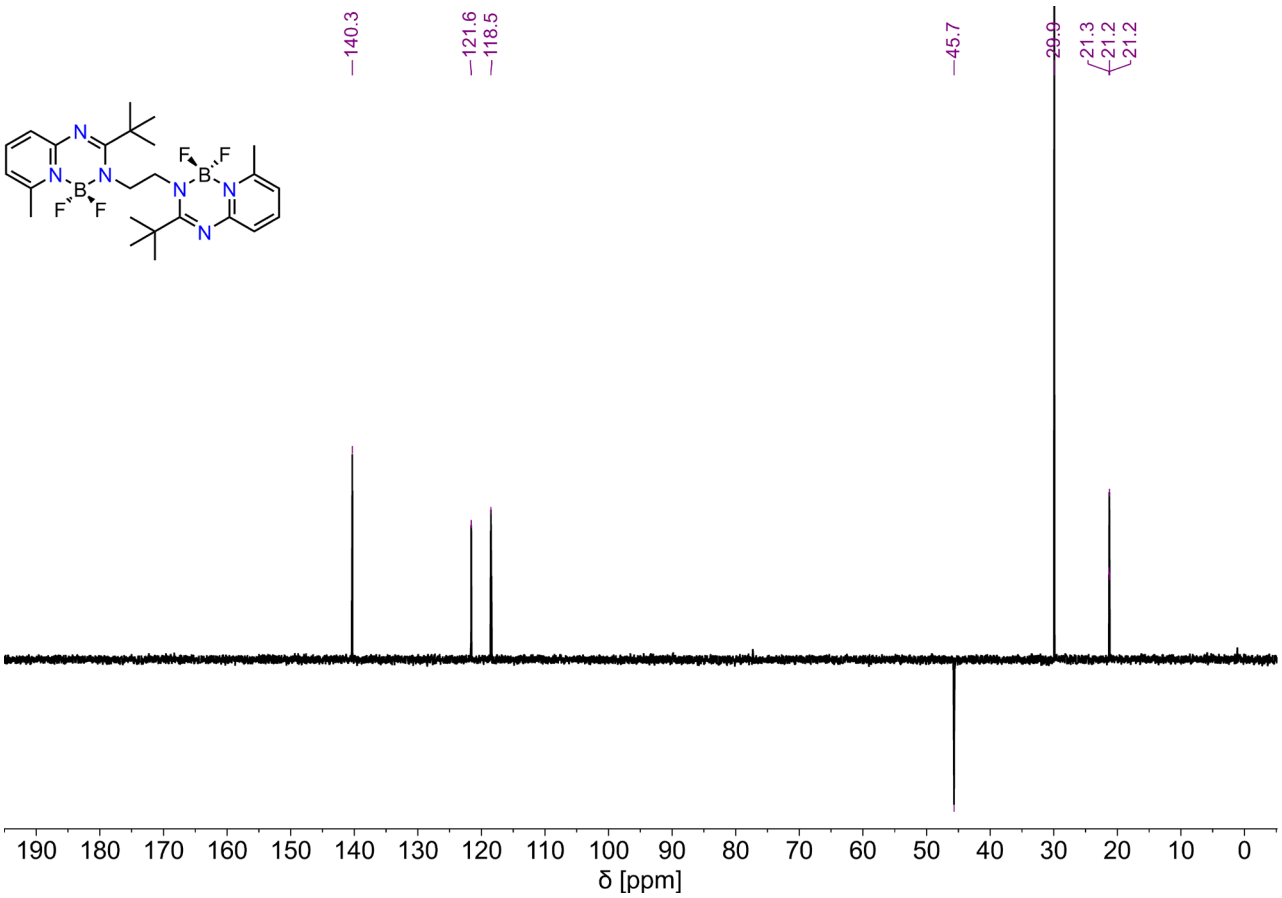

Figure S24. DEPT 135 NMR spectrum of **2** ($CDCl_3$, 150.9 MHz).

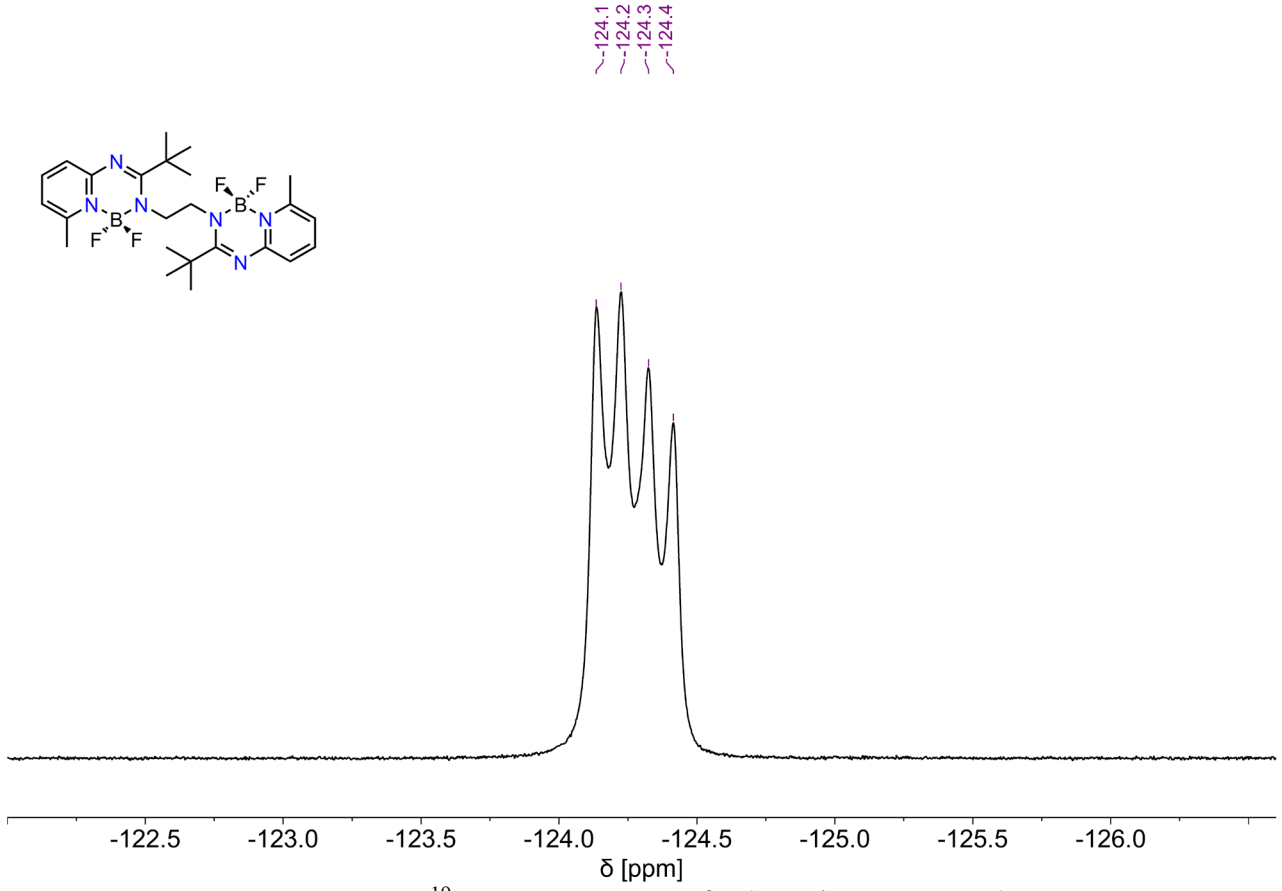

Figure S25. ^{19}F NMR spectrum of **2** ($CDCl_3$, 376.5 MHz).

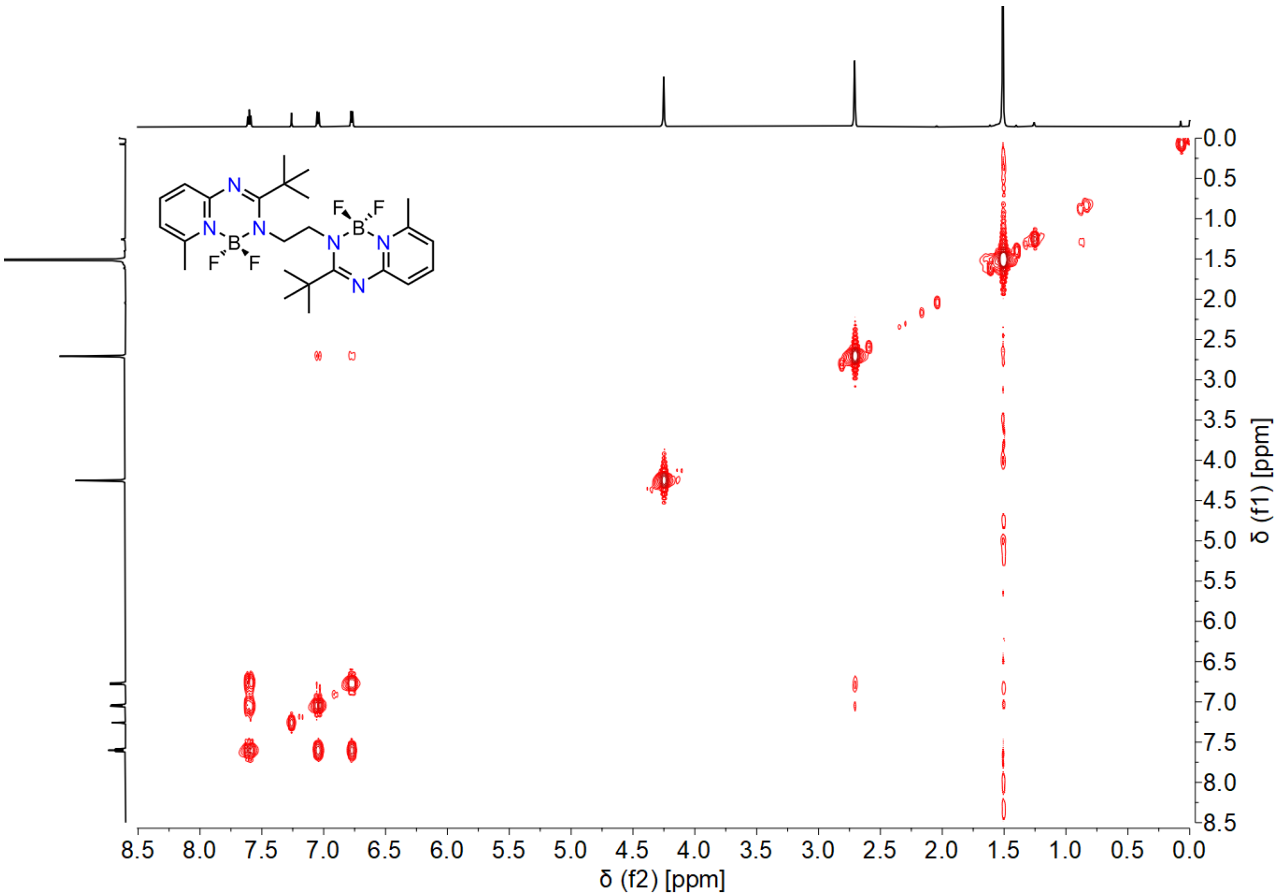

Figure S26. (^{1}H, ^{1}H)-COSY NMR spectrum of **2** ($CDCl_3$, 600.2 MHz).

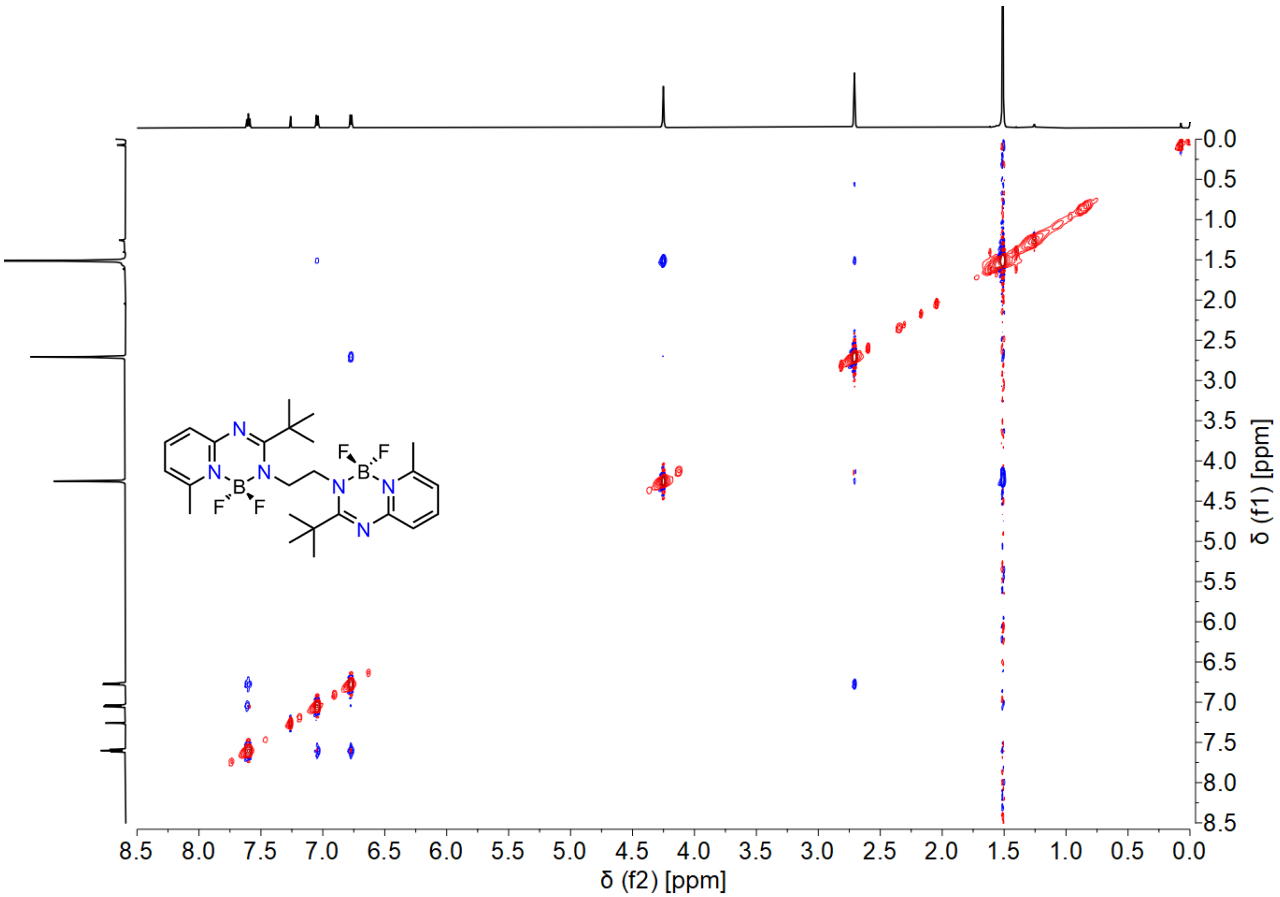

Figure S27. (^{1}H, ^{1}H)-NOESY NMR spectrum of **2** ($CDCl_3$, 600.2 MHz).

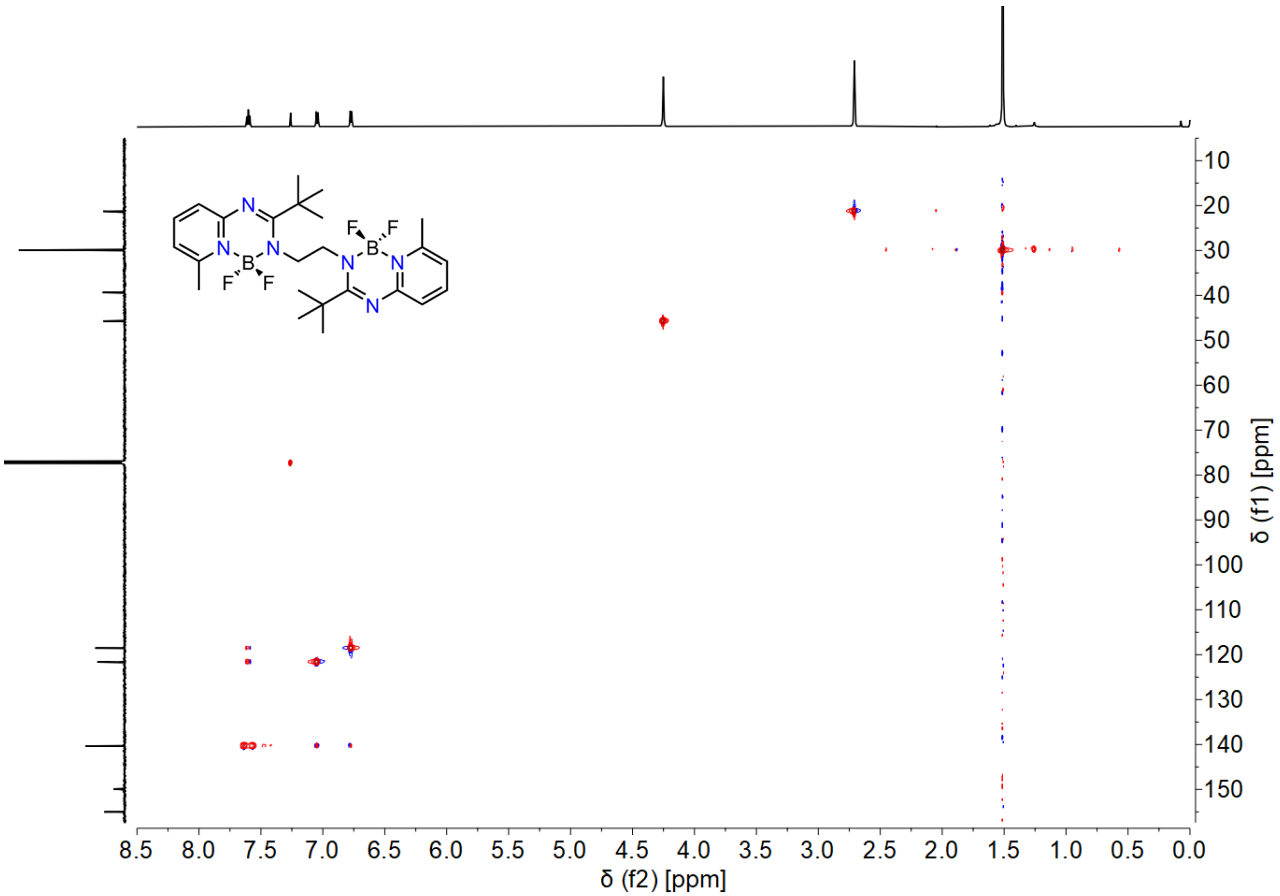

Figure S28. (^{1}H, ^{13}C)-HSQC NMR spectrum of **2** ($CDCl_3$, 600.2, 150.9 MHz).

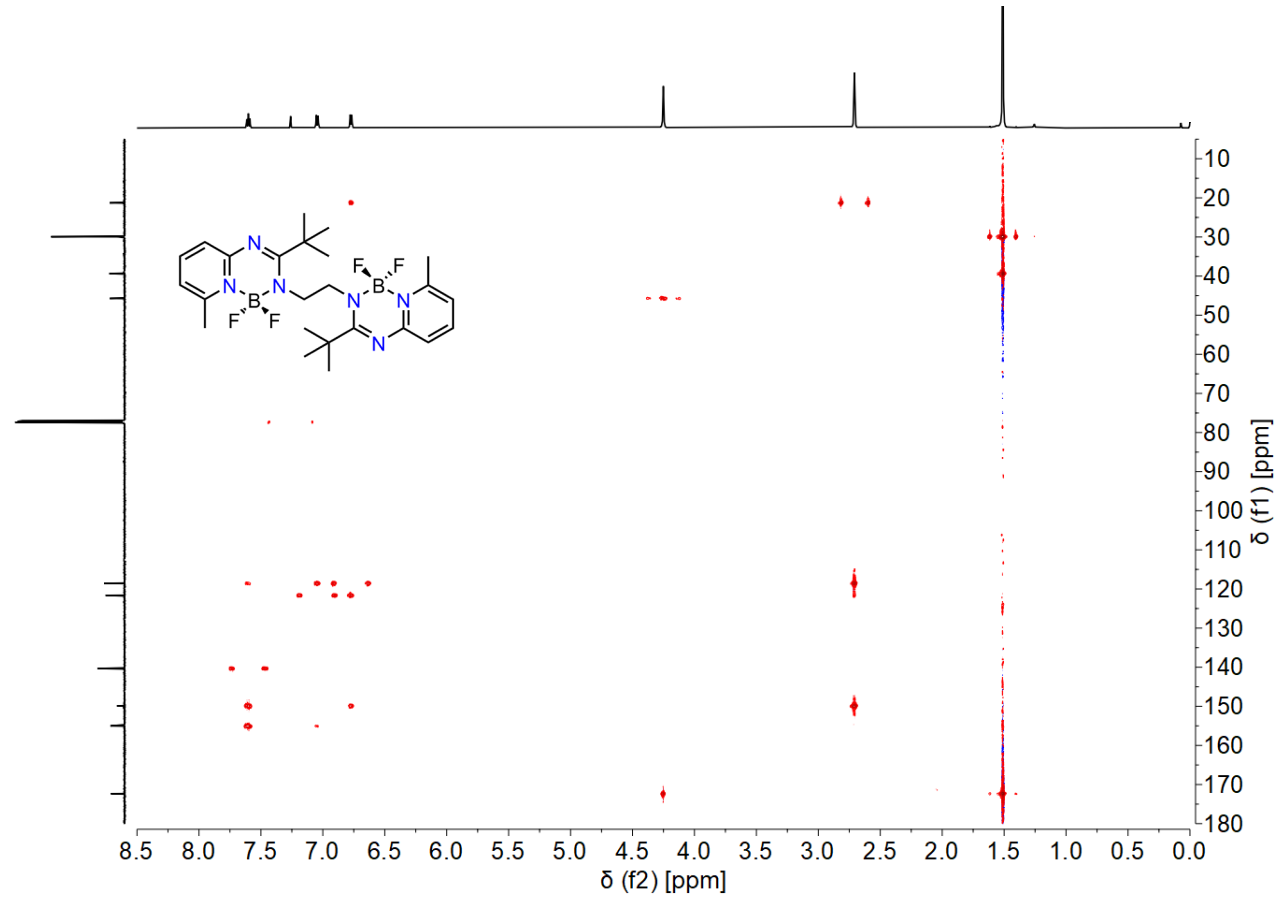

Figure S29. (^{1}H, ^{13}C)-HMBC NMR spectrum of **2** ($CDCl_3$, 600.2, 150.9 MHz).

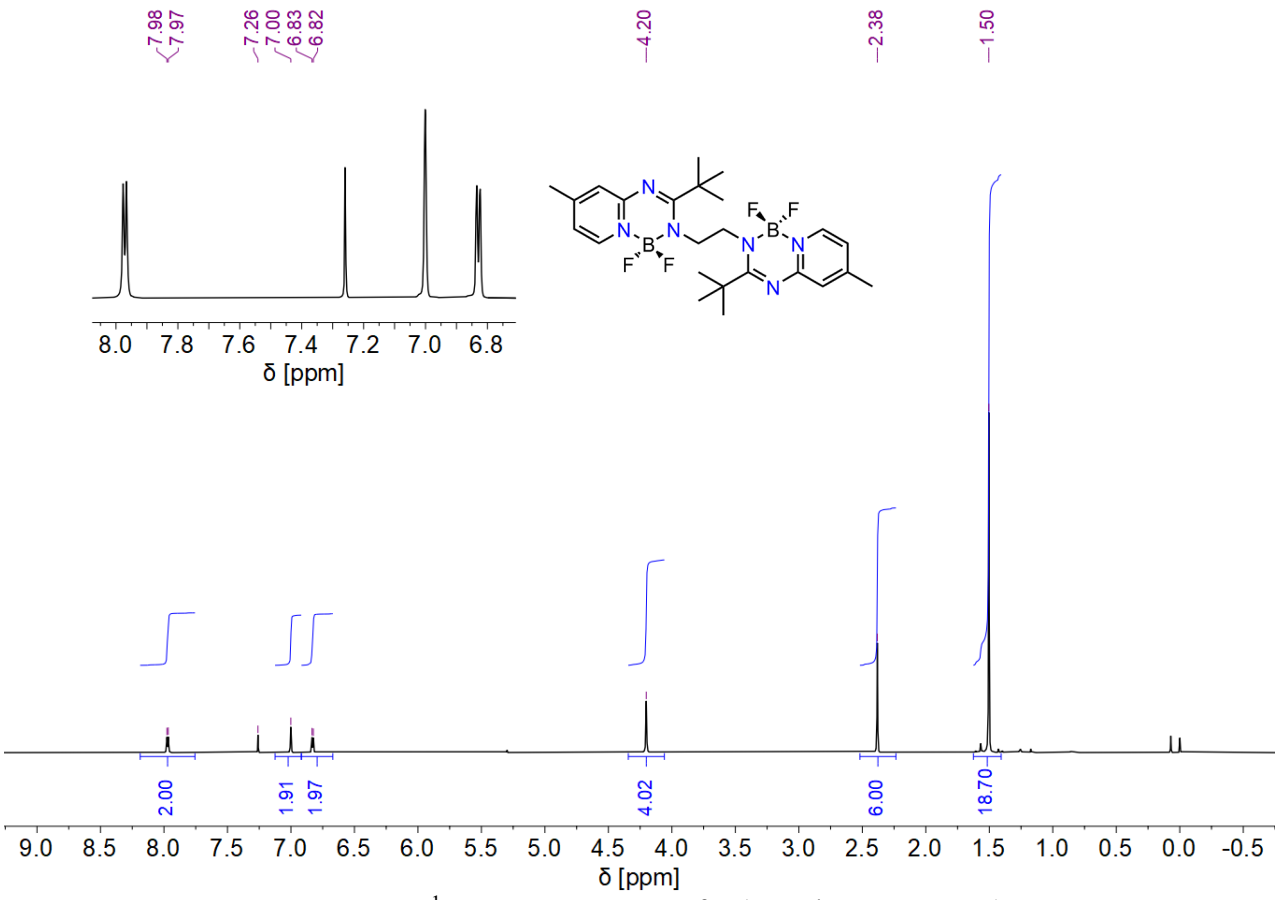

Figure S30. ^{1}H NMR spectrum of **3** ($CDCl_3$, 600.2 MHz).

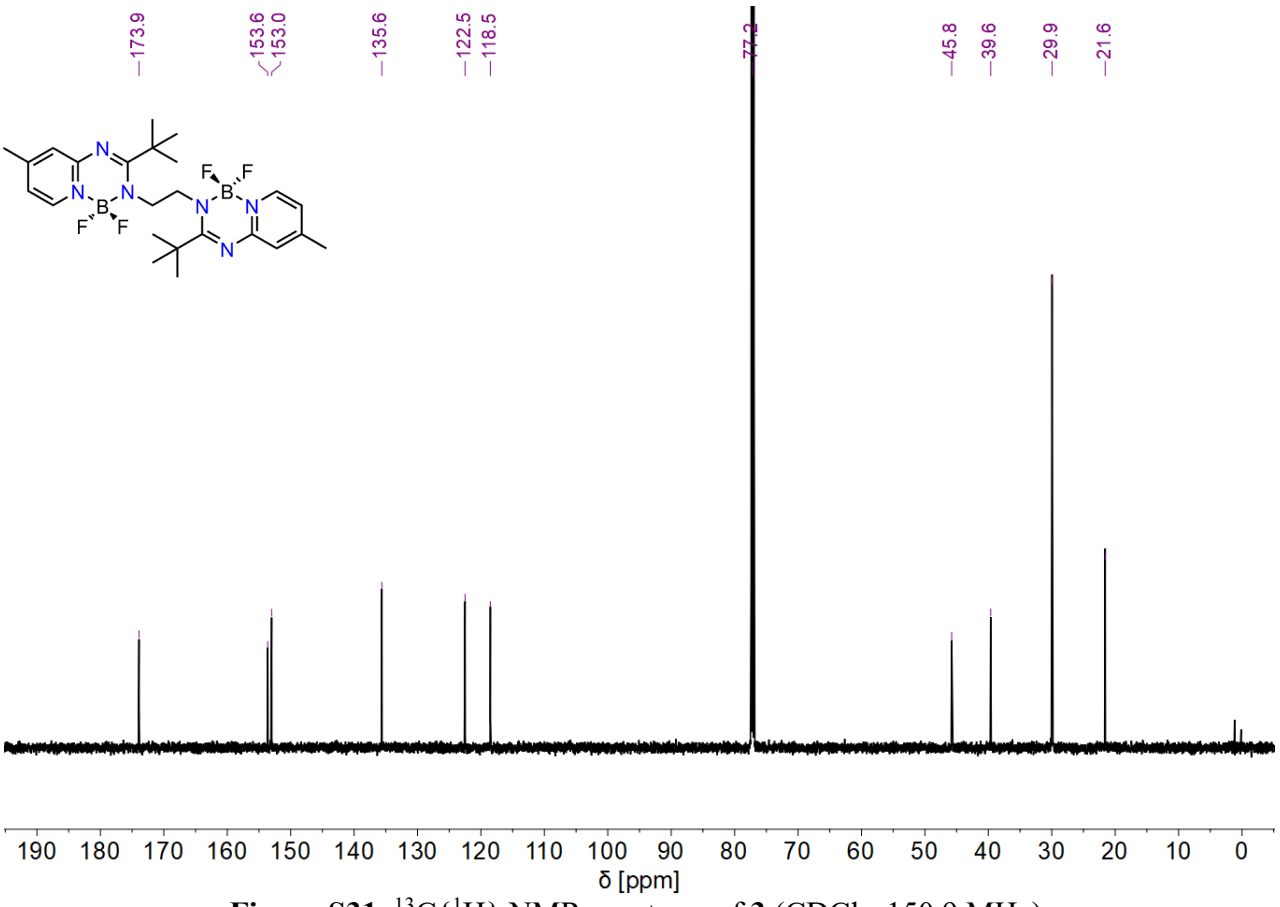

Figure S31. $^{13}C\{^{1}H\}$ NMR spectrum of **3** ($CDCl_3$, 150.9 MHz).

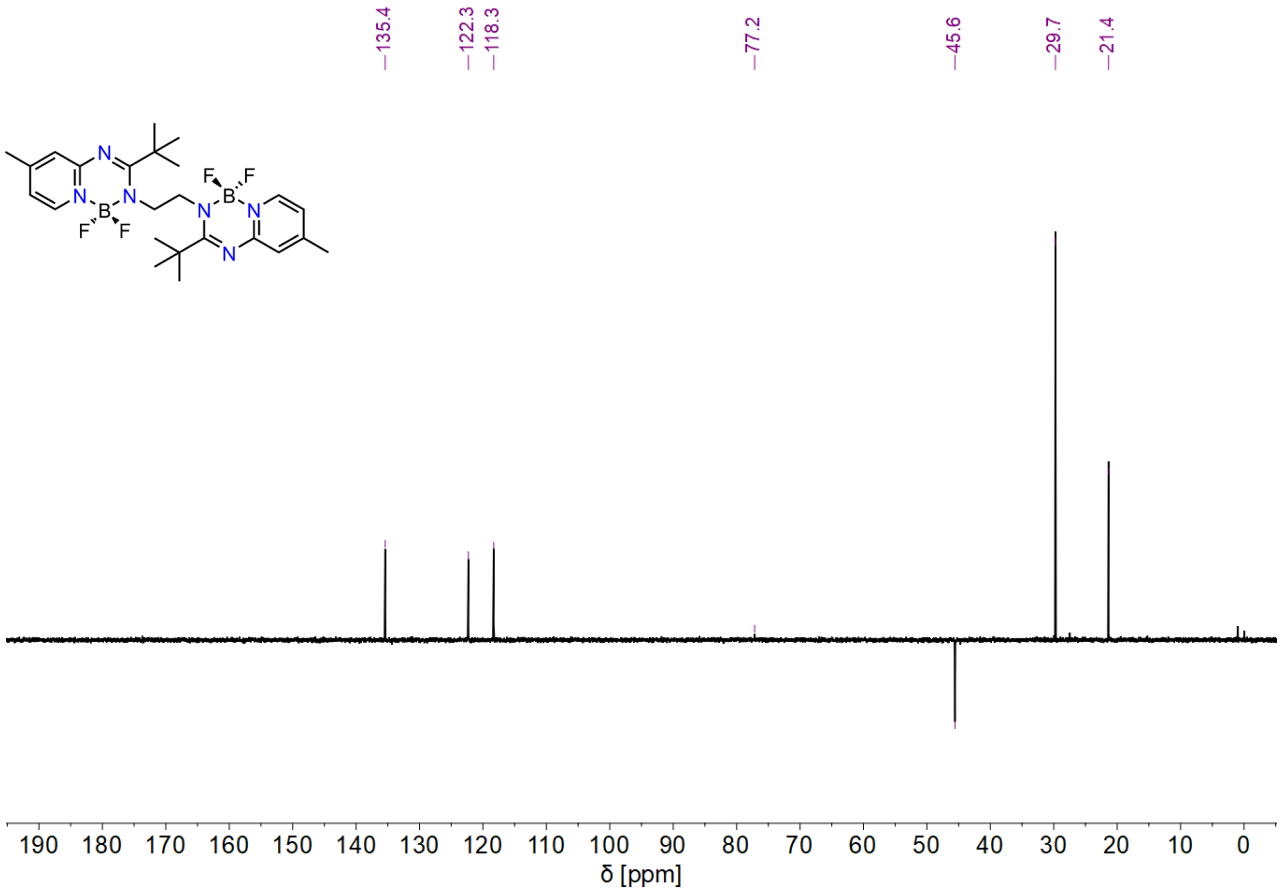

Figure S32. DEPT 135 NMR spectrum of **3** ($CDCl_3$, 150.9 MHz).

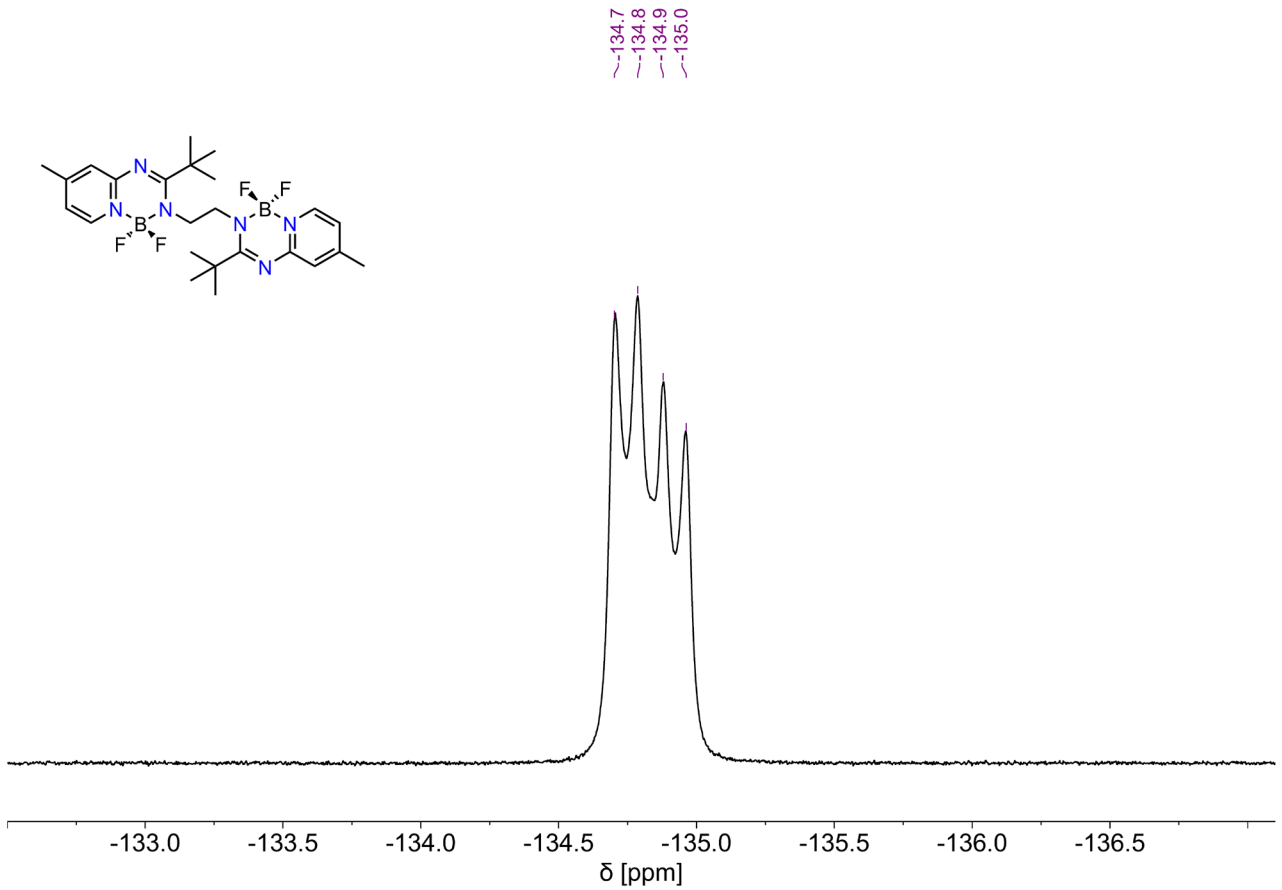

Figure S33. ^{19}F NMR spectrum of **3** ($CDCl_3$, 376.5 MHz).

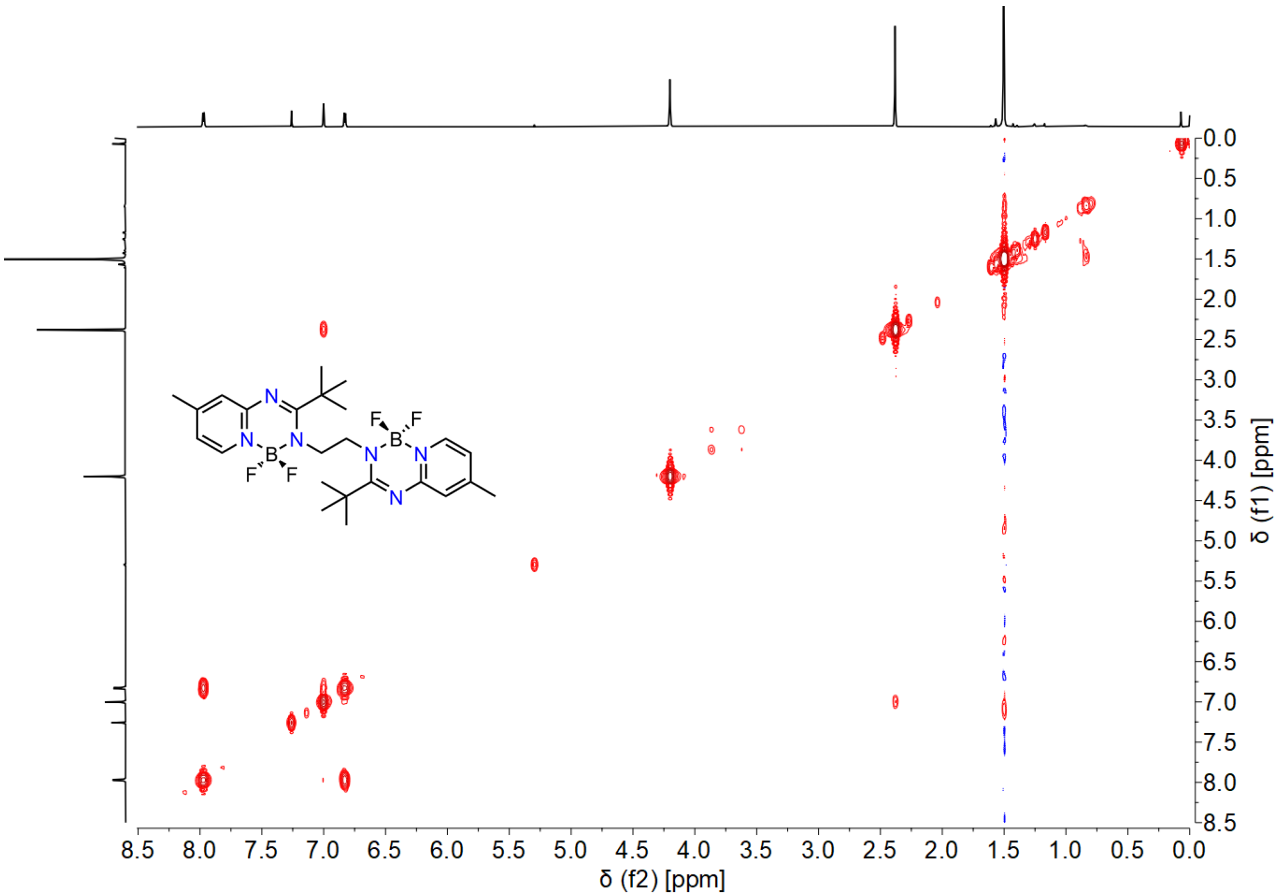

Figure S34. (^{1}H, ^{1}H)-COSY NMR spectrum of **3** ($CDCl_3$, 600.2 MHz).

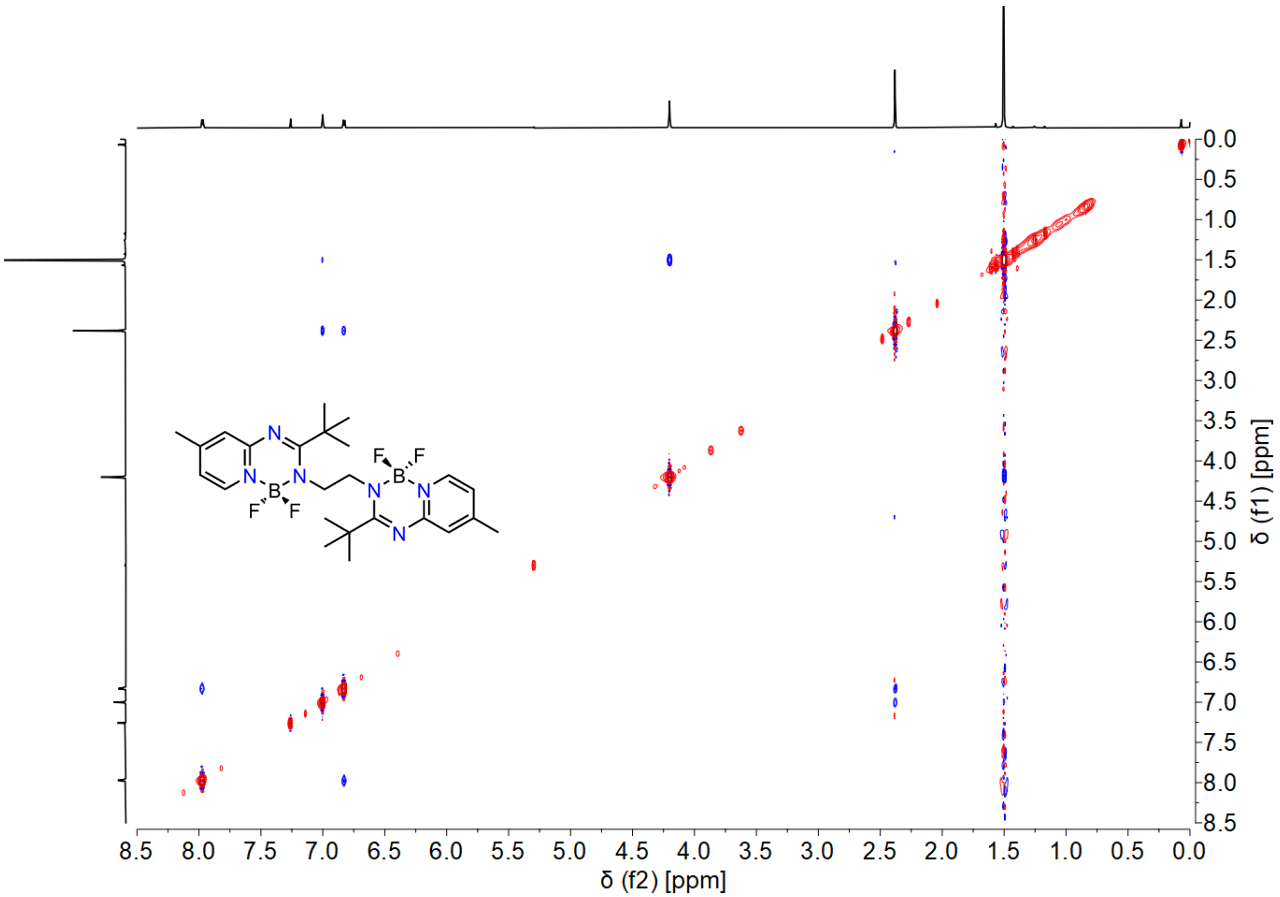

Figure S35. (^{1}H, ^{1}H)-NOESY NMR spectrum of **3** ($CDCl_3$, 600.2 MHz).

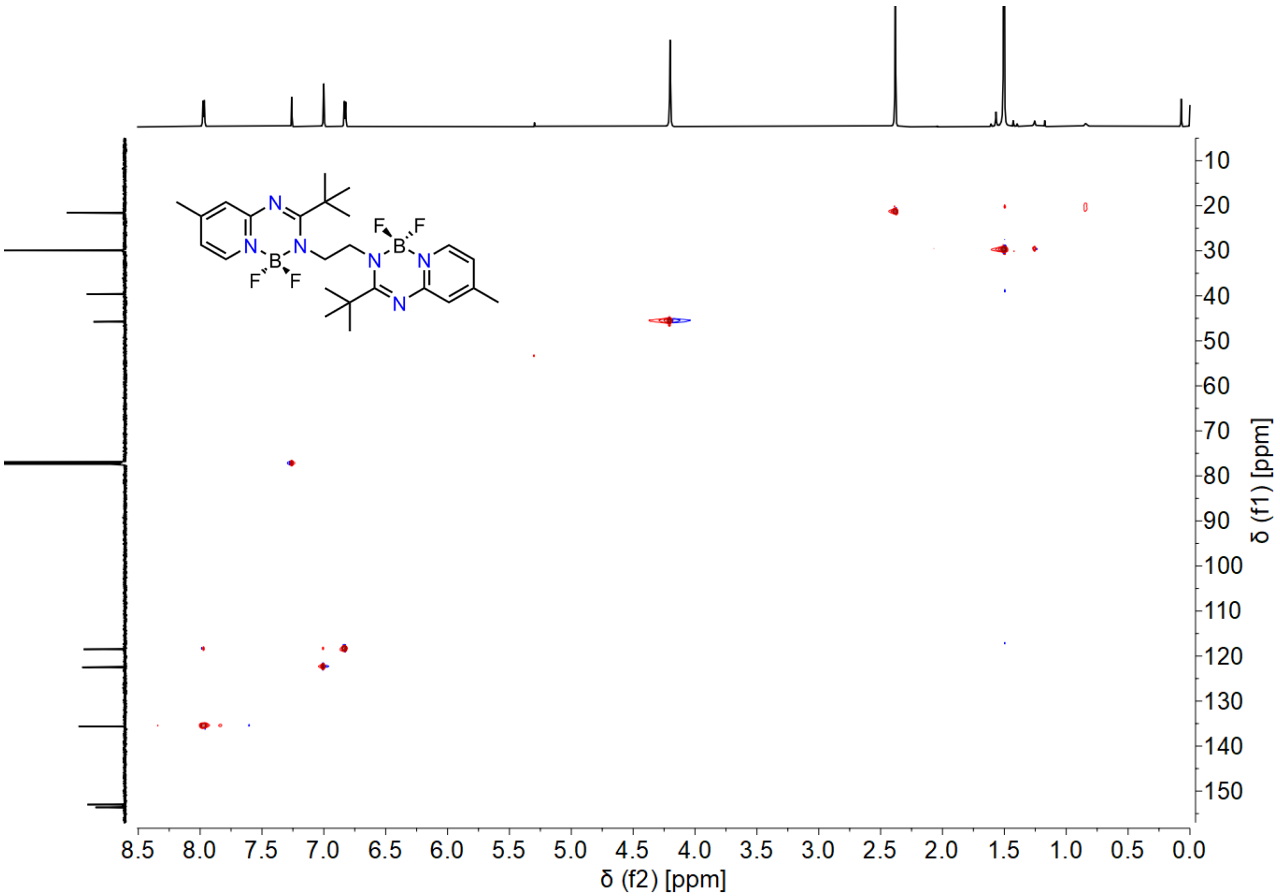

Figure S36. (^{1}H, ^{13}C)-HSQC NMR spectrum of **3** ($CDCl_3$, 600.2, 150.9 MHz).

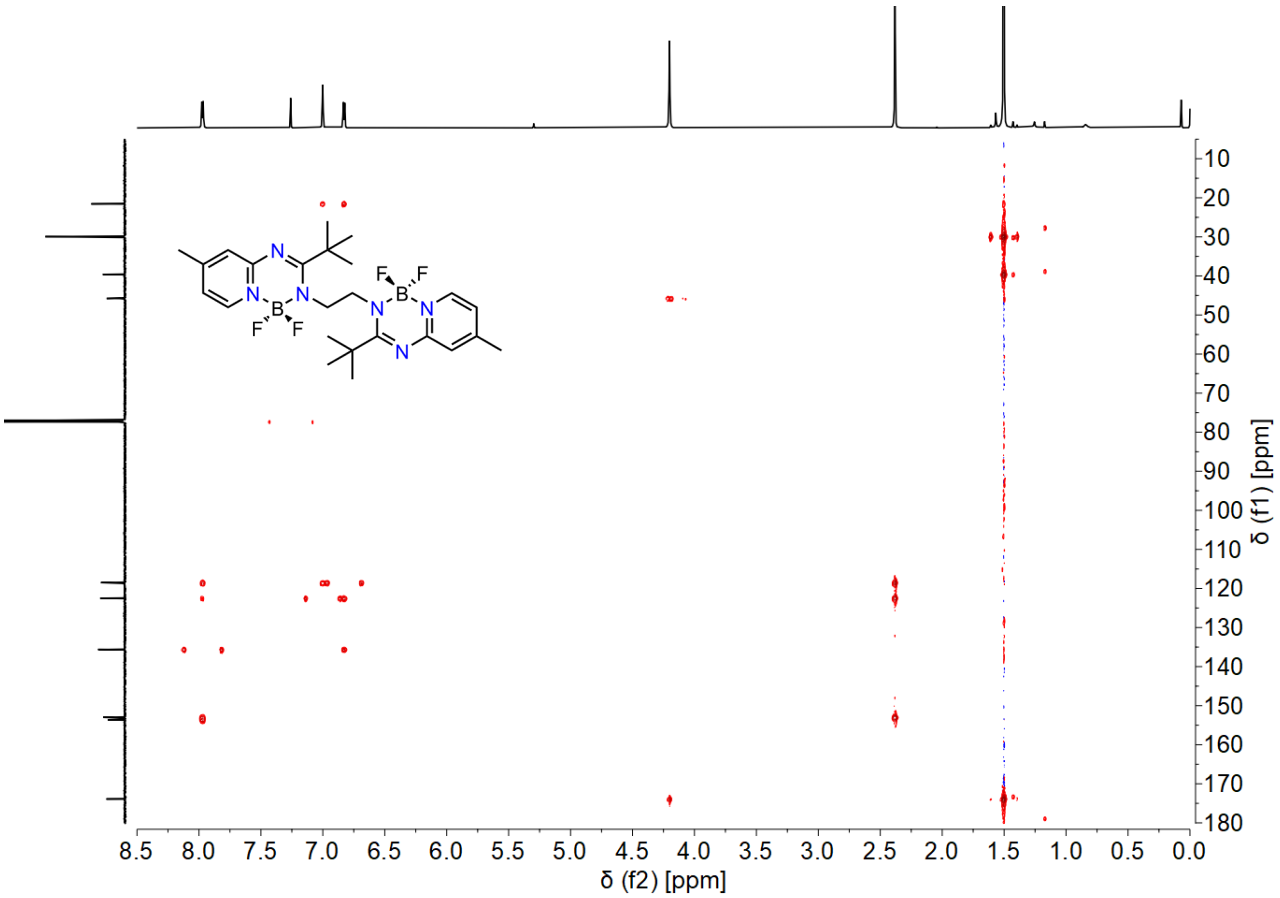

Figure S37. (^{1}H, ^{13}C)-HMBC NMR spectrum of **3** ($CDCl_3$, 600.2, 150.9 MHz).

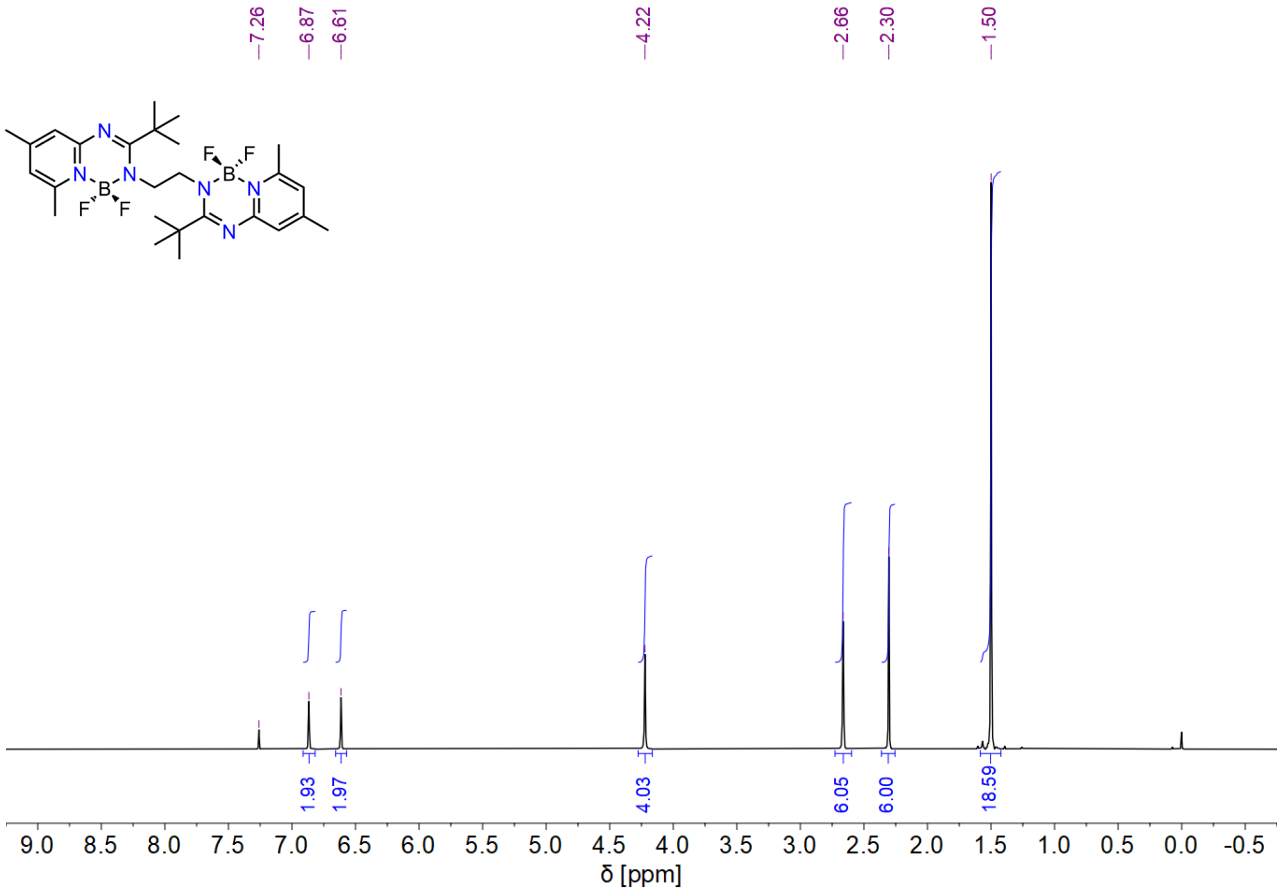

Figure S38. ^{1}H NMR spectrum of **4** ($CDCl_3$, 600.2 MHz).

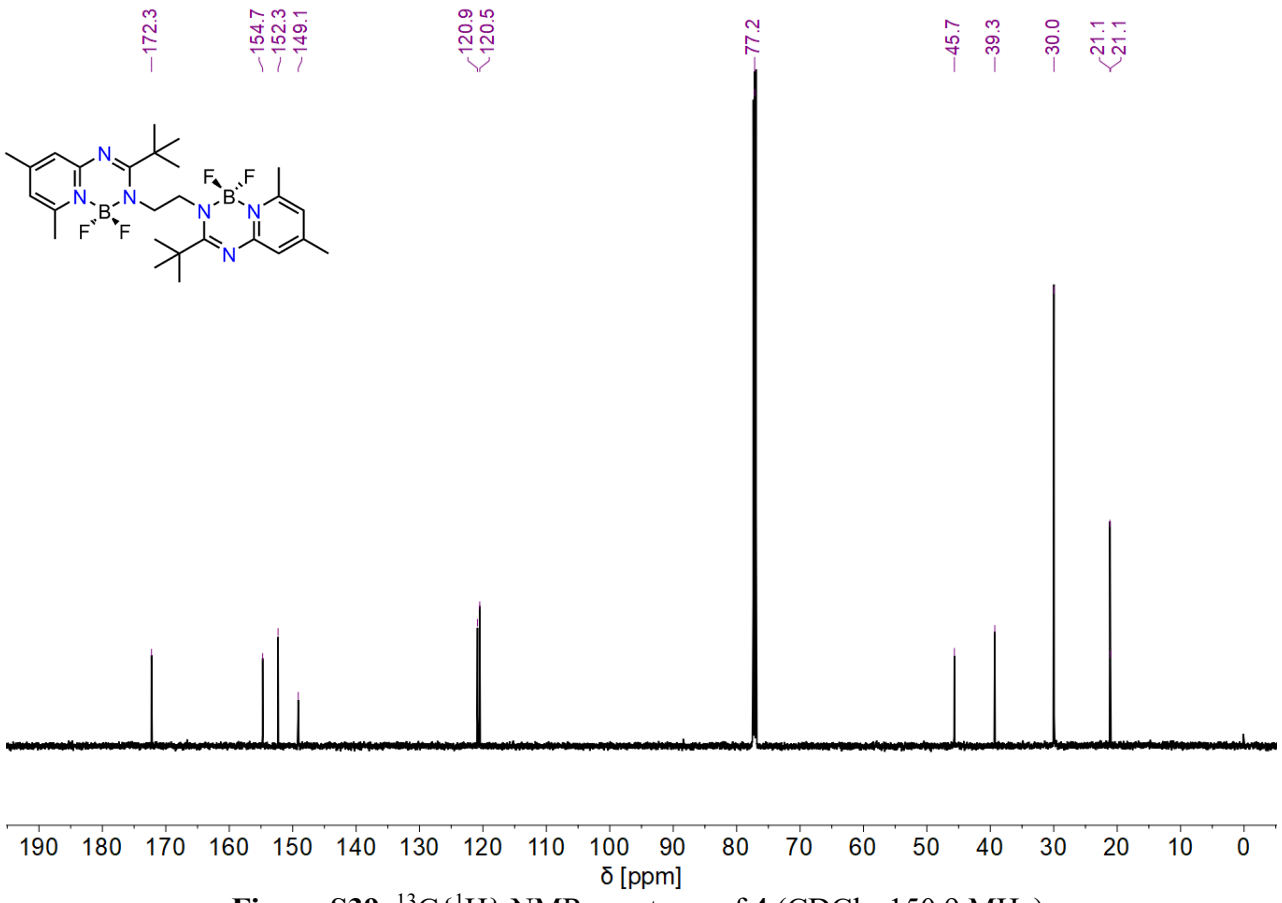

Figure S39. $^{13}C\{^{1}H\}$ NMR spectrum of **4** ($CDCl_3$, 150.9 MHz).

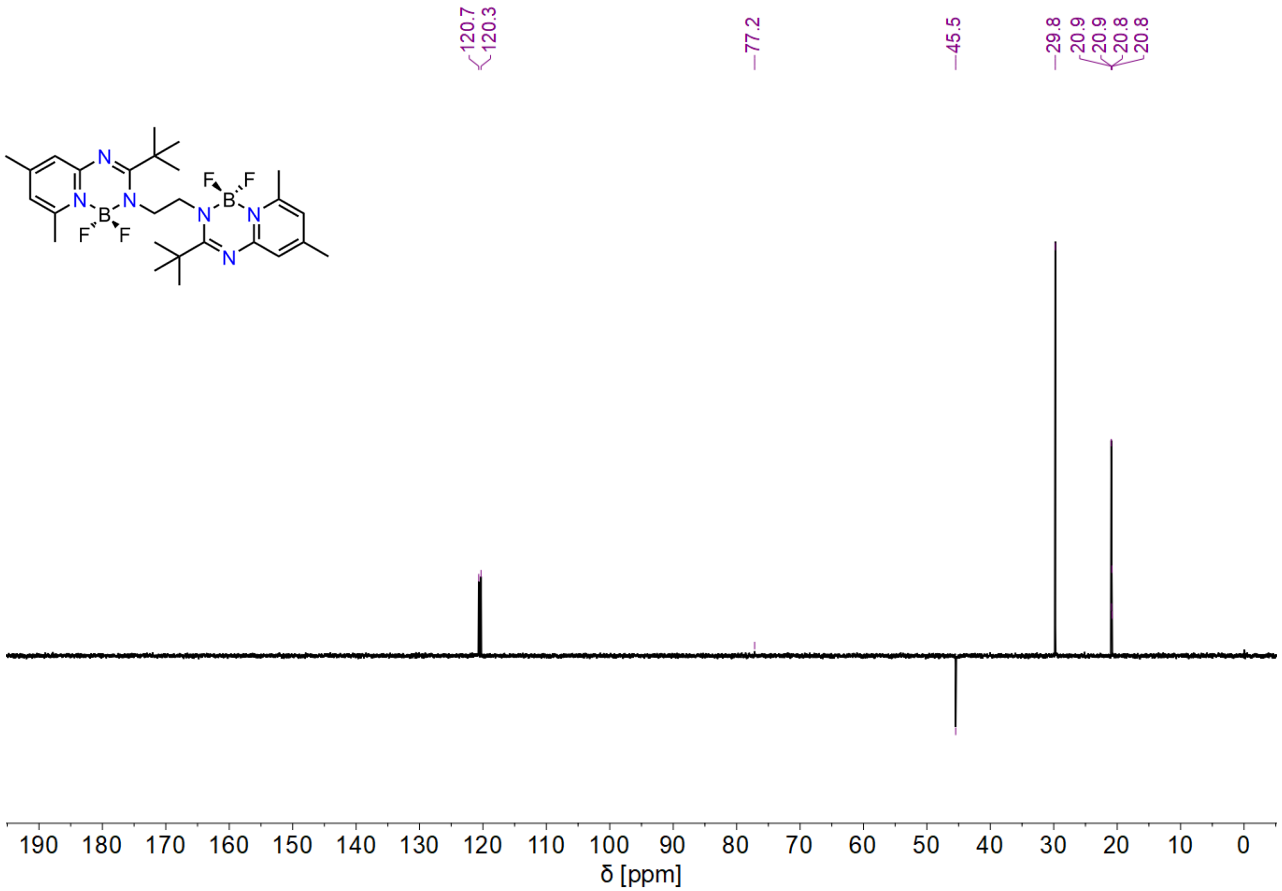

Figure S40. DEPT 135 NMR spectrum of **4** ($CDCl_3$, 150.9 MHz).

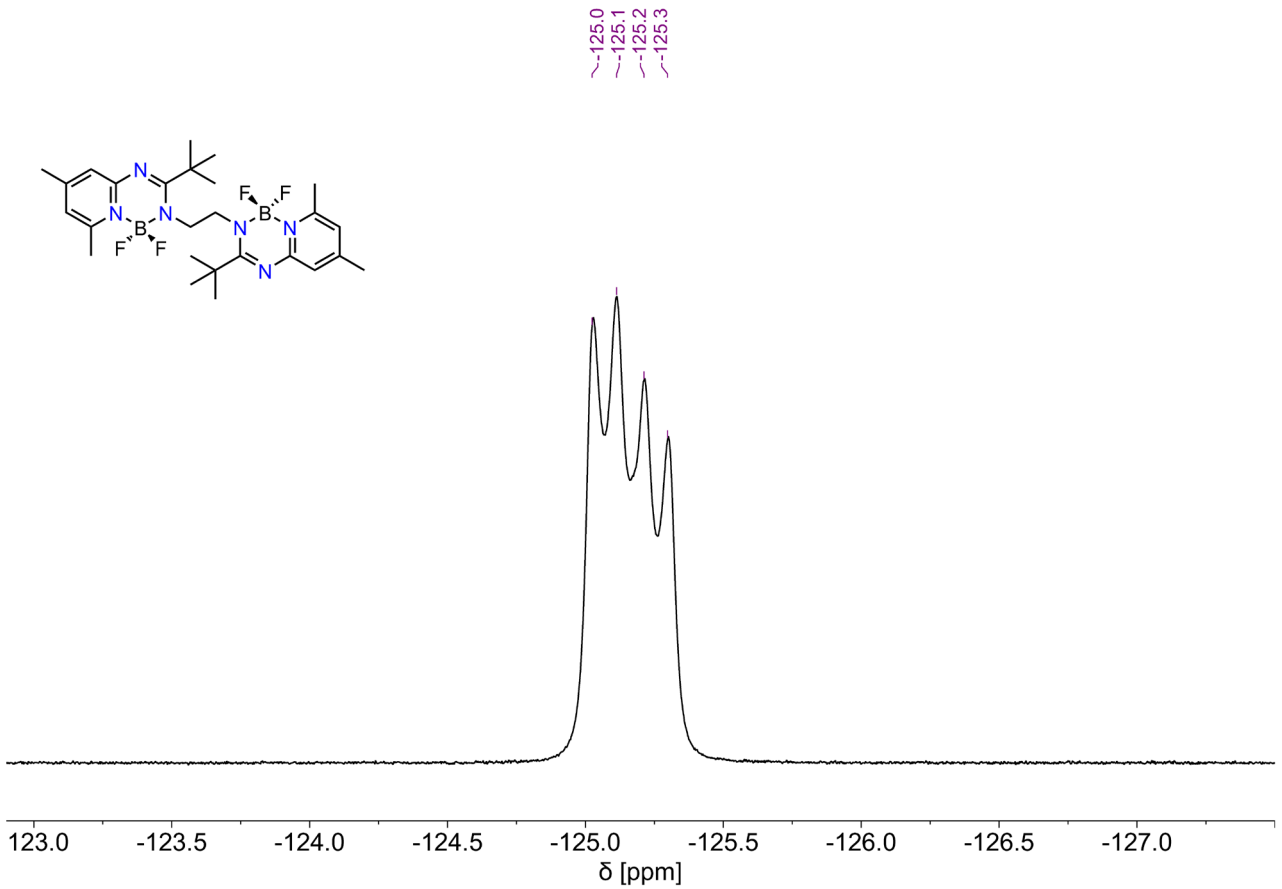

Figure S41. ^{19}F NMR spectrum of **4** ($CDCl_3$, 376.5 MHz).

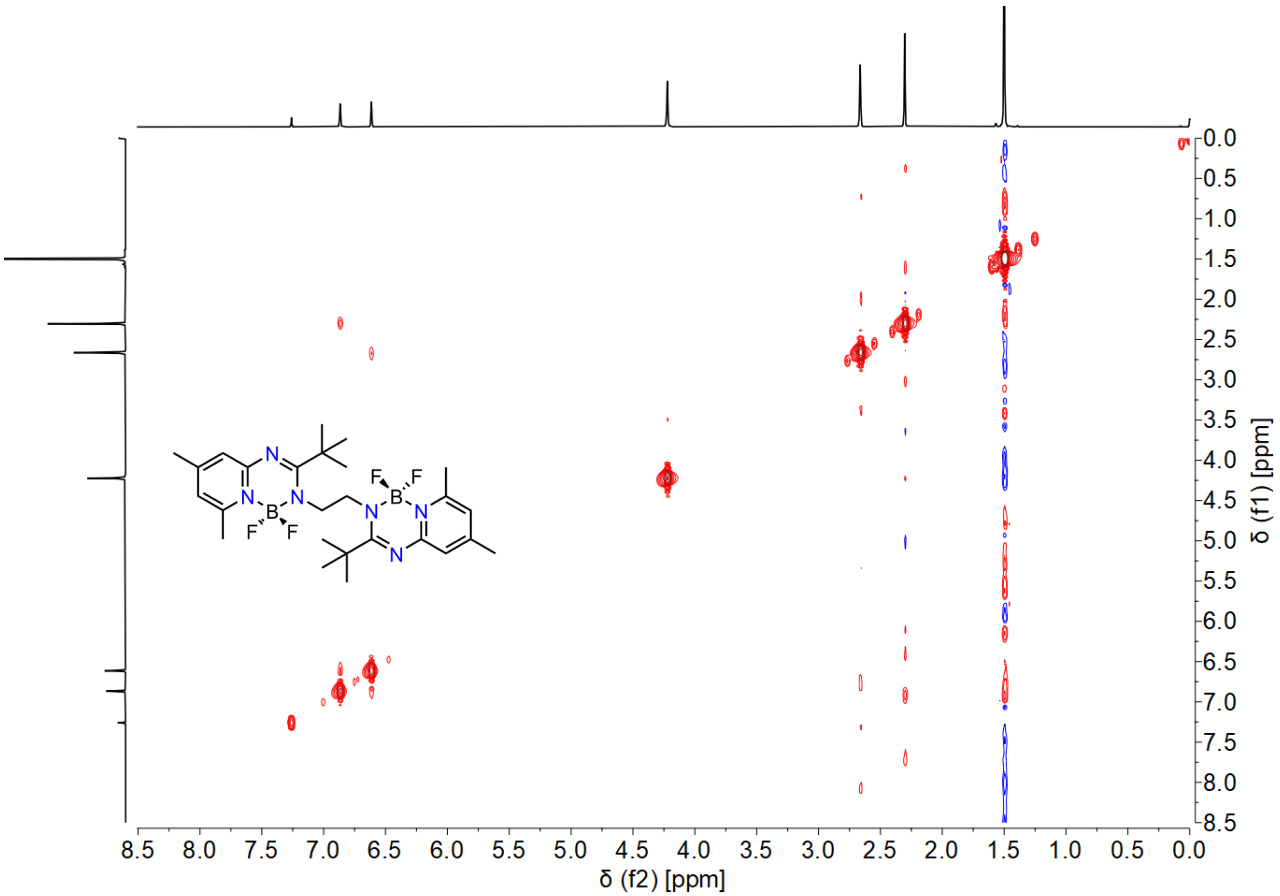

Figure S42. (^{1}H, ^{1}H)-COSY NMR spectrum of **4** ($CDCl_3$, 600.2 MHz).

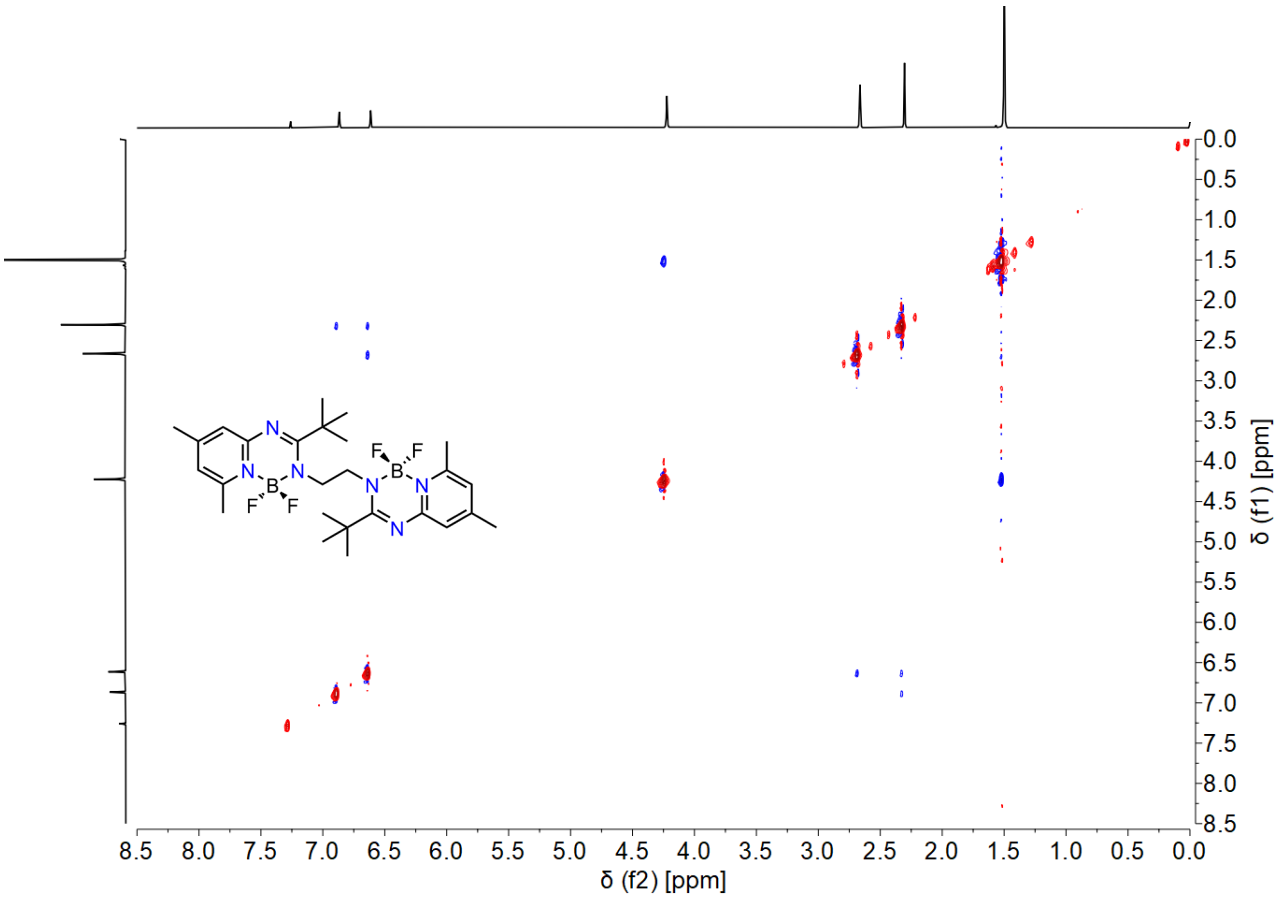

Figure S43. (^{1}H, ^{1}H)-NOESY NMR spectrum of **4** ($CDCl_3$, 600.2 MHz).

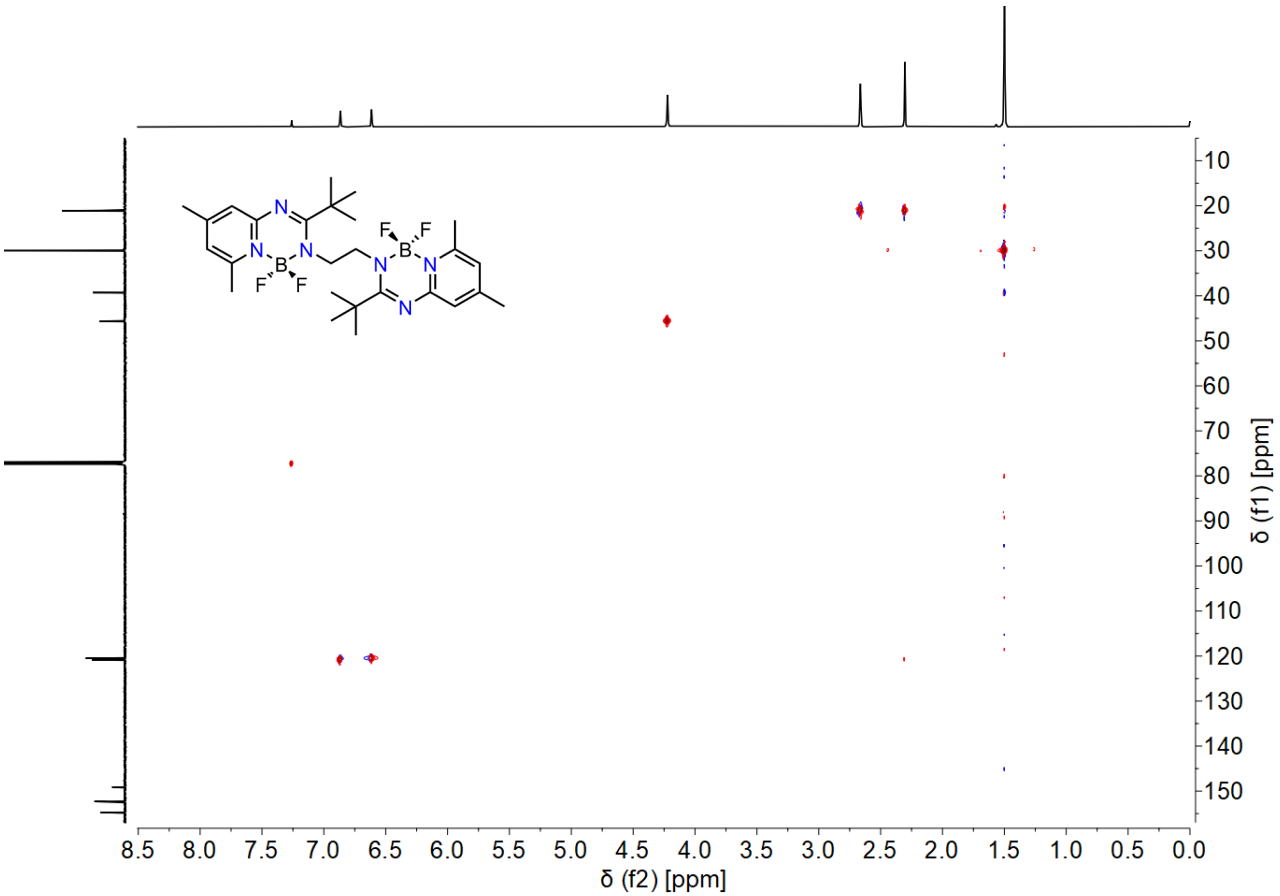

Figure S44. (^{1}H, ^{13}C)-HSQC NMR spectrum of **4** ($CDCl_3$, 600.2, 150.9 MHz).

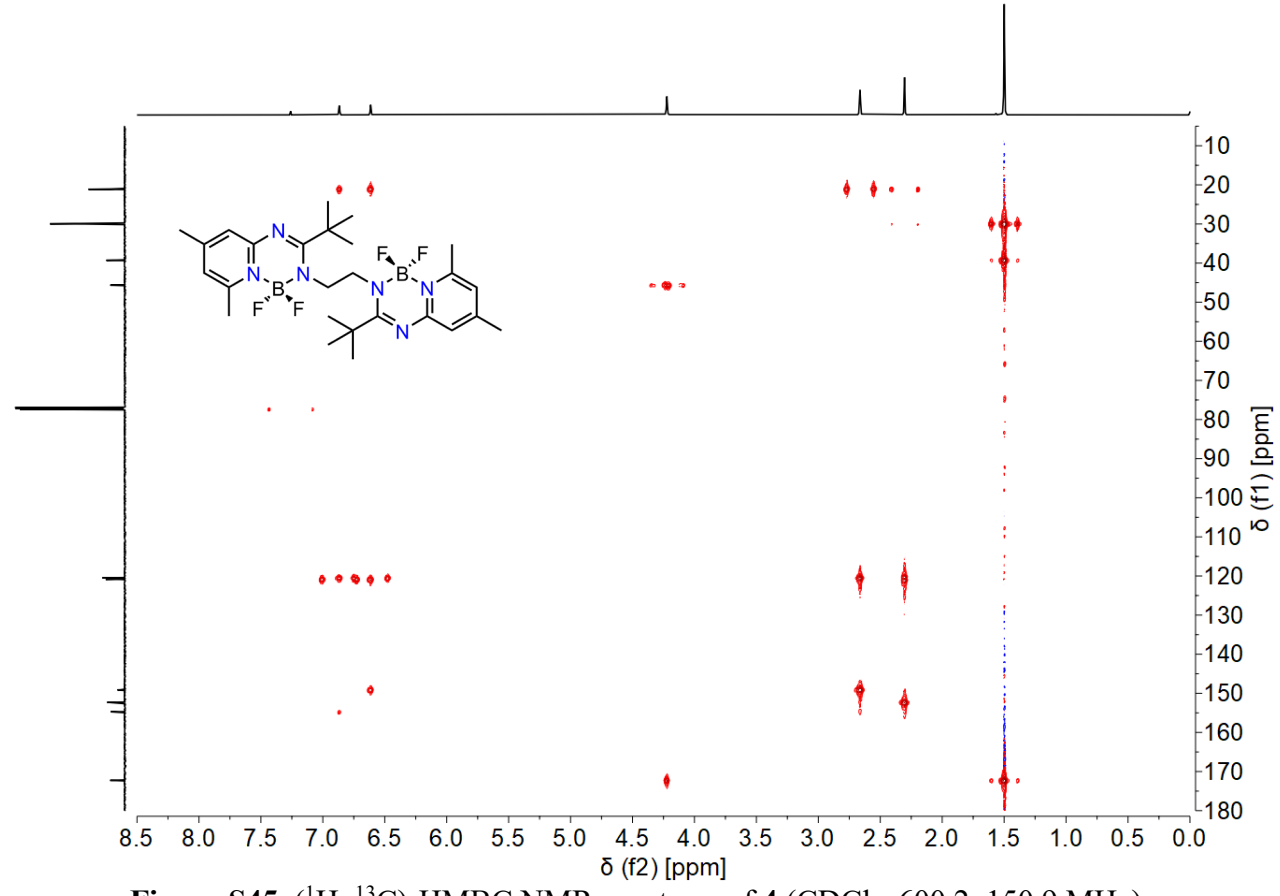

Figure S45. (^{1}H, ^{13}C)-HMBC NMR spectrum of **4** ($CDCl_3$, 600.2, 150.9 MHz).

Table S5. Selected ^{1}H NMR shifts of **1**–**4**.

	1	**2**	**3**	**4**
			δ ($CDCl_3$) [ppm]	
CH_3 (^{t}Bu)	1.52	1.51	1.50	1.50
NCH_2	4.23	4.25	4.20	4.22
Py H^3	7.19	7.05	7.00	6.87
Py H^5	7.00	6.77	6.83	6.61

Table S6: Selected $^{13}C\{^{1}H\}$ NMR shifts of **1**–**4**.

	1	**2**	**3**	**4**
			δ ($CDCl_3$) [ppm]	
$C(\underline{C}H_3)_3$	29.9	29.9	29.9	30.0
$\underline{C}(CH_3)_3$	39.7	39.4	39.6	39.3
NCH_2	45.8	45.7	45.8	45.7
C (Py C^2)	153.9	155.0	153.6	154.7
CH (Py C^3)	123.5	121.6	122.5	120.9
C/CH (Py C^4)	140.7	140.3	153.0	149.1
CH (Py C^5)	116.5	118.6	118.5	120.5
C/CH (Py C^6)	136.2	149.9	135.6	152.3
^{t}Bu$\underline{C}N_2$	174.0	172.3	173.9	172.3

Table S7. ^{19}F NMR shifts of **1**–**4**.

1	**2**	**3**	**4**
		δ ($CDCl_3$) [ppm]	
–134.3	–124.3	–134.8	–125.2

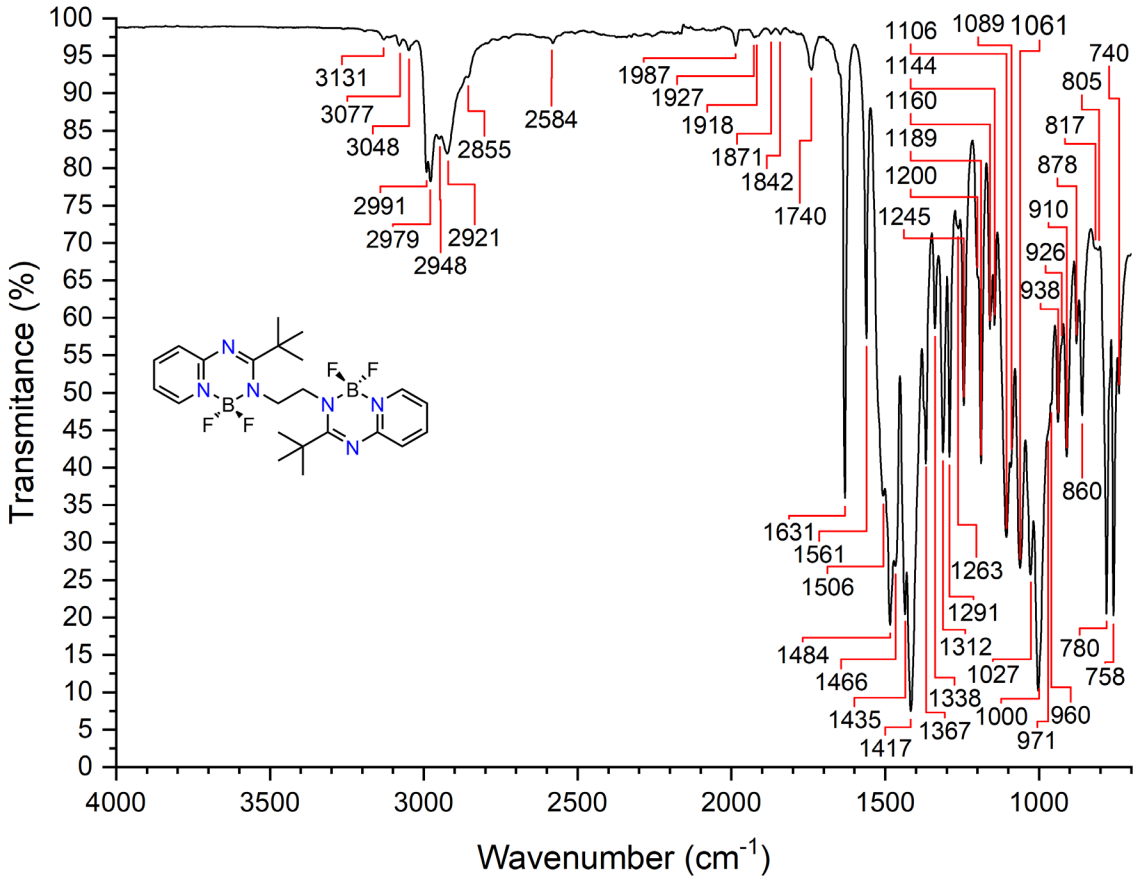

Figure S46. IR spectrum of **1** (ATR).

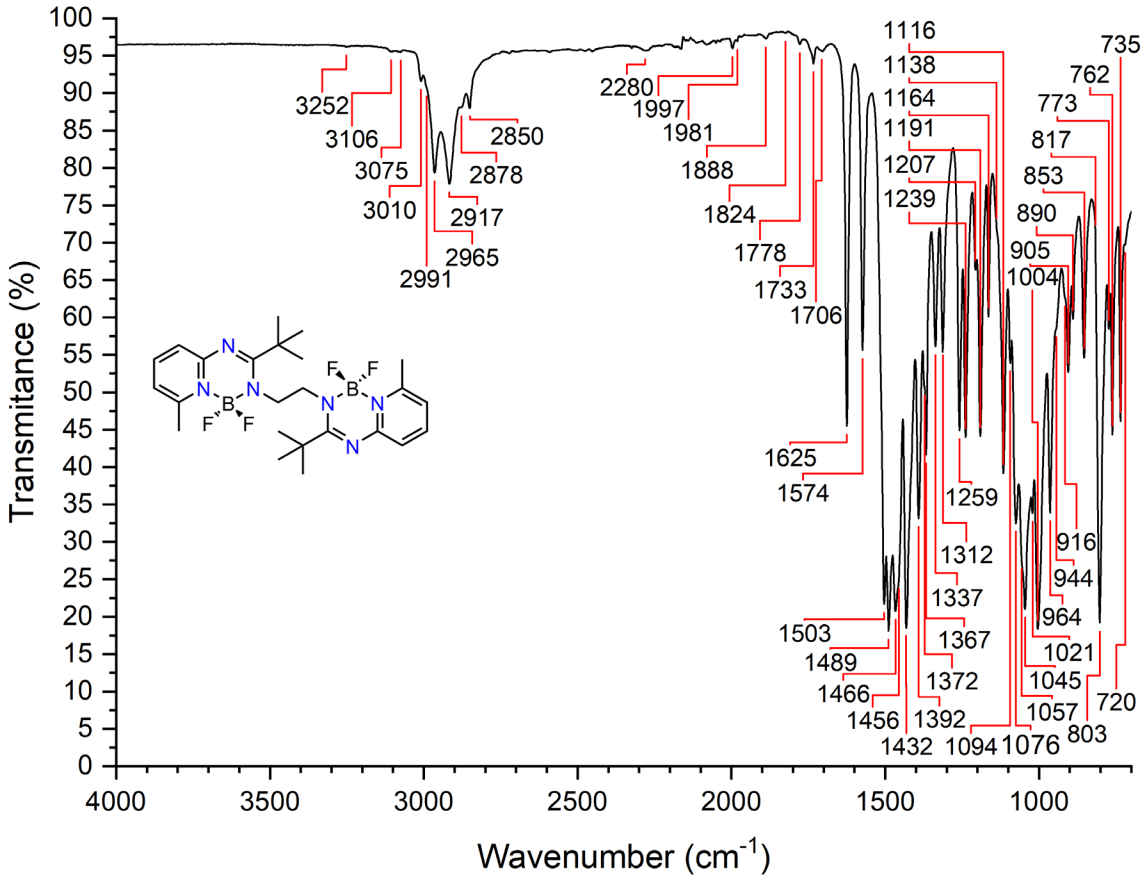

Figure S47. IR spectrum of **2** (ATR).

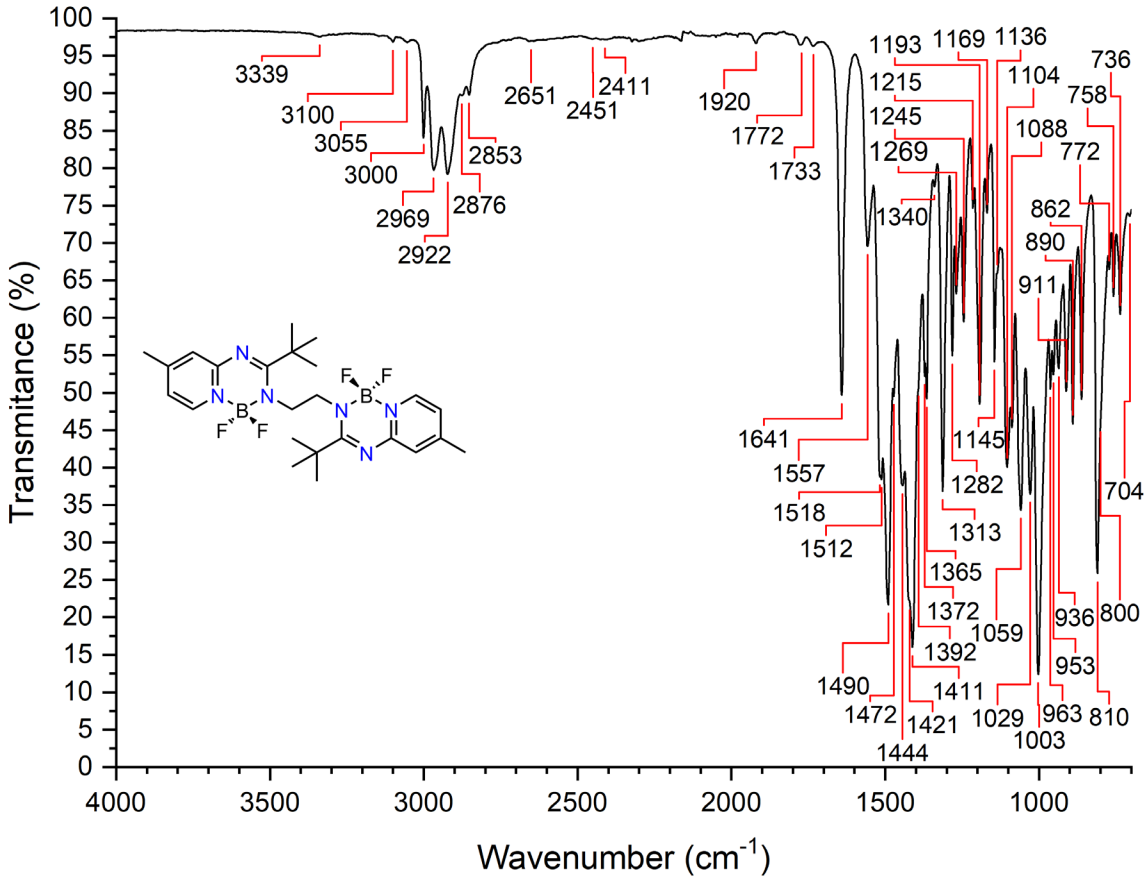

Figure S48. IR spectrum of **3** (ATR).

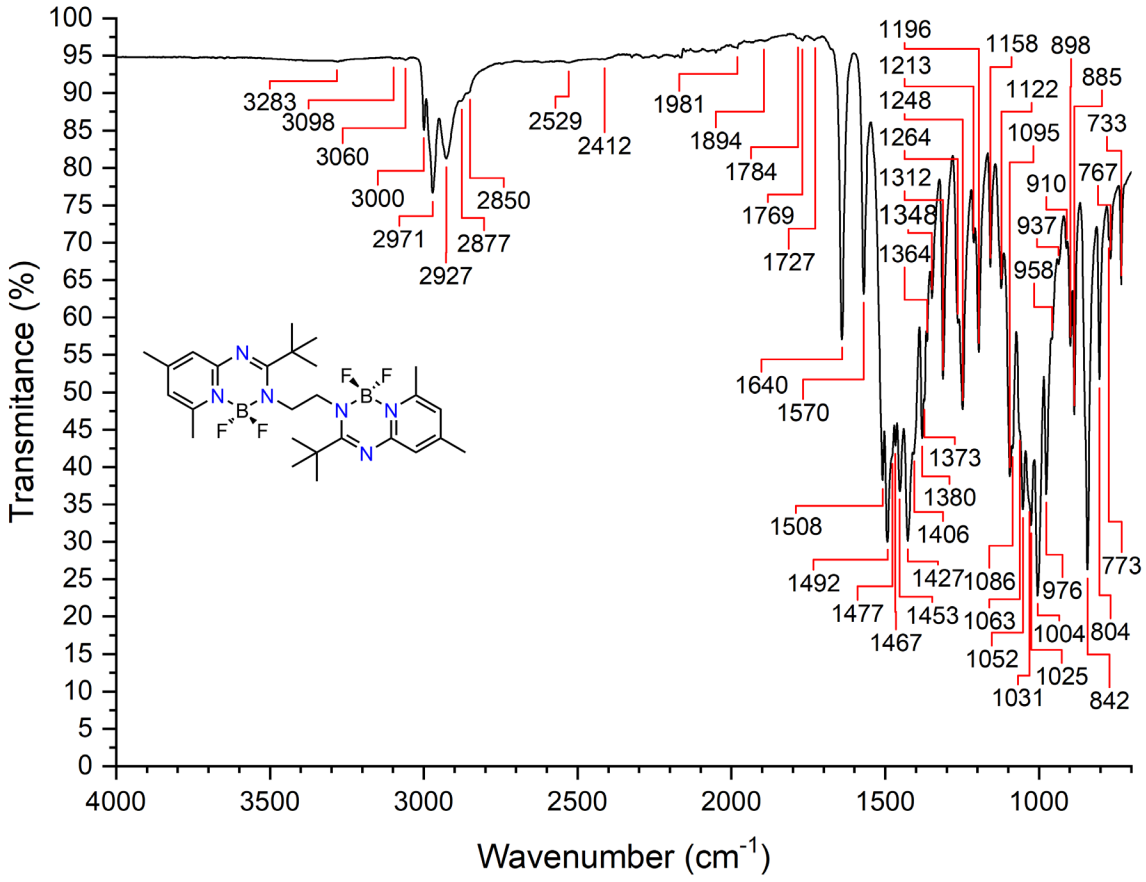

Figure S49. IR spectrum of **4** (ATR).

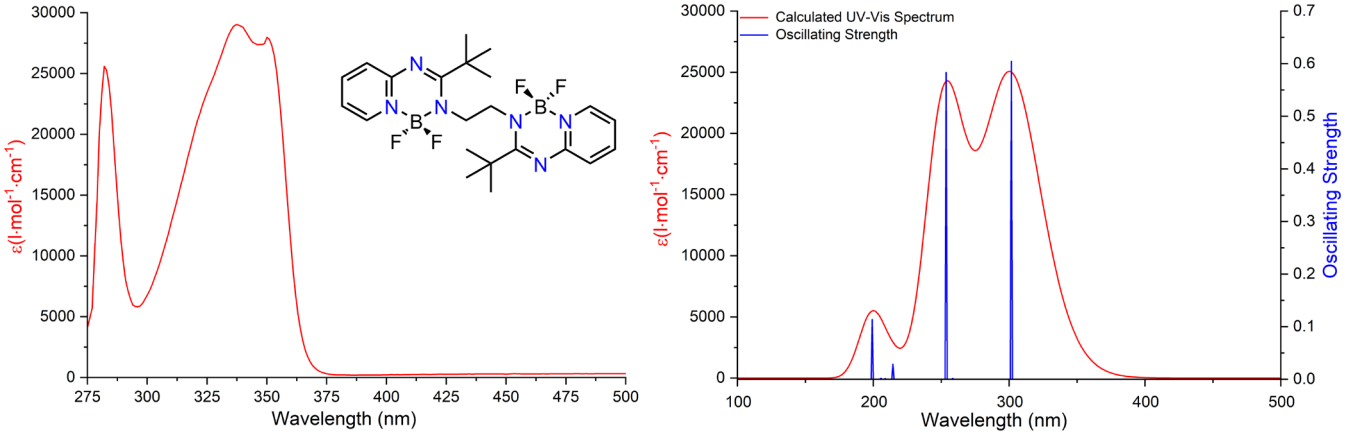

Figure S50. Experimental (left) and calculated (right) UV–Vis spectrum of **1**.

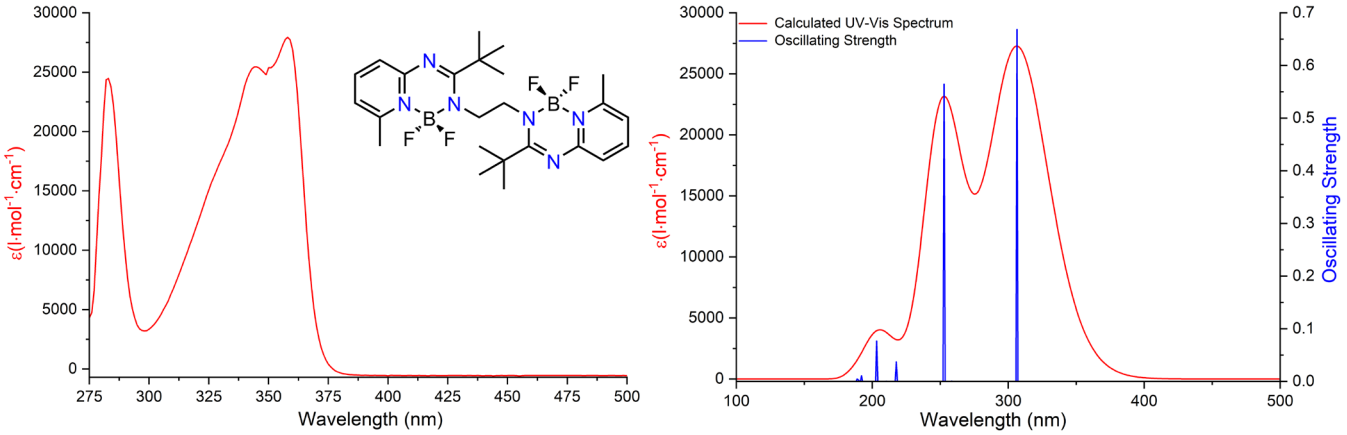

Figure S51. Experimental (left) and calculated (right) UV–Vis spectrum of **2**.

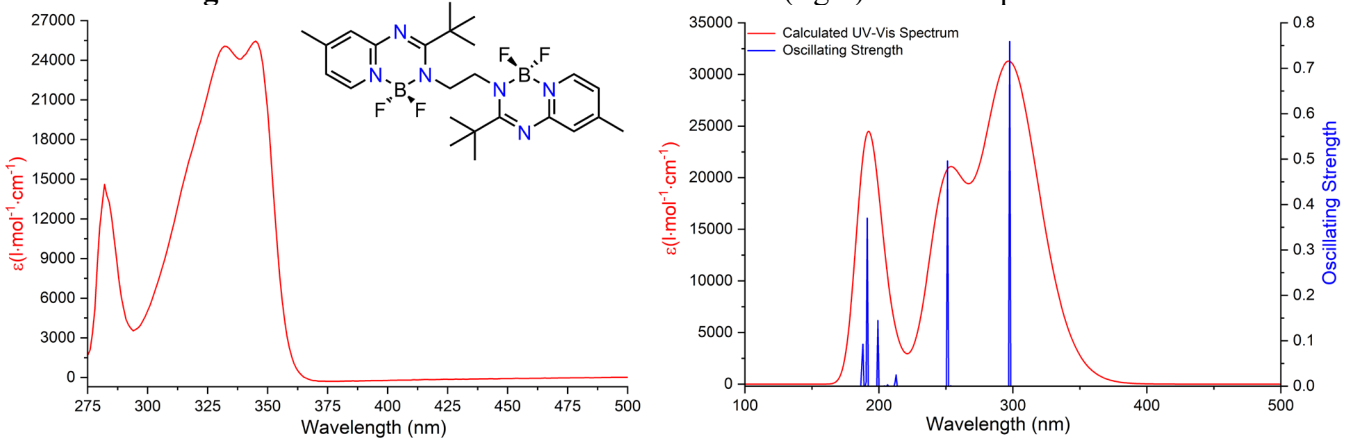

Figure S52. Experimental (left) and calculated (right) UV–Vis spectrum of **3**.

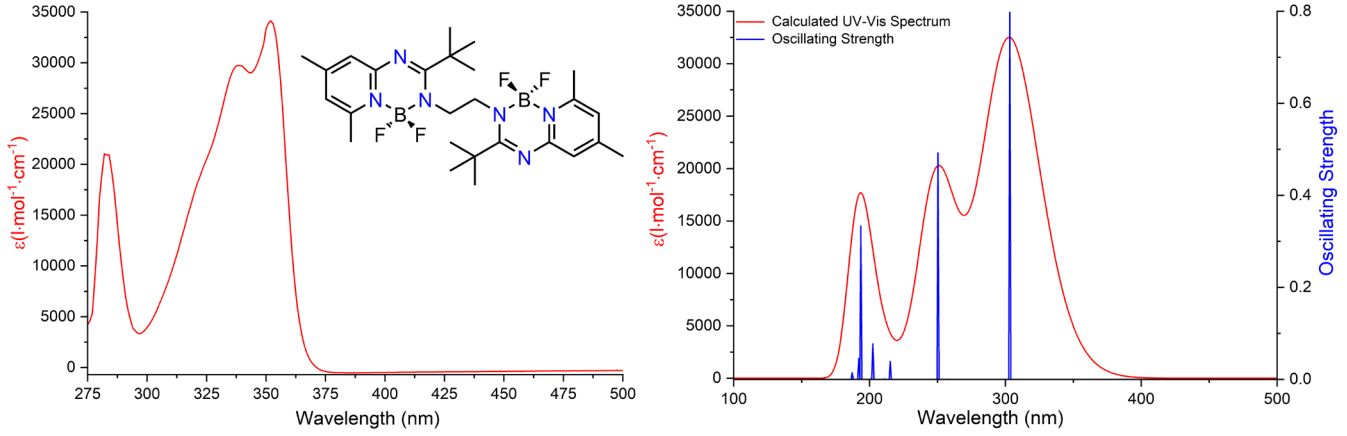

Figure S53. Experimental (left) and calculated (right) UV–Vis spectrum of **4**.

Table S8. UV–Vis parameters of **1–4** in solution (THF).

1	**2**	**3**	**4**
λ_{max} [nm] (ε [10^4 L·mol^{-1}·cm^{-1}])			
282 (2.56)	283 (2.45)	282 (1.46)	282 (2.11)
337 (2.90)	345 (2.55)	332 (2.51)	338 (2.98)
350 (2.80)	358 (2.79)	345 (2.55)	352 (3.41)

Table S9. Calculated first excited (S_1) states of **1**–**4**.

	1	**2**	**3**	**4**
Energy (eV)	4.1115	4.0409	4.1621	4.0896
Wavelength λ (nm)	301.56	306.82	297.89	303.17
Oscillation Factor *f*	0.6047	0.6685	0.7593	0.7981
HOMO-1 → LUMO+1	124 → 127	132 → 135	132 → 135	140 → 143
Singlet-AU (coefficient)	0.45649	0.44671	-0.45426	-0.44471
Orbital Contribution (%)	45.55%	41.53%	43.08%	41.25%
HOMO → LUMO	125 → 126	133 → 134	133 → 134	141 → 142
Singlet-AU (coefficient)	0.52108	0.53001	0.52207	0.53074
Orbital Contribution (%)	55.44%	58.46%	56.91%	58.75%

Table S10. Calculated higher excited states of **1**–**4** (4.89–4.95 eV).

	1	**2**	**3**	**4**
Energy (eV)	4.8921	4.9127	4.9267	4.9523
Wavelength λ (nm)	253.44	252.44	251.66	250.36
Oscillation Factor *f*	0.5832	0.5646	0.4960	0.4923
HOMO-1 → LUMO+3	124 → 129	132 → 137	132 → 137	140 → 145
Singlet-AU (coefficient)	0.45398	0.44528	0.44637	0.44881
Orbital Contribution (%)	43.69%	43.25%	43.67%	43.53%
HOMO → LUMO+2	125 → 128	133 → 136	133 → 136	141 → 145
Singlet-AU (coefficient)	0.51537	0.50989	0.50689	0.51114
Orbital Contribution (%)	56.31%	56.75%	56.33%	56.47%

Table S11. Calculated higher excited states of **1**–**4** (6.21–6.45 eV).

	1	**2**	**3**	**4**
Energy (eV)	6.2093	6.0877	6.2438	6.4457
Wavelength λ (nm)	199.68	203.66	199.59	192.35
Oscillation Factor f	0.1139	0.0769	0.1450	0.3336
HOMO-8 → LUMO+2	-	125 → 136	125 → 134	-
Singlet-AU (coefficient)	-	0.10638	0.11472	-
Orbital Contribution (%)	-	2.50%	2.91%	-
HOMO-7 → LUMO+5	-	-	126 → 137	-
Singlet-AU (coefficient)	-	-	0.11241	-
Orbital Contribution (%)	-	-	2.79%	-
HOMO-7 → LUMO+3	-	-	126 → 135	-
Singlet-AU (coefficient)	-	-	0.19669	-
Orbital Contribution (%)	-	-	8.55%	-
HOMO-7 → LUMO+2	117 → 128	-	-	-
Singlet-AU (coefficient)	0.15499	-	-	-
Orbital Contribution (%)	5.60%	-	-	-
HOMO-7 → LUMO+1	-	-	-	134 → 143
Singlet-AU (coefficient)	-	-	-	0.36455
Orbital Contribution (%)	-	-	-	31.27%
HOMO-6 → LUMO+3	118 → 129	126 → 137	-	-
Singlet-AU (coefficient)	0.15422	0.12291	-	-
Orbital Contribution (%)	5.55%	3.33%	-	-
HOMO-6 → LUMO+2	-	-	127→ 134	-
Singlet-AU (coefficient)	-	-	0.39201	-
Orbital Contribution (%)	-	-	33.99%	-
HOMO-6 → LUMO	-	133 → 134	-	135 → 142
Singlet-AU (coefficient)	-	0.12201	-	0.38710
Orbital Contribution (%)	-	3.29%	-	35.25%

Table S11. Calculated higher excited states of **1**–**4** (6.21–6.45 eV, continued).

	1	**2**	**3**	**4**
Energy (eV)	6.2093	6.0877	6.2438	6.4457
Wavelength λ (nm)	199.68	203.66	199.59	192.35
Oscillation Factor f	0.1139	0.0769	0.1450	0.3336
HOMO-5 → LUMO+3	-	-	128 → 135	136 → 145
Singlet-AU (coefficient)	-	-	0.35232	0.15965
Orbital Contribution (%)	-	-	27.45%	5.99%
HOMO-4 → LUMO+4	-	-	129 → 136	-
Singlet-AU (coefficient)	-	-	0.18987	-
Orbital Contribution (%)	-	-	7.97%	-
HOMO-4 → LUMO+3	-	-	-	137 → 145
Singlet-AU (coefficient)	-	-	-	0.20405
Orbital Contribution (%)	-	-	-	9.79%
HOMO-4 → LUMO+1	120 → 127	128 → 135	-	-
Singlet-AU (coefficient)	0.38339	0.39944	-	-
Orbital Contribution (%)	34.30%	35.28%	-	-
HOMO-3 → LUMO	121 → 126	129 → 134	-	-
Singlet-AU (coefficient)	0.43873	0.43627	-	-
Orbital Contribution (%)	44.92%	42.08%	-	-
HOMO-1 → LUMO+5	-	-	132 → 137	-
Singlet-AU (coefficient)	-	-	0.12250	-
Orbital Contribution (%)	-	-	2.32%	-
HOMO-1 → LUMO+2	-	-	-	140 → 144
Singlet-AU (coefficient)	-	-	-	0.13121
Orbital Contribution (%)	-	-	-	4.05%
HOMO-1 → LUMO	123 → 126	131 → 134	-	-
Singlet-AU (coefficient)	0.10543	0.14160	-	-
Orbital Contribution (%)	2.59%	4.43%	-	-

Table S11. Calculated higher excited states of **1**–**4** (6.21–6.45 eV, continued).

	1	**2**	**3**	**4**
Energy (eV)	6.2093	6.0877	6.2438	6.4457
Wavelength λ (nm)	199.68	203.66	199.59	192.35
Oscillation Factor f	0.1139	0.0769	0.1450	0.3336
HOMO → LUMO+8	-	-	-	141 → 150
Singlet-AU (coefficient)	-	-	-	0.15265
Orbital Contribution (%)	-	-	-	5.48%
HOMO → LUMO+4	-	-	133 → 136	-
Singlet-AU (coefficient)	-	-	0.24239	-
Orbital Contribution (%)	-	-	12.99%	-
HOMO → LUMO+3	-	-	-	141 → 145
Singlet-AU (coefficient)	-	-	-	0.18603
Orbital Contribution (%)	-	-	-	8.14%
HOMO → LUMO+1	124 → 127	132 → 135	-	-
Singlet-AU (coefficient)	0.17345	0.20244	-	-
Orbital Contribution (%)	7.02%	9.06%	-	-

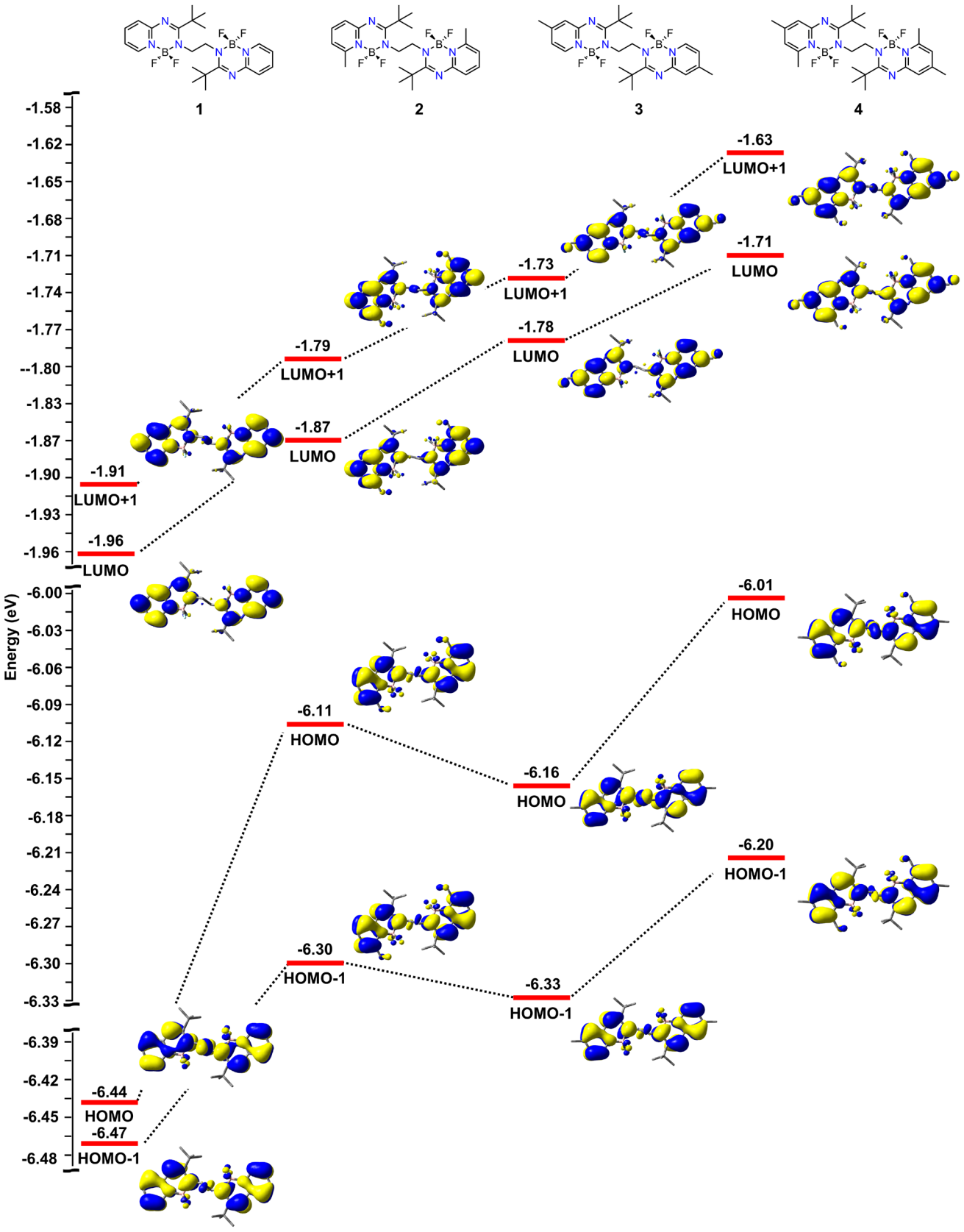

Figure S54. Calculated orbital energies and modeled frontier molecular orbitals of **1**–**4** (isovalue = 0.04 a.u.).

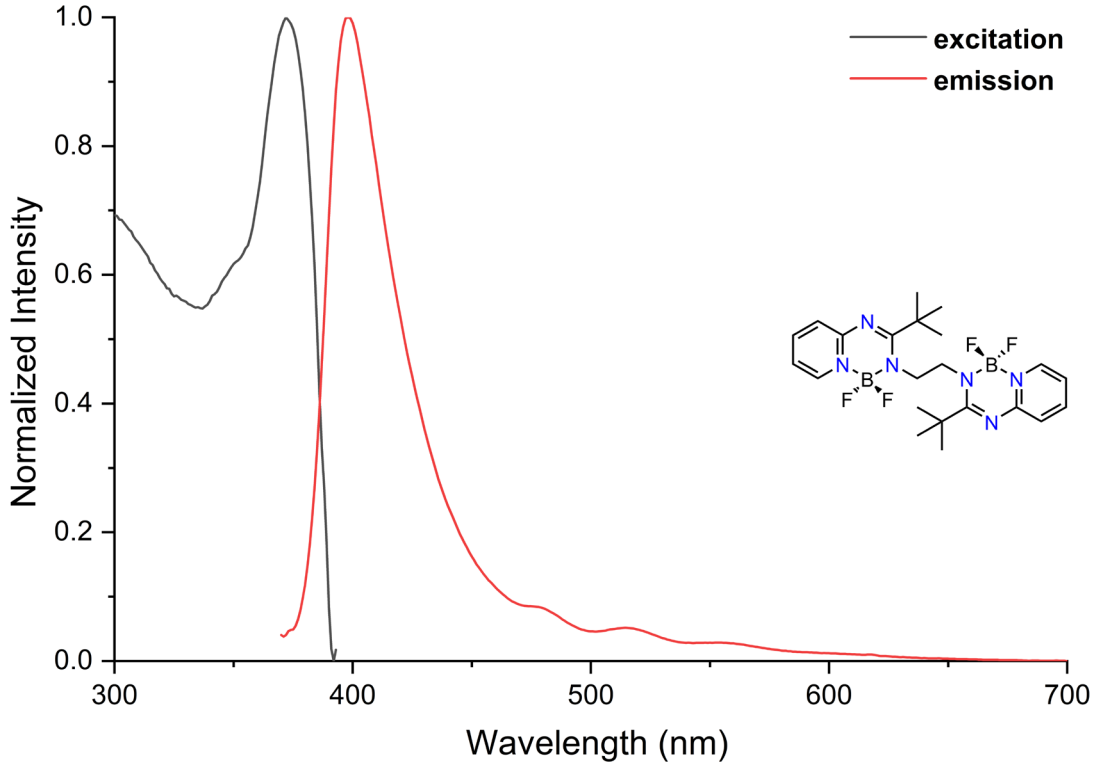

Figure S55. Normalized photoluminescence excitation and emission spectra of **1** in the solid state at 300 K.

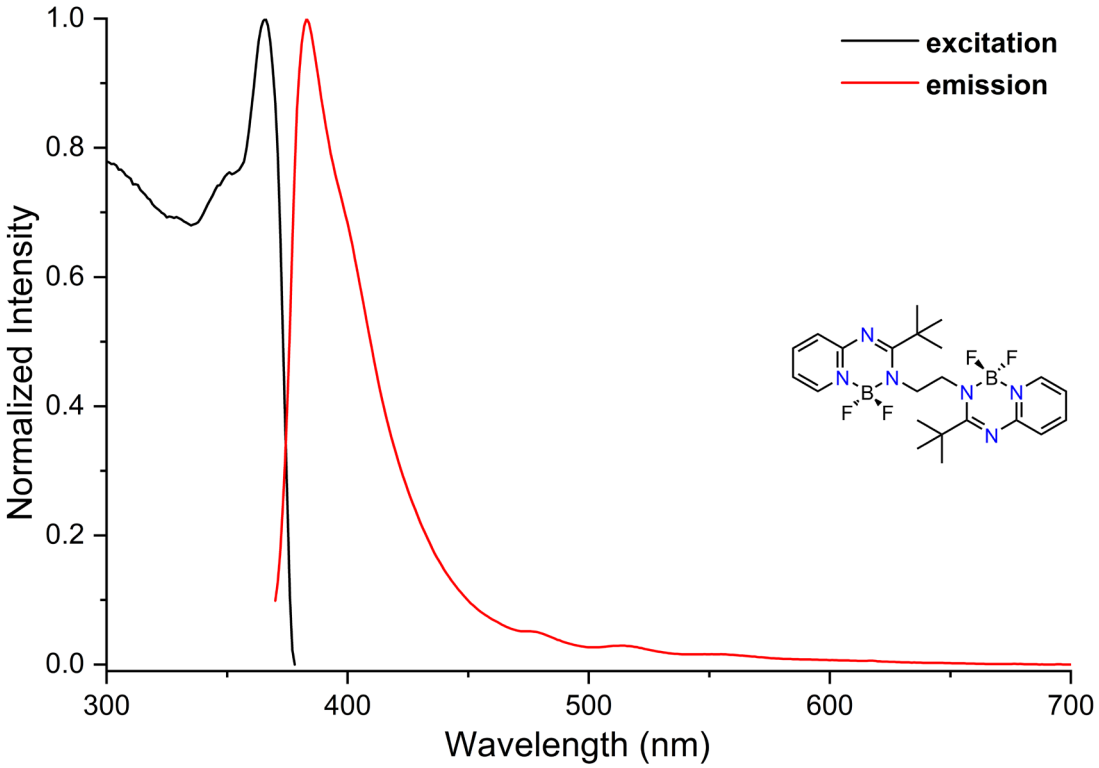

Figure S56. Photoluminescence excitation and emission spectra of **1** in the solid state at 77 K.

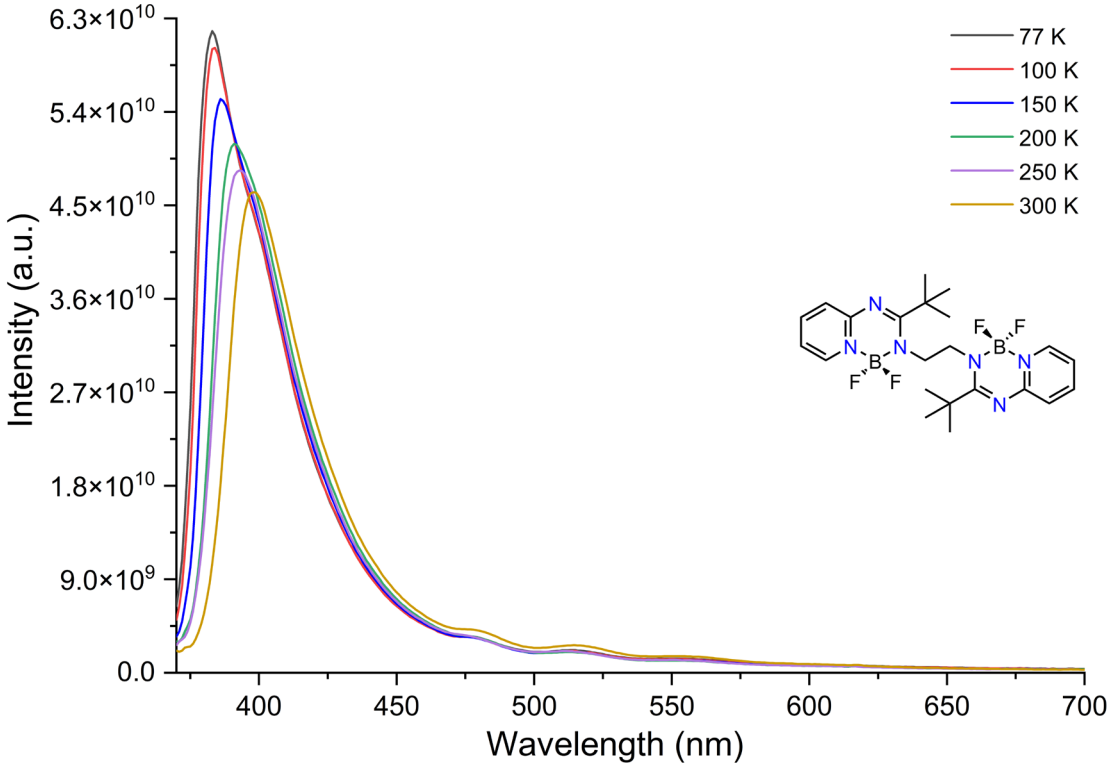

Figure S57. Variable-temperature photoluminescence emission spectra of **1** in the solid state.

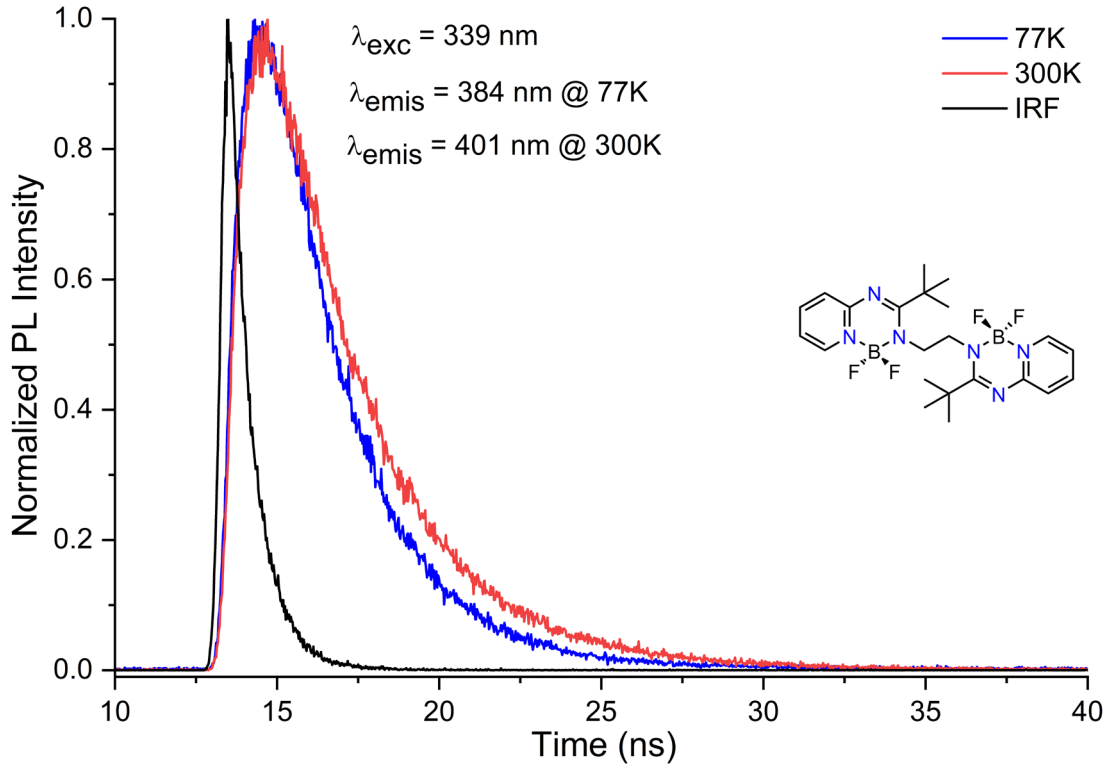

Figure S58. Emission decay traces of **1** in the solid state at 77 and 300 K under ns-pulsed excitation at 339 nm (IRF = Instrument Response Function). The decay can be fit with monoexponential curves, with τ = 2.31 and 2.93 ns, respectively.

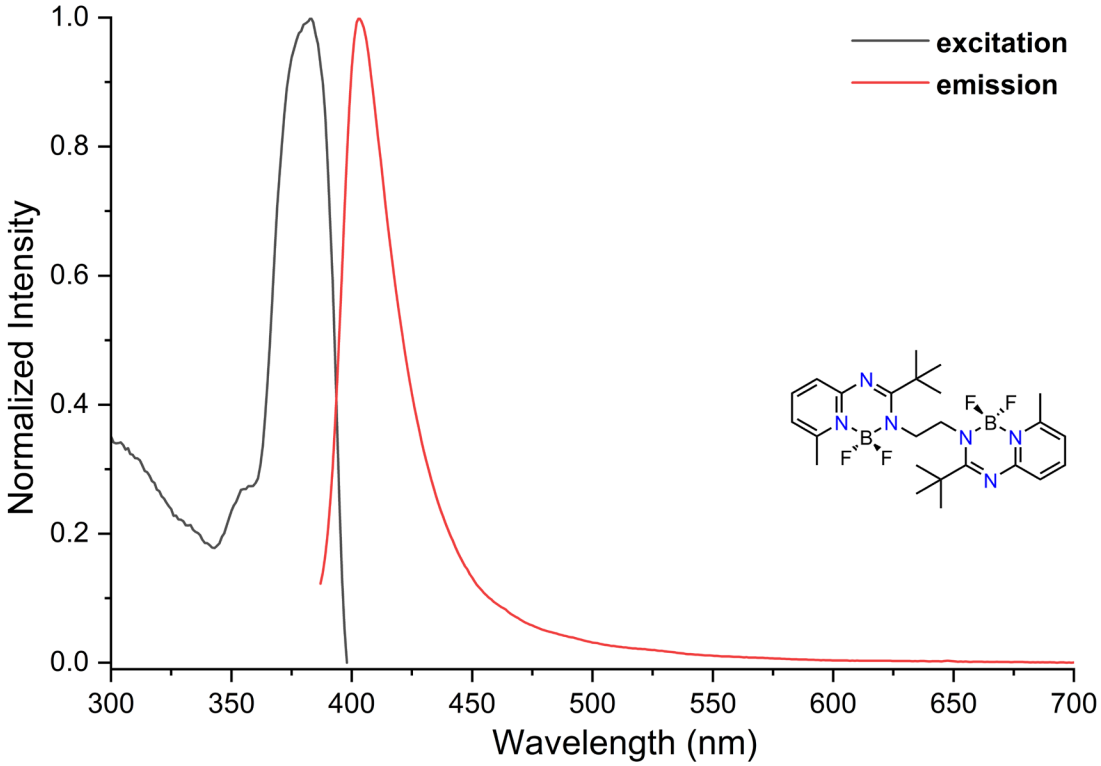

Figure S59. Normalized photoluminescence excitation and emission spectra of **2** in the solid state at 300 K.

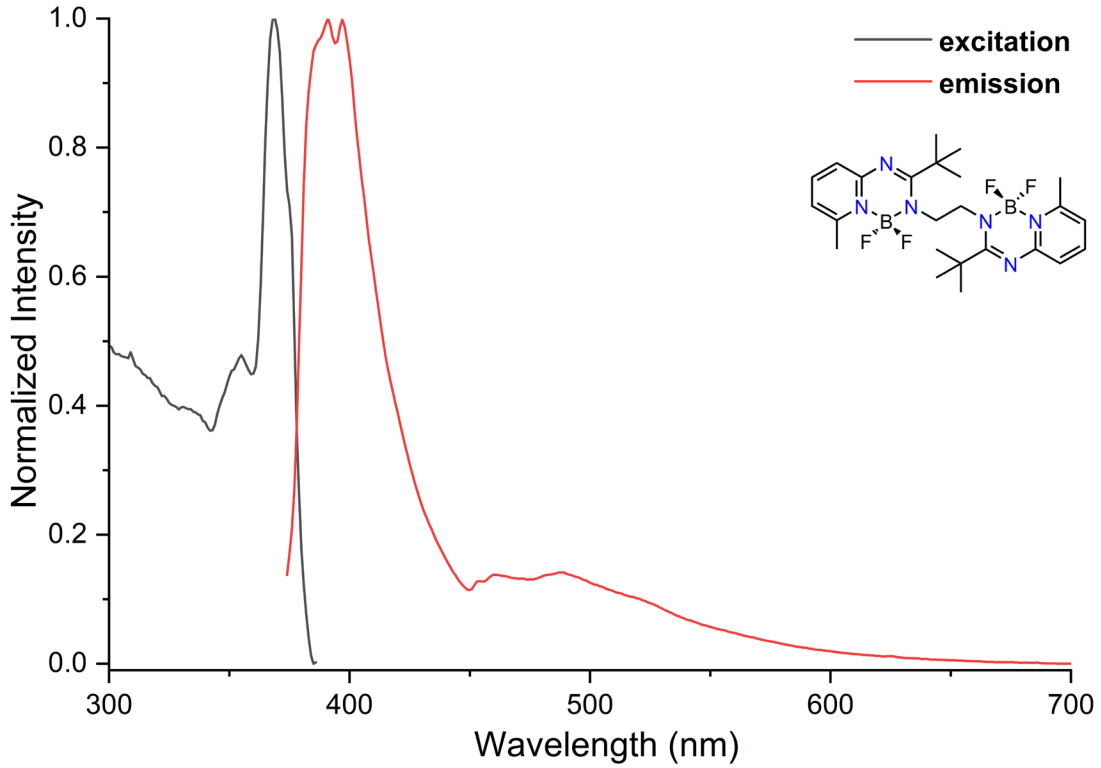

Figure S60. Photoluminescence excitation and emission spectra of **2** in the solid state at 77 K.

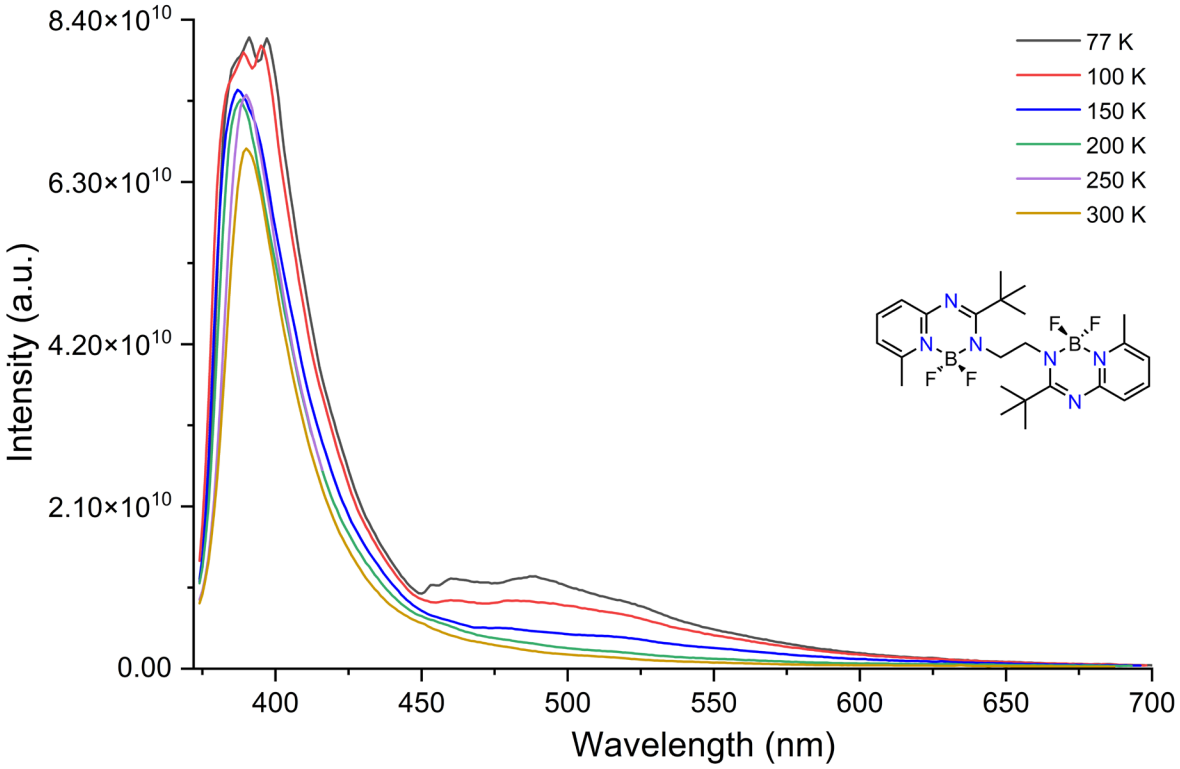

Figure S61. Variable-temperature photoluminescence emission spectra of **2** in the solid state.

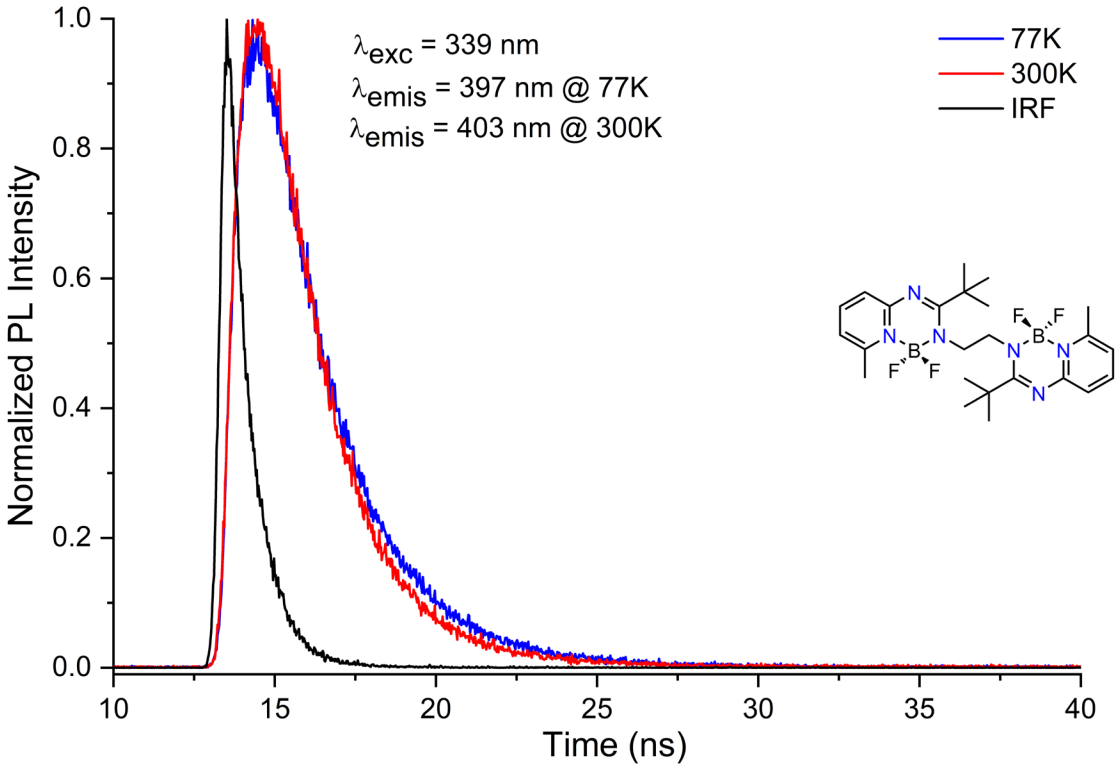

Figure S62. Emission decay traces of **2** in the solid state at 77 and 300 K under ns-pulsed excitation at 339 nm (IRF = Instrument Response Function). The decay can be fit with monoexponential curves, with τ = 1.74 and 2.02 ns, respectively.

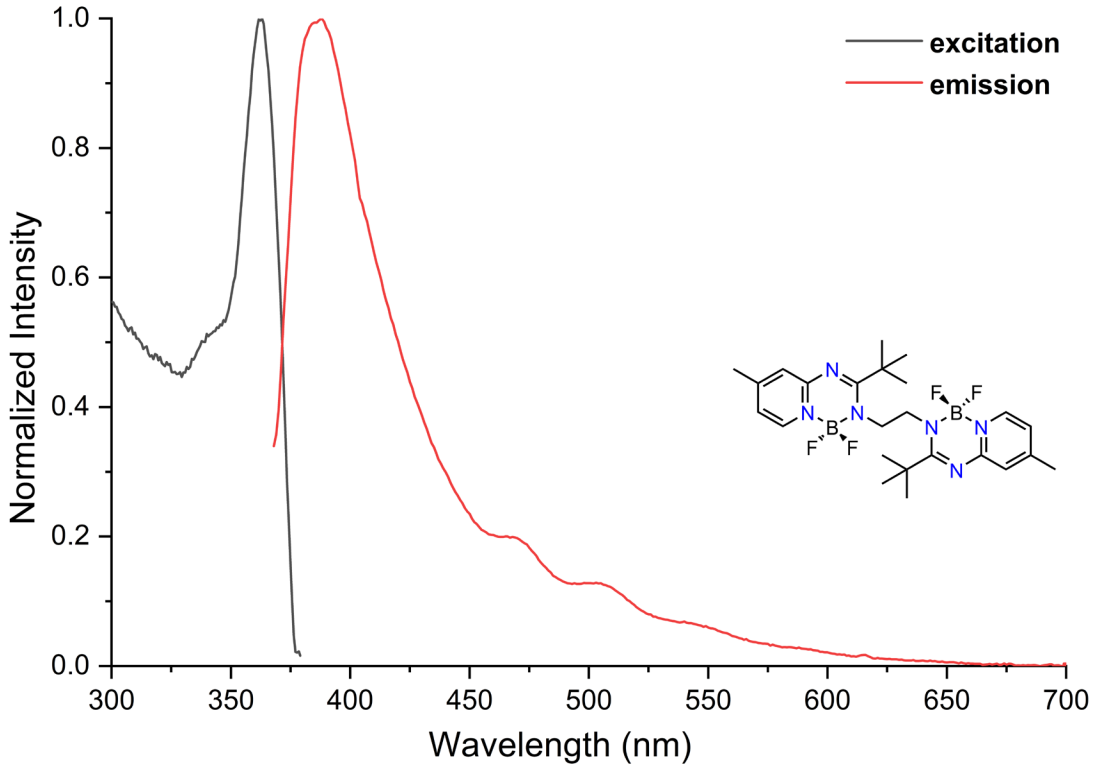

Figure S63. Normalized photoluminescence excitation and emission spectra of **3** in the solid state at 300 K.

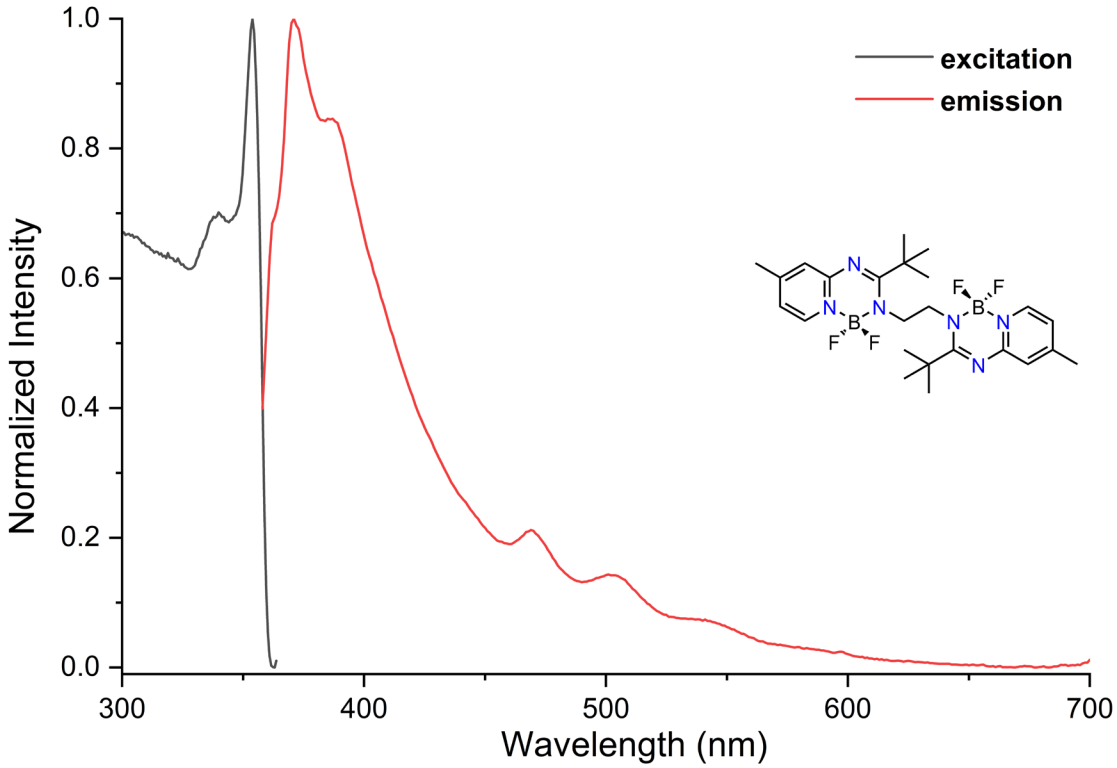

Figure S64. Photoluminescence excitation and emission spectra of **3** in the solid state at 77 K.

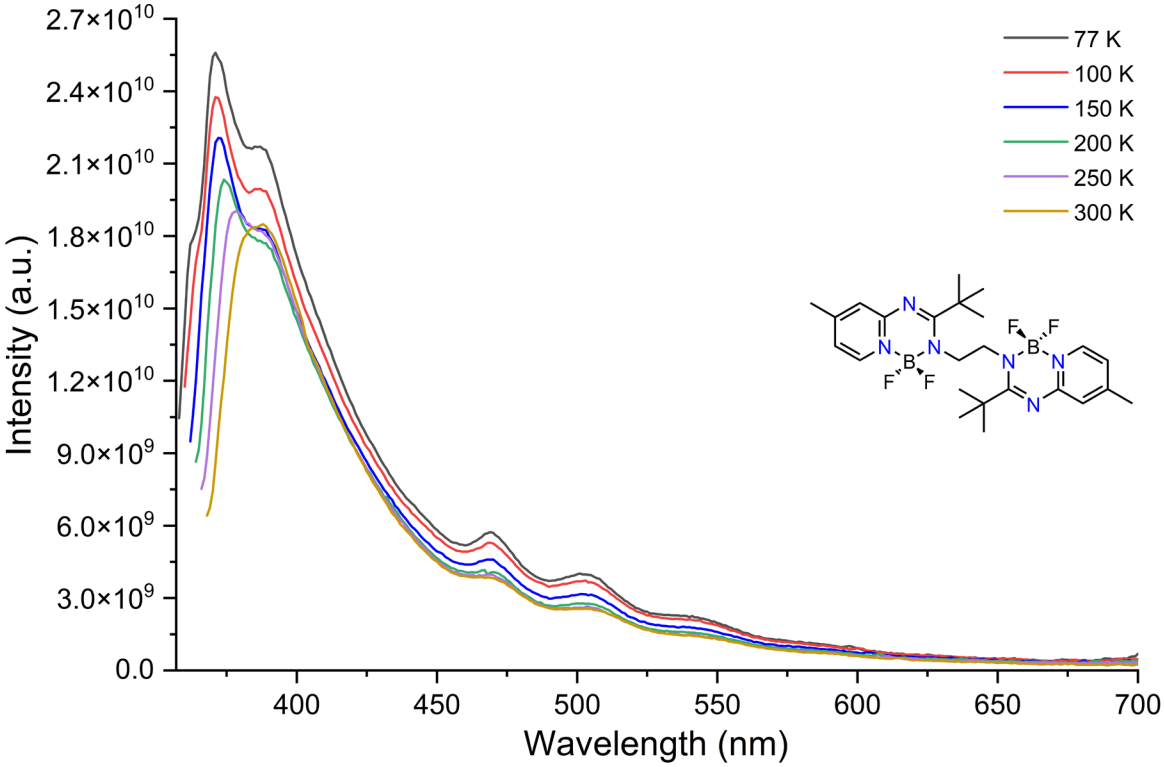

Figure S65. Variable-temperature photoluminescence emission spectra of **3** in the solid state.

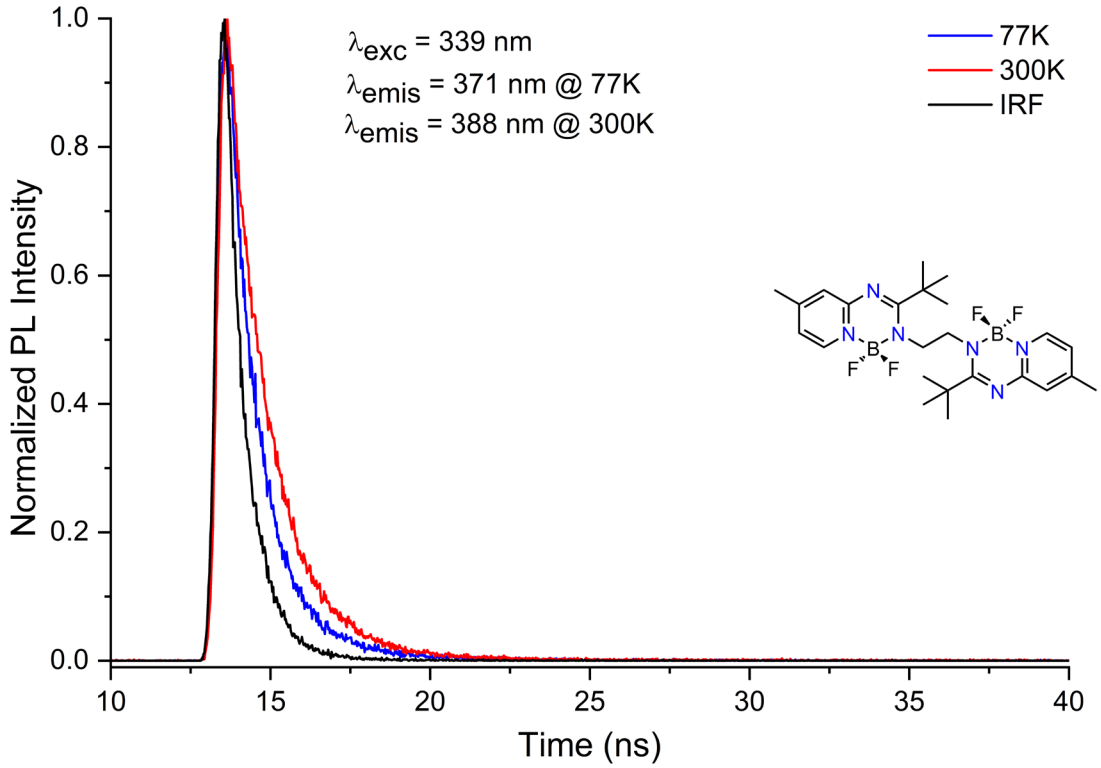

Figure S66. Emission decay traces of **3** in the solid state at 77 and 300 K under ns-pulsed excitation at 339 nm (IRF = Instrument Response Function). The decay can be fit with monoexponential curves, with τ = 4.15 and 7.36 ns, respectively.

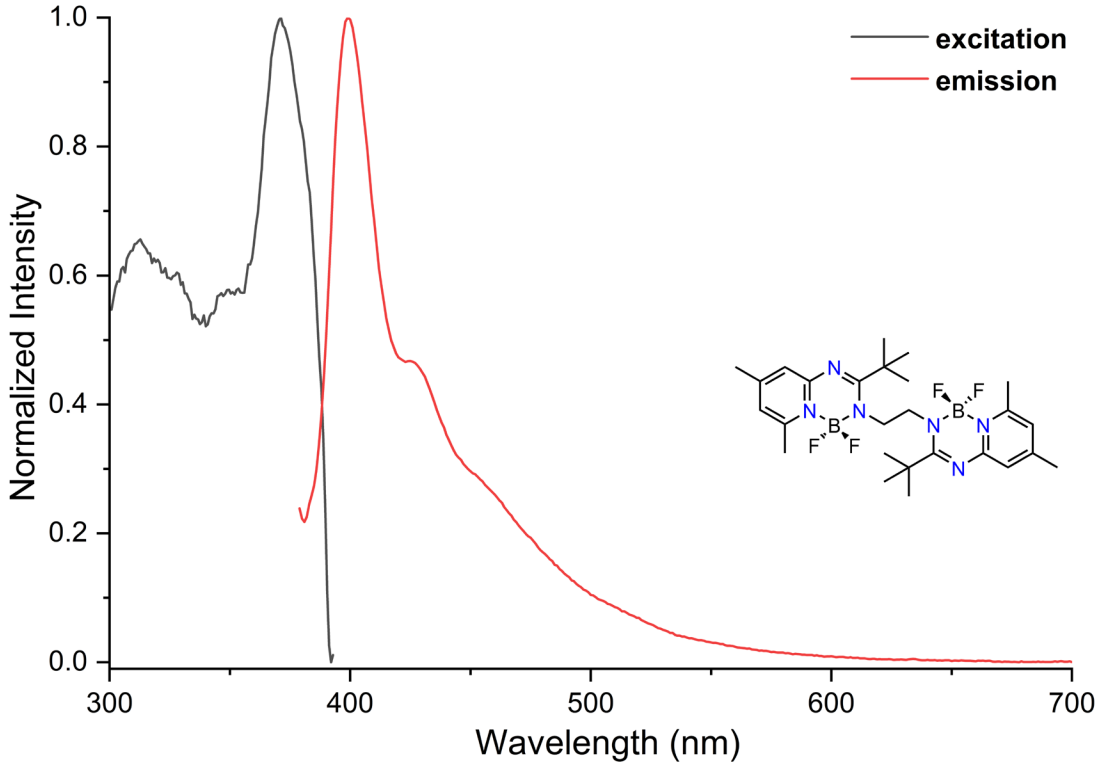

Figure S67. Normalized photoluminescence excitation and emission spectra of **4** in the solid state at 300 K.

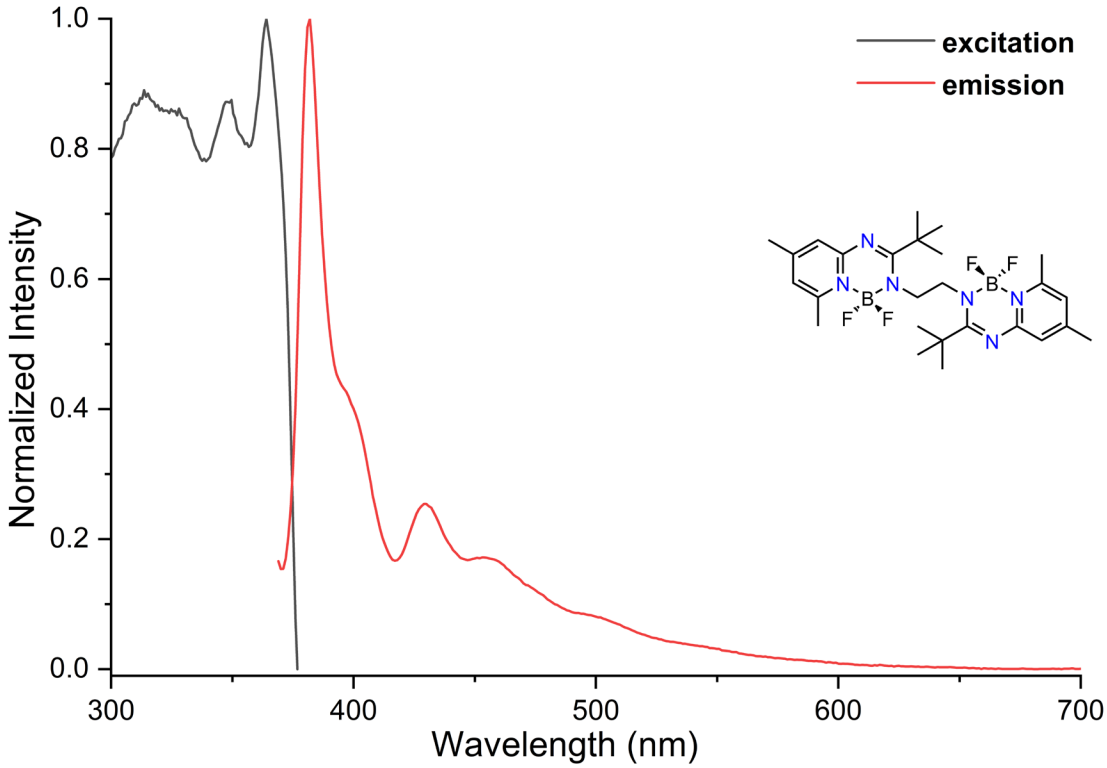

Figure S68. Photoluminescence excitation and emission spectra of **4** in the solid state at 77 K.

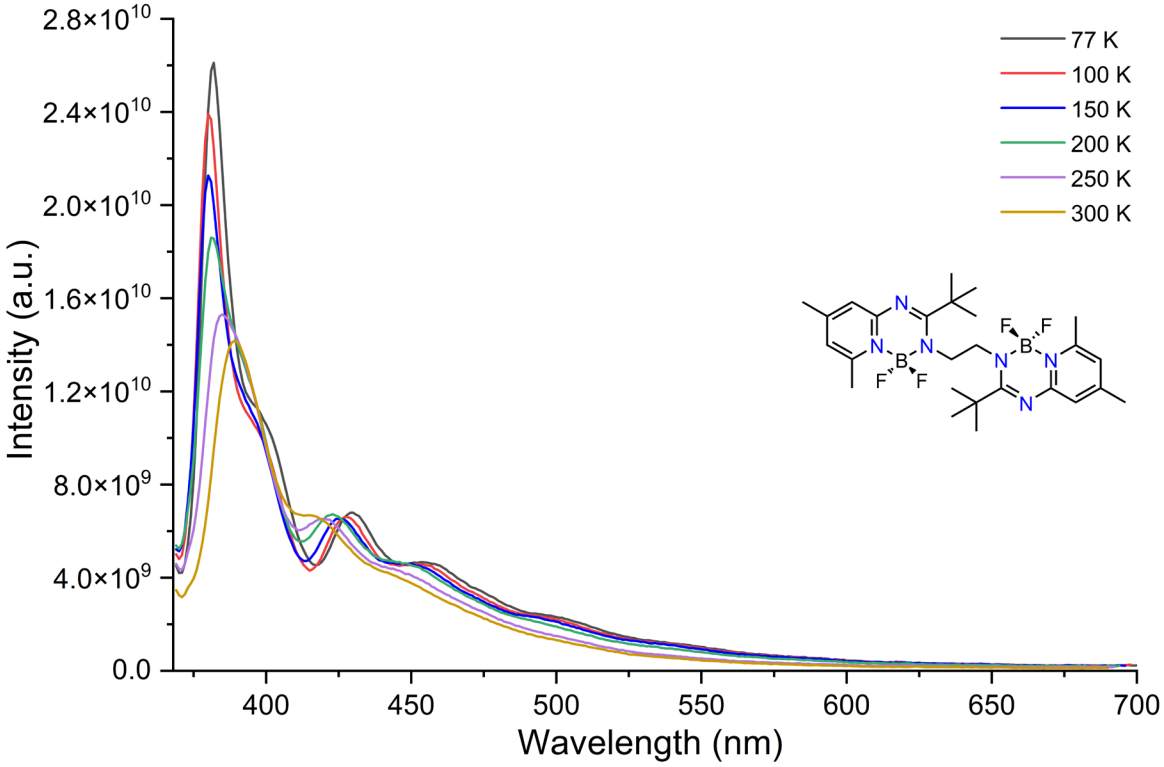

Figure S69. Variable-temperature photoluminescence emission spectra of **4** in the solid state.

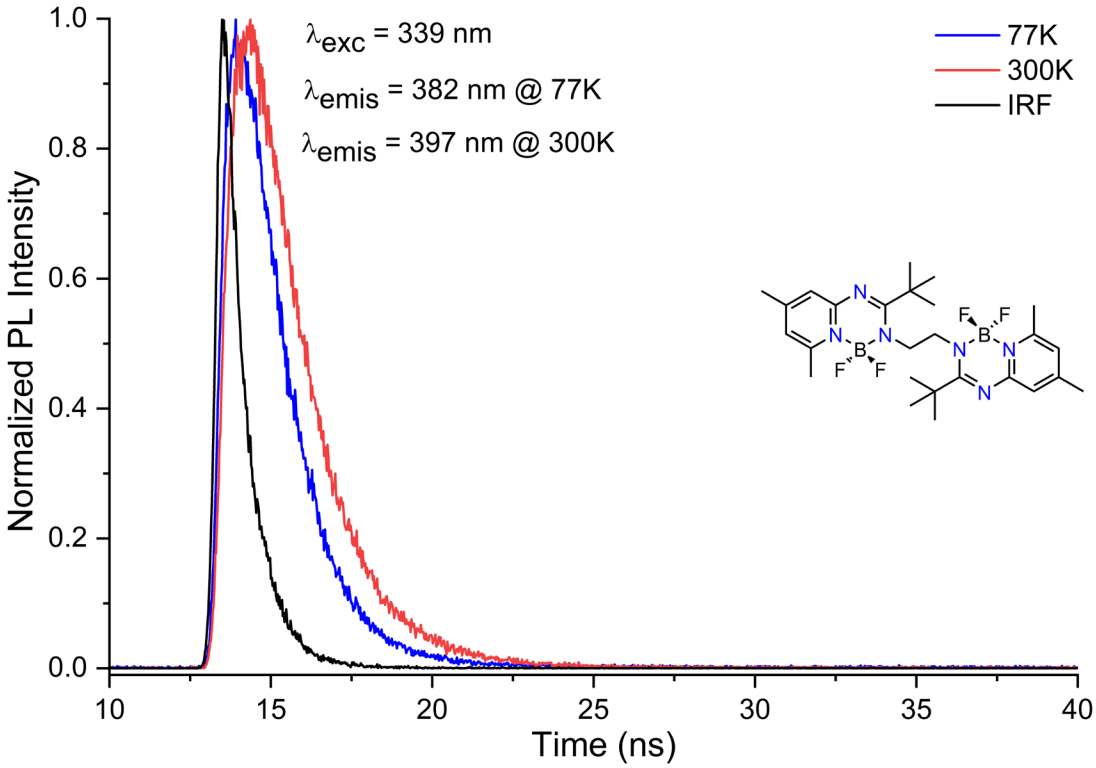

Figure S70. Emission decay traces of **4** in the solid state at 77 and 300 K under ns-pulsed excitation at 339 nm (IRF = Instrument Response Function). The decay can be fit with monoexponential curves, with τ = 1.05 and 1.48 ns, respectively.

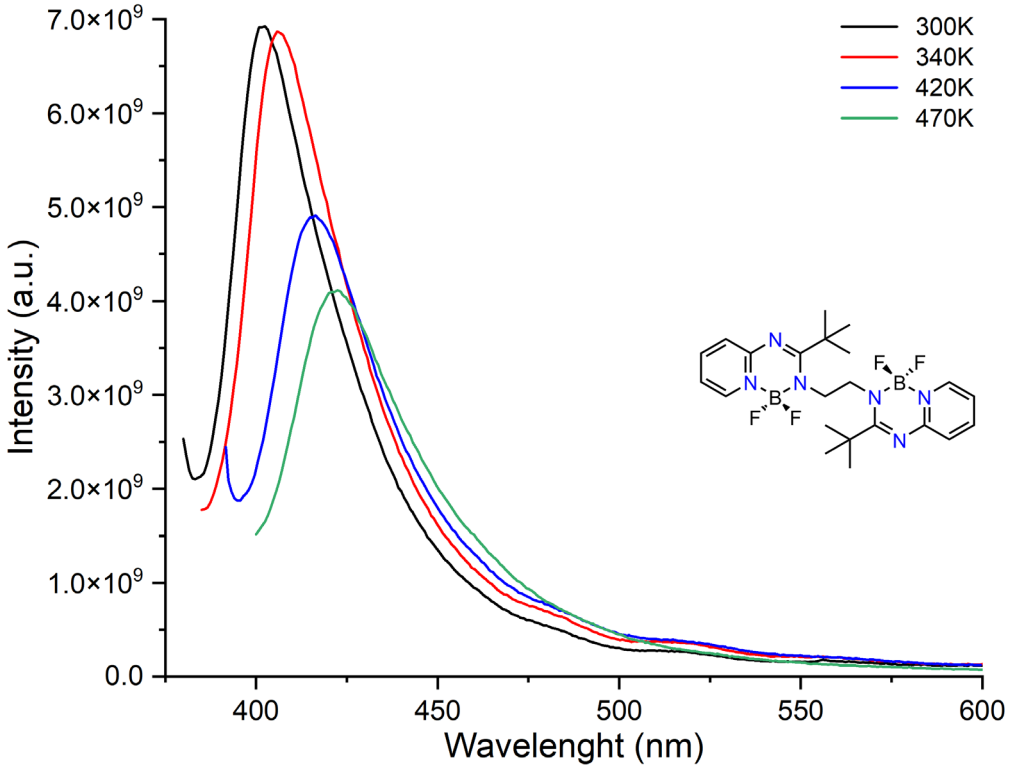

Figure S71. Variable-temperature photoluminescence emission spectra of **1** in the solid state (300–470K).

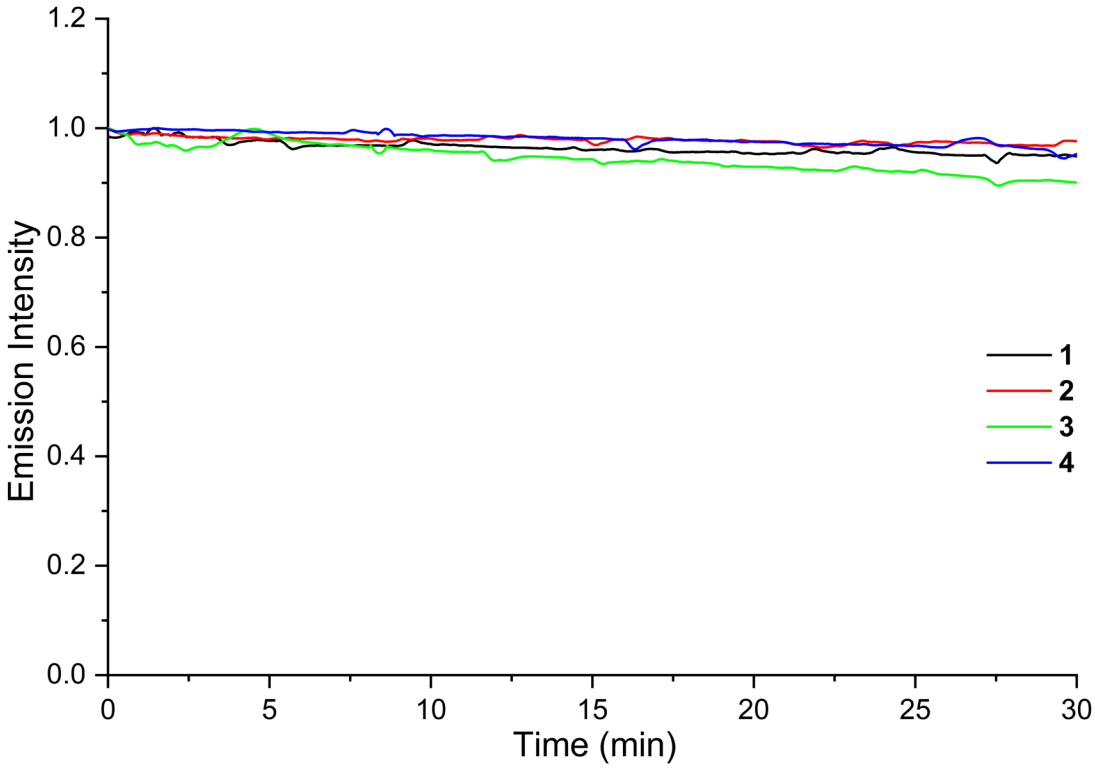

Figure S72. Photostability of **1–4** in the solid state.

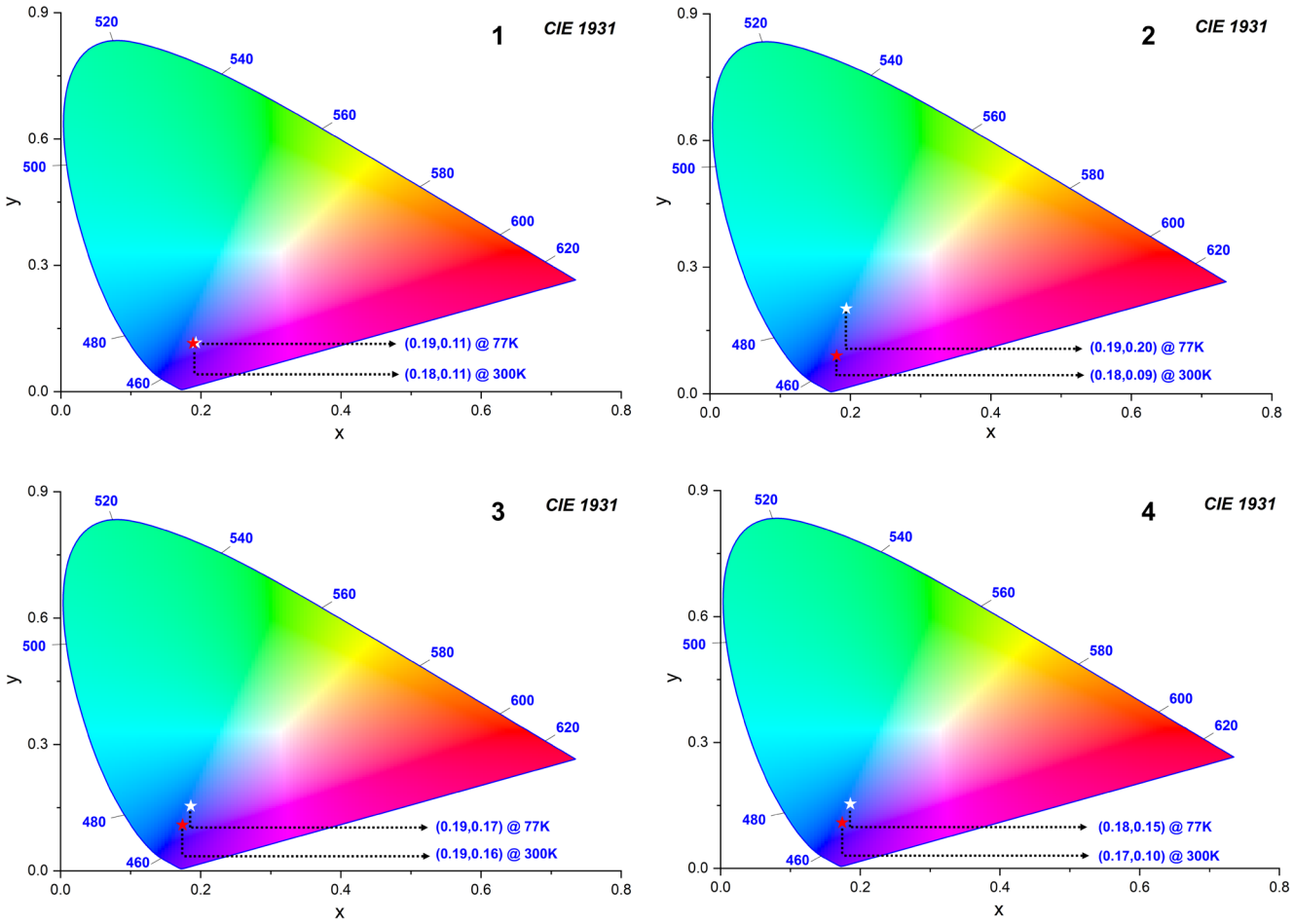

Figure S73. Commission Internationale de l'Eclairage (CIE) 1931 plots of **1–4**.

References and Footnotes

[S1] Graphics were generated using the following program: DIAMOND—Crystal and Molecular Structure Visualization (version 3.2k), CRYSTAL IMPACT, Dr. H. Putz and Dr. K. Brandenburg GbR, Kreuzherrenstr. 102, 53227 Bonn (Germany).

[S2] O'Dea, C.; Ugarte Trejo, O.; Arras, J.; Ehnbom, A.; Bhuvanesh, N.; M. *J. Org. Chem.* **2019**, *84*, 14217–14226.

[S3] Fulmer, G. R.; Miller, A. J. M.; Sherden, N. H.; Gottlieb, H. E.; Nudelman, A.; Stoltz, B. M.; Bercaw, J. E.; Goldberg, K. I. *Organometallics* **2010**, *29*, 2176–2179.

[S4] Harris, R. K.; Becker, E. D.; Cabral de Menezes, S. M.; Goodfellow, R.; Granger, P. *Pure Appl. Chem.* **2001**, *73*, 1795–1818.

[S5] (a) *APEX2: Program for Data Collection on Area Detectors*; BRUKER AXS Inc., 5465 East Cheryl Parkway, Madison, WI 53711–5373 USA. (b) *APEX3: Program for Data Collection on Area Detectors*; BRUKER AXS Inc., 5465 East Cheryl Parkway, Madison, WI 53711–5373, USA. (c) *APEX4: Program for Data Collection on Area Detectors*; BRUKER AXS Inc., 5465 East Cheryl Parkway, Madison, WI 53711–5373, USA.

[S6] Sheldrick, G.M. *SADABS: Program for Absorption Correction of Area Detector Frames*; University of Göttingen, Göttingen, Germany, 2008.

[S7] (a) Sheldrick, G.M. *Acta Crystallogr.* **2008**, *A64*, 112–122. (b) Sheldrick, G. M. *Acta Crystallogr.* **2015**, *C71*, 3–8.

[S8] (a) Spek, A. L. *PLATON: A Multipurpose Crystallographic Tool*, Utrecht University, Utrecht, The Netherlands 2008. (b) Spek, A. L. *J. Appl. Cryst.* **2003**, *36*, 7–13.

[S9] (a) Perdew, J. P.; Burke, K.; Ernzerhof, M. *Phys. Rev. Lett.* **1996,** *77*, 3865−3868. (b) Ernzerhof, M.; Scuseria, G. E. *J. Chem. Phys.* **1999**, *110*, 5029−5036. (c) Adamo, C.; Barone, V. *J. Chem. Phys.* **1999**, *110*, 6158−6170.

[S10] Yanai, T.; Tew, D.P.; Handy, N.C. *Chem. Phys. Lett.* **2004,** *393*, 51−57.

[S11] Frisch, M. J.; Trucks, G. W.; Schlegel, H. B.; Scuseria, G. E.; Robb, M. A.; Cheeseman, J. R.; Scalmani, G.; Barone, V.; Petersson, G. A.; Nakatsuji, H.; Li, X.; Caricato, M.; Marenich, A. V.; Bloino, J.; Janesko, B. G.; Gomperts, R.; Mennucci, B.; Hratchian, H. P.; Ortiz, J. V.; Izmaylov, A. F.; Sonnenberg, J. L.; Williams; Ding, F.; Lipparini, F.; Egidi, F.; Goings, J.; Peng, B.; Petrone, A.; Henderson, T.; Ranasinghe, D.; Zakrzewski, V. G.; Gao, J.; Rega, N.; Zheng, G.; Liang, W.; Hada, M.; Ehara, M.; Toyota, K.; Fukuda, R.; Hasegawa, J.; Ishida, M.; Nakajima, T.; Honda, Y.; Kitao, O.; Nakai, H.; Vreven, T.; Throssell, K.; Montgomery Jr., J. A.; Peralta, J. E.; Ogliaro, F.; Bearpark, M. J.; Heyd, J. J.; Brothers, E. N.; Kudin, K. N.; Staroverov, V. N.; Keith, T. A.; Kobayashi, R.; Normand, J.; Raghavachari, K.; Rendell, A. P.; Burant, J. C.; Iyengar, S. S.; Tomasi, J.; Cossi, M.; Millam, J. M.; Klene,

M.; Adamo, C.; Cammi, R.; Ochterski, J. W.; Martin, R. L.; Morokuma, K.; Farkas, O.; Foresman, J. B.; Fox, D. J. *Gaussian 16 Rev. C.01*, Wallingford, CT, 2016.

[S12] These torsion angles were calculated with the program DIAMOND 4.6.8.

[S13] Distance between F atom and a plane defined by the constituting atoms of the difluoroborylamidinate heterocycle except for the sp^3 hybridized B atom.

[S14] Distance between F atom and the centroid of the difluoroborylamidinate heterocycle.

[S15] Distance between Py^5 H atom and a plane defined by the constituting atoms of the difluoroborylamidinate heterocycle except for the sp^3 hybridized B atom.

[S16] Distance between Py^5 H atom and the centroid of the difluoroborylamidinate heterocycle.

[S17] Distance between the centroids of the 4,6-dimethylpyridyl-heteroaromatic rings.

[S18] Häfelinger, G.; Kuske, F. K. H. In The Chemistry of Amidines and Imidates; Patai, S., Rappoport, Z., Eds.; John Wiley & Sons, Ltd.: Chichester, UK, 1991; pp 1−100.